UNDERSTANDING THE RELATIONSHIP BETWEEN FIRE, CLIMATE, AND POPULATION IN CENTRAL UGANDA FROM 1990-2010

by

Ashley Powell

A thesis submitted to the faculty of
The University of Utah
in partial fulfillment of the requirements for the degree of

Master of Science

Department of Geography

The University of Utah

December 2012

The University of Utah Graduate School

STATEMENT OF THESIS APPROVAL

The thesis of **Ashley Powell**

has been approved by the following supervisory committee members:

Philip E. Dennison	, Chair	**08/20/12** Date Approved
Andrea Brunelle	, Member	**08/20/12** Date Approved
Mitchell Power	, Member	Date Approved

and by **George Hepner**, Chair of the Department of **Geography**

and by Charles A. Wight, Dean of The Graduate School.

ABSTRACT

Fire is a form of natural disturbance that can keep ecosystems in balance, but fire in Africa is neither entirely natural nor anthropogenic due to the hundreds of thousands of years of coexistence between fire and humans. In central Uganda fires can easily reach the size of 200 km^2 and fire is an effective way for farmers and pastoralists to clear away dead grasses that can give way to new growth. There is little to no research on fire as a disturbance in Uganda, nor on relationships between fire and climate and fire and population. Remotely sensed data allow analysis of geographic regions that may have limited access. This study generated a decision tree using six Landsat (TM and EMT+) bands, three indices (Normalized Difference Vegetation Index (NDVI), Normalized Burn Ratio (NBR), and Tassel Cap transformation) and a DEM to produce classified images. Classified images collected in five years had three classes: no burn, new burn and old burn. These classes provided a way to map fires and quantify the area burned in each scene. Population data were gridded and contained population density for the years 1990, 1995, 2000, and 2005, with a spatial resolution of 2.5 degrees, and were provided by the Socioeconomic Data and Applications Center (SEDAC) from Columbia University. Climate data used were reanaylsis datasets from the collaboration by the National Center for Atmospheric Research (NCAR) and the National Centers for Environmental Prediction (NCEP), which provides continuous global climate data from 1948 to present. The three variables analyzed were: precipitation rate, temperature and, soil moisture from

0-10 cm in depth. Within regions of lower populations and drier climates, there was more burned area than in areas of wetter climate and higher population densities. As a result of the coarse spatial resolution of climate and population data, linkages between climate, fire, and people in Uganda were difficult to ascertain. However, this study suggests that in regions with fewer people, more burning occurs regardless of how dry conditions are.

TABLE OF CONTENTS

LIST OF FIGURES

LIST OF TABLES

1 INTRODUCTION

Vegetation change is a natural process that can be measured; Milne (1988) defines change as "an alteration in the surface components of the vegetation cover." Natural and anthropogenic causes of vegetation change include avalanches, earthquakes, wildfire, flooding, landslides, outbreaks of disease or pests, wind storms, agriculture, grazing, urbanization, war, commercial logging, mining, human induced fire, and road building (Copeland et al., 1996; Sala et al., 2000; MacDonald, 2003). Fire is the most well-defined and studied form of disturbance on land and is not always viewed as a favorable one due to destruction of personal property (MacDonald, 2003).

Fire is a natural disturbance that keeps ecosystems in balance and plays a positive role in various ways, but it can also radically alter the landscape in a negative way. Fire clears accumulated leaf litter and returns nutrients from living and dead vegetation back into the soil for further growth. Some seeds require heat and chemical reactions that accompany fire for germination (MacDonald, 2003). Canopy fires allow sun light to penetrate down to the forest floor where smaller seedlings and shrubs were once shaded, and some taxa benefit from or actually require ash and mineral soils for establishment (Pyne et al., 1996; MacDonald, 2003). In addition to rich soils being favorable for native plants, these enhanced soils are also beneficial for planting a new crop or to promote new growth in grassy areas for grazing, which is why fire is a useful tool in agriculture communities (Pyne et al., 1996). Fire can also be detrimental in agriculture when

1 INTRODUCTION

Vegetation change is a natural process that can be measured; Milne (1988) defines change as "an alteration in the surface components of the vegetation cover." Natural and anthropogenic causes of vegetation change include avalanches, earthquakes, wildfire, flooding, landslides, outbreaks of disease or pests, wind storms, agriculture, grazing, urbanization, war, commercial logging, mining, human induced fire, and road building (Copeland et al., 1996; Sala et al., 2000; MacDonald, 2003). Fire is the most well-defined and studied form of disturbance on land and is not always viewed as a favorable one due to destruction of personal property (MacDonald, 2003).

Fire is a natural disturbance that keeps ecosystems in balance and plays a positive role in various ways, but it can also radically alter the landscape in a negative way. Fire clears accumulated leaf litter and return nutrients from living and dead vegetation back into the soil for further growth. Some seeds require heat and chemical reactions that accompany fire for germination (MacDonald, 2003). Canopy fires allow sun light to penetrate down to the forest floor where smaller seedlings and shrubs were once shaded, and some taxa benefit from or actually require ash and mineral soils for establishment (Pyne et al., 1996; MacDonald, 2003). In addition to rich soils being favorable for native plants, these enhanced soils are also beneficial for planting a new crop or to promote new growth in grassy areas for grazing, which is why fire is a useful tool in agriculture communities (Pyne et al., 1996). Fire can also be detrimental in agriculture when

frequent high intensity fires remove much of the vegetation cover which results in an increase in surface temperatures and loss of nutrients which leads to the area being classified as inhospitable (Pyne et al., 1996). Frequent fires can deplete the once nitrogen rich soil and decrease the rate at which water can permeate the soil, which negatively effects the regeneration of new plant life (Asner et al., 2004; Mills & Fey, 2004).

Landscapes that have experienced fire can readily be visually detected due to the apparent physical changes that occur, such as vegetation and soil charring (Kokaly et al., 2007). Mapping area burned on the ground, if possible, can be an arduous and a costly process. Remote sensing is an appropriate technology for mapping vegetation change and disturbances temporally and spatially. Remote sensing is a useful tool to map areas that are more difficult to get to. Little is known about the fire regimes in Sub-Saharan Africa. There is a need for adequate knowledge of land cover changes, specifically fire, in areas of Africa, because land cover change is regarded as one of the most important variables of global change affecting ecological systems (Vitousek, 1994; Cooke et al., 1996; Otukei & Blaschke, 2010).

While the series of Landsat sensors has been obtaining data throughout the world since the 1970s, spatial and temporal coverage is sparse for many portions of Sub-Saharan Africa, and only a few sporadic years of data are available in many regions. Another issue with studying vegetation change and fire regimes in Africa is the lack of ground-truth data and accessibility to remote areas. While a few studies have been completed in Uganda, and those that do focus on the southwestern portion of the country where there is higher population density (Mugisha, 2002; Namaalwa et al., 2009; Nakaaawa et al., 2011), this study aims to map burned area, calculate the total area

burned, to explain temporal trends in burned area during the past two decades and understand the relationships between climate, fire, and population in Central Uganda from 1989 to 2010. By addressing these objectives this study will determine if the variation in burned area within the study region can be explained through climate variables (precipitation rate, soil moisture, and temperature), or if the variation in burned area is driven by population density and/or population change.

2 BACKGROUND

The study area for this project is in Central Uganda, a land locked country in the Great Lakes region of East Africa. The area is north of the capital Kampala and totals 185km^2 with Lake Kyoga in the center (Figure 1). Uganda has a subtropical climate with rainfall patterns related to the movement of the Inter-tropical Convergence Zone (ITCZ). As the sun's declination migrates between the Tropic of Cancer (23.5° N) and the Tropic of Capricorn (23.5° S), the ITCZ lags behind the sun's path bringing rain a month after the sub-solar point has passed (Christopherson, 2000). The ITCZ moves across the area biannually creating a bimodal rainfall pattern. There are two rainy seasons, one in March, April and May (MAM), the dominant rainy season; and the second rainy season occurs during the months of October, November, and December (OND). The moisture comes from the northeasterly winds picking up moisture across the Indian Ocean (Ogallo, 1988; Mutai et al., 1998).

In Northern Uganda the time between the end of the first rainy season and the start of the second rainy season is close together, creating a unimodal rainfall distribution, with little precipitation the rest of the calendar year. There has yet to be a clear explanation behind why there is both a bimodal and unimodal rainfall distribution in Uganda, though the variable topography and two large bodies of water, Lake Victoria and Lake Kyoga, can influence the spatial distribution of rainfall within the region (Ogallo,1989).

Most of the research that has been done on sea surface temperature (SST) and sea-level pressure in Eastern Africa has focused on the second and shorter rainy season, peaking

in November. No significant relationship between the variables: SSTs, sea level pressures, and MAM rainy season has yet to be determined; MAM rains seem to have little to no interannual variability (Mutai et al., 1998).

There have been a few studies that have shown a relationship between El Niño-Southern Oscillation (ENSO) and OND rainfall (Phillips & McIntyre, 2000). Phillips and McIntyre (2000) concluded that during years of el niño, the bimodal region (Southern Uganda) sees an increase in rainfall, whereas during la niña the same region receives less precipitation. The unimodal region (Northern Uganda) does not see a change in the amount of precipitation during ENSO, but rather a shift in the rainy season peak. The peaks are later during years of el niño, whereas during a la niña the peak occurs earlier in the year (Phillips & McIntyre, 2000).

The southern region of Uganda tends to receive more precipitation, an average of 2500 mm of annual precipitation, whereas in the north it is drier in comparison, an average of 750 mm of annual precipitation (Nicholson 2001; Eriksen et al., 2008; McSweeney et al., 2008; Apuuli et al., 2000). The annual mean temperature for Uganda is 22°C with a mean minimum of 17°C and a mean maximum of 27°C (Apuuli et al., 2000).

Many regions of the world that have a subtropical grassland and/or savanna climate regime experience frequent fires every 1 to 5 years due to low topographic variation, quick regeneration of annual vegetation, frequent winds, low humidity, high temperatures, and frequent lighting strikes (Pyne et al., 1996; MacDonald, 2003). While there are many natural factors that affect the size, frequency, and intensity of fires, human activities play an integral role.

Fire occurs regularly in Africa, but is neither entirely natural nor anthropogenic due to the hundreds of thousands of years of coexistence between fire and humans. Between 60-80% of biomass burning worldwide takes place in tropical savannas and open woodlands, which are dominated by grasses, limited trees, and woody shrubs (Cooke et al., 1996; MacDonald, 2003). Lightning strikes are the leading cause of naturally occurring fires, whereas humans are the major source of ignition for all fires. Fire on the landscape allowed humans to alter a wild landscape into a grazing habitat or farmland (Pyne et al., 1996; MacDonald, 2003). The process of burning large areas of lands is one that has been historically used in Uganda prior to Western influences and is useful for regeneration of new vegetation and the creation of charcoal as a fuel source (Cooke et al., 1996; Pyne et al., 1996; MacDonald, 2003). In Central Uganda fires can easily reach the size of 200 km^2 and fire is an effective way for farmers and pastoralists to clear away dead grasses that can give way to new growth (Buechner & Dawkins, 1961). Domestic and wild herbivores forage on new vegetation which is higher in essential nutrients that can lead to an increase in mass of the animals (Van de Vijver et al., 1999). Not only does burning provide new vegetation, but it also removes vegetation that could decrease the visibility and accessibility to animals (Buechner & Dawkins, 1961).

Fire provides an important energy source for Ugandans. Over 90% of all energy used in Uganda comes from forest biomass, and 15.4% of that is for the production of charcoal (Namaalwa et al., 2009; Nakaaawa et al., 2011). Firewood is predominately used by rural populations, which makes up 88% of Uganda's overall population, and charcoal tends to be used by urban populations (Namaalwa et al., 2009). Because wood

is primarily used for energy production, wood collection it is the leading cause of forest degradation and deforestation in Uganda (Namaalwa et al., 2009; Nakaaawa et al., 2011). Forested areas that are lost are then converted to grasslands or agricultural land, which can in turn be burned during the dry season.

Topography, fuel type, and weather (the most dynamic factor) affect when and how fire burns (Pyne et al., 1996). Climatic drivers such as air temperatures and the amount and timing of precipitation can affect fire regimes. Irregular cold conditions over the Atlantic and Indian Oceans increase precipitation, while warmer conditions decrease rainfall in Uganda (Nicholson 2001; Osbahr et al., 2010). Uganda has experienced a decrease in precipitation of 3.5% annually and an increase in mean annual temperature by 1.4˚C since the 1960s. Seven different droughts were noted during 1991-2000, with the most severe drought during that time occurring 1999-2000 (McSweeney et al., 2008; Osbahr, 2010).

Remote sensing has been a useful tool for detecting vegetation and vegetation change on the African continent in general and Uganda specifically. Mugisha (2002) set out to quantify, with the use of remote sensing, land cover/use changes and determine the source of change in five areas of Uganda: Sango Bay, Lake Mburo National Park and adjacent areas, Kabale/Ntungamo Border, areas adjacent to Kibale National Park, and Katakwi/Karamoja. Four out of the five sites saw a significant decrease in tropical rain forest, savanna and wetlands, and a significant increase in subsistence farming. While they were able to successfully analyze four areas, results were inconclusive in the Katakwi/Karamoja border area, which covers portions of this current project. Nakakaawa et al. (2011) were able to classify the vegetation cover and change over the

entire country in 1995 and 2000. They determined that there was a decrease in forest and woodland areas and an increase in subsistence farming and grazing and commercial production of wood for fuel during that time period. This study also pointed out that the majority of the area that saw an increase in subsistence farming and grazing was in Central and Northern Uganda due to the large subsistence rural population and unsustainable farming practices (Nakakaawa et al., 2011). While both of these studies provide a better understanding of Uganda's land cover, there has yet to be a study on the role of fire as an ecosystem process and potential drivers of fire activity on the landscape in Central Uganda.

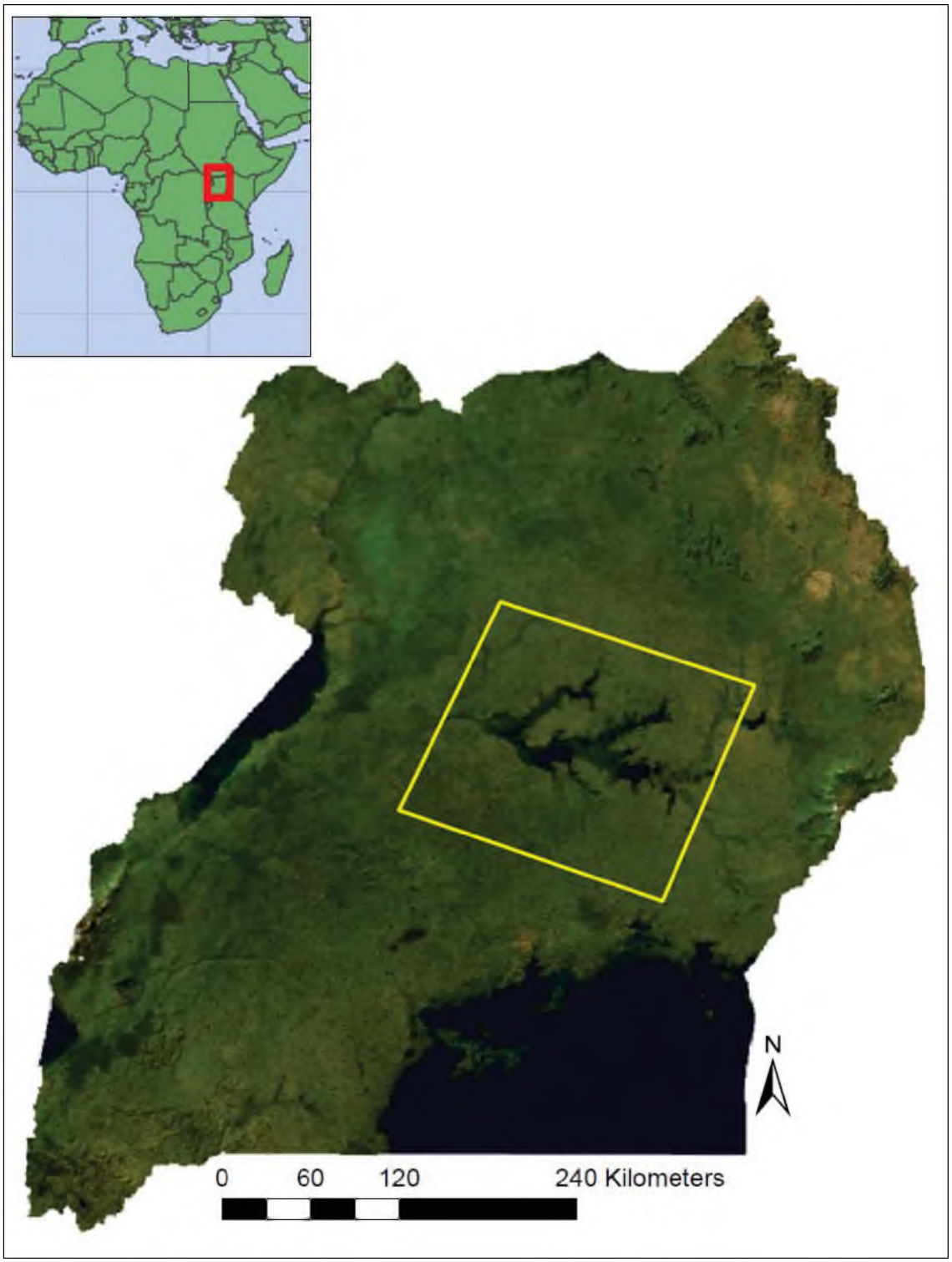

Figure 1. Location map of study area. The red box in the upper left corner indicates the location of Uganda. The yellow box indicates the specific study area in Uganda.

3 METHODOLOGY

The Thematic Mapper (TM) sensors on the Landsat 4 and 5 satellites were launched in the mid-1980s, and Landsat 5 TM operated from 1984 until 2011. TM was a mechanical optical scanner that recorded energy reflected by or emitted from the earth's surface in the visible, reflective-infrared, and thermal infrared portions of the electromagnetic spectrum (Jensen, 2000). Landsat TM sensors had seven spectral bands with specific wavelength ranges to optimize the detection of vegetation absorption and reflection, wetlands, plant and soil moisture, water penetration, differentiate between clouds, snow and ice, and identification of certain rock types (Jensen, 2000). The specific wavelengths and region of the electromagnetic spectrum for each band were as follows: band 1: 0.45 to 0.52 μm (blue), band 2: 0.52 to 0.60 μm (green), band 3: 0.63-0.69 μm (red), band 4: 0.76 to 0.90 μm (near infrared), band 5: 1.55 to 1.75 μm (mid infrared), band 6: 10.4 to 12.5 μm (thermal infrared), band 7: 2.08 to 2.35 μm (shortwave infrared). Band 1-5 and 7 had the same spatial resolution of 30 x 30 meter at nadir (perpendicular downward-facing viewing geometry), whereas band 6 had a spatial resolution of 120 x 120 meter at nadir (Huang et al., 2010; Jensen, 2000).

Landsat 7 ETM+ has the same seven spectral bands and Landsat TM sensors; band 6 has an improved spatial resolution of 60 x 60 meter, and has an additional panchromatic band, band 8. The panchromatic band spans across the blue, green and red portions of the electromagnetic spectrum, and is useful for visual inspection, especially with a better spatial

resolution (15 m) than the other bands (Chander et al., 2009; Huang et al., 2010; Jensen, 2000). Landsat 7 launched in 1999, but suffered a scan line corrector failure in 2003 which caused ETM+ to return incomplete data.

The specific Landsat tile that was used for this study is path 171 and row 59, and the tile dimensions are approximately 175 km by 183 km. It was important to obtain scenes during the months of December through February; December is the beginning of the dry season whereas February, on average, is the end of the dry season. During this time, grasses are senesced and fires are actively burning and/or recent burn scars are more visible, and there is a greater likelihood of obtaining cloud free scenes. Anniversary dates or anniversary windows, using the same Julian date each year, are ideal. Due to limited data availability and gaps in the data, good scenes during December through February were not always available (Coppin et al., 2004). Despite these challenges there were five different scenes spanning this seasonal window captured during the last 20 years (Table 1). Data were ordered from the US Geological Survey (USGS) as level 1G products, and were then atmospherically corrected and radiometrically calibrated.

Remotely sensed data allow researchers to study geographic regions that may not be easily accessible and/or on the other side of the world, but the collected data are not final products. Various indices can be calculated in order to more accurately interpret and analyze the imagery such as: Normalized Difference Vegetation Index (NDVI), Normalized Burn Ratio (NBR), and Tassel Cap transformation (Healey et al., 2005; Miller & Thode 2005; Pettorelli et al., 2005). The NDVI is a measure of green vegetation cover and leaf area index using near infrared (NIR) and red bands represented

by the equation;

$$NDVI = \frac{R_{NIR} - R_{red}}{R_{NIR} + R_{red}} \quad (1)$$

where R_{NIR} is near infrared band reflectance and R_{red} is red band reflectance. Chlorophyll absorption occurs in the red portion of the electromagnetic spectrum, whereas the structure of leaves reflect or transmit most NIR wavelengths (Jensen, 2005; Miller & Thode, 2005; Otukei & Blaschke, 2010; Pettorelli et al., 2005). Normalized burn ratio (NBR) is similar to NDVI except the red band is removed and replaced with a shortwave infrared (SWIR) band. SWIR band reflectance (R_{SWIR}) is sensitive to the presence of water in vegetation and soils.

$$NBR = \frac{R_{NIR} - R_{SWIR}}{R_{NIR} + R_{SWIR}} \quad (2)$$

The difference between pre-fire and post-fire (dNBR) determines fire severity by calculating a burn ratio, which also has a range from -1 to 1 (Miller & Thode, 2007).

$$dNBR = NBR_{pre-fire} - NBR_{post-fire} \quad (3)$$

Tassel Cap transformation enhances the spectral information within Landsat TM and ETM+ data by reducing the number of bands to three standard principal components referred to as brightness, greenness, and wetness (Healey et al., 2005).

NDVI, NBR and Tassel Cap transformation are all individually useful indices to analyze remote sensing images. However, with the use of data mining all three processes can be used together to generate a decision tree. Data mining programs such as WEKA, from the University of Waikato in New Zealand, creates decision trees more efficiently than manually constructing a decision tree in ENVI and uses an automated process to create decision boundaries (Otukei & Blaschke, 2010). Otukei and Blaschke (2010) state that with the use of data mining nodes a decision tree can be replicated without the disagreement of expert classification from varying opinions.

The five Landsat scenes used in this study were normalized to apparent surface reflectance using Atmospheric CORection Now (ACORN) which corrects for atmospheric attenuation that occurs due to absorption and scattering by gases and particles in the atmosphere. Only one image went through the rigorous process of running ACORN. Additional calibration needed to be completed in order to correct the remaining images to the atmospherically corrected image. Iteratively Re-weighted Multivariate Alteration Detection (IR-MAD) radiometrically normalizes an uncorrected image to one that has been atmospherically corrected.

Once preprocessing was completed, the next task was to stack Landsat bands 1-5 and 7 with the output layers of NBR, NDVI, Tassel Cap and a data elevation model (DEM). The purpose of using a DEM was to account for any variation in elevation that could lead to more or less burning, if this variation existed. Masks for Lake Kyoga and

the scene edges were then created to prevent these areas from being classified as burned or unburned. Within a few bands the spectral response of the lake and areas on the edges of the scenes were similar to burned areas and had the potential to be misclassified.

Regions of interests (ROIs) are areas that are archetypical of a spectral response for a specific land cover type. ROIs were selected for each of the three land cover classes: new burn, old burn, or no burn. ROIs for each class were chosen based on their color and shape—visual characteristics within the images. Three bands were used to create a false color composite within ENVI: band 5 (shortwave infrared), band 4 (near infrared), and band 3 (red). The no burn class was characterized by surface materials such as green vegetation, senesced vegetation, bare soil, water, clouds, and cloud shadows. New burn ROIs were characterized by a dark purple/maroon color in the image. The distribution of new burn did not appear to be random and the shape of the burned areas tended to be irregular. The old burn class was determined by appearing to be a lighter purple/maroon than the new burn; old burn tended to be close in proximity to the new burn areas. The old burn class was the most difficult to determine because at times the colors consistent with old burn were similar to bare soil and/or senesced vegetation. All of the ROIs were imported into a data mining program WEKA (Waikato Environment for Knowledge Analysis) in order to build a decision tree based off of the inputs. Additional inputs, such as NBRI, NDVI, Tassel Cap, and a data elevation model (DEM) were used to most effectively classify each pixel in every image.

The output of WEKA is a decision tree based on the inputs for each image. In order to classify the image, the decision tree was transferred into a decision tree within ENVI. The output from ENVI is a classified image that can be analyzed. In order to

properly analyze the classified images, it is important to separate the data into training and accuracy assessment data. ROIs for both the training and accuracy assessment were selected at the same time and randomly divided into 2 groups. In order to reduce accuracy bias, the training ROIs used for the development of the decision tree were used independently of the accuracy assessment. Training ROIs were chosen for all 3 classes and used to create the decision tree. Once the classified image was completed it was tested for its overall accuracy. The accuracy assessment was completed within ENVI using a confusion matrix to determine which pixels the classified image defined as new burn, old burn, or no burn verses the validation ROIs that were chosen at the same time as the training ROIs for the same classifications. This process demonstrates how accurately the decision tree was able to classify the image.

A map of burn frequencies was created in order to determine if and where particular areas had burned more than once throughout all 5 Landsat scenes. The same decision tree as previously discussed was used, but modified by changing the output of 3 classes to only 2 classes, no burn and burn. Pixels of no burn were given a value of 0, whereas pixels that burned were given a value of 1. Each image ran through the 2 class decision tree and within ENVI a layer stack was created using all image outputs. The output file had values between 0 and 5. If a pixel did not burn in all 5 scenes, it was given a 0 value. If a pixel burned once, then the pixel value was 1. The maximum value for a single pixel is 5, if that particular pixel burned in all 5 scenes. The output map can help determine how many times an area has burned, indicate if there is a pattern, and point to a reason behind the burning.

Once burned area mapping was completed, potential explanations for temporal trends were explored with the use of climate and population data. The poor temporal resolution of remotely sensed data of Uganda makes it difficult to say whether burned area is increasing or decreasing over the last 20 years, but climate and population data could correlate with changes in fire area over time. Weather station and census data are spatially and temporally sparse, but with the use of gridded datasets it may be possible to make a link to either climate and/or humans. The study region of Central Uganda was divided into four quadrants, as seen in Figure 2, to determine the total area burned and to more accurately compare averaged population data and averaged precipitation data over the same region.

The Socioeconomic Data and Applications Center from Columbia University has gridded data that contain population density for the years 1990, 1995, 2000, and 2005, with a spatial resolution of 2.5', which is about 21.2 km^2. Settlement points were also available for download, but were only available for the year 2000. Population density was averaged and summed for the entire scene and for 4 subsets of the scene within ArcGIS.

Weather station data that are used to understand the climate in Uganda are also temporally and spatially sparse so gridded datasets were used. The National Center for Atmospheric Research (NCAR) and the National Centers for Environmental Prediction (NCEP) collaborated together to produce reanaylsis datasets that provide continuous global climate data from 1948 to present. The program R was used to extract the specific area and time within the climate NetCDF files. The reanalysis data have many variables. However, this project focused specifically on 3 variables: precipitation rate, skin

temperature (temperature at the surface) and soil moisture from 0-10 cm in depth. All 3 variables are available in daily averages and have a spatial coverage of the T62 Gaussian grid (192 x 94 data points). The T62 Gaussian grid is typically used for modeling a sphere, such as the earth. The coordinates for the grid cell that encompass the study area are centered at 31.875° east and 0.952° north. The years that were examined were 1988-2010, 1 year prior to the first year Landsat data are available for this area. Precipitation rate is measured in $kg/m^2/s$, temperature is measured in kelvin, and soil moisture is measured in fractions.

The climate variables chosen were used to determine if there were any trends in the climate data that could explain differences in the area burned from year to year. Precipitation, soil moisture, and temperature have daily values that were averaged for the time periods of October-February (preceding wet season), March-February (preceding year), and 24 months March-February (two preceding years). Yearly averages were also calculated for the same 3 time periods. Z-scores were calculated from monthly and yearly values using the following equation:

$$z = \frac{x - \mu}{\sigma} \tag{4}$$

where x is the climate variable, μ is the average of a group of climate variables, and σ represents the standard deviation. The z-score was calculated to normalize climate variables for comparison.

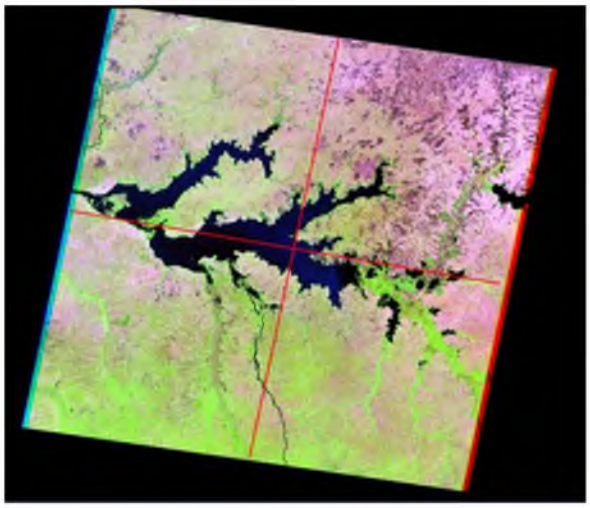

Figure 2. The four quadrants of a Landsat image.

Table 1. Year, Julian data and Landsat sensor type for acquired data. Landsat Thematic Mapper is "TM" and "ETM+" is Landsat Enhanced Thematic Mapper Plus.

Year	Julian Date	Sensor
1989	058	TM4
1995	019	TM5
2001	027	ETM+ 7
2003	017	ETM+ 7
2010	028	TM5

4 RESULTS

The total area burned, new burn, and old burn for each date were calculated from the classified images. For the image taken in 1989, the total area burned was 644.4 km^2, with 205.0 km^2 new burn and 439.4 km^2 old burn (Figure 3). The classified 1989 image had a kappa coefficient of 0.944 and the confusion matrix had an overall accuracy of 97.2%. Within the confusion matrix, the new burn class had a total of 60 reference pixels chosen with 52 of those pixels correctly classified as new burn in the classified image, whereas eight pixels were misclassified as no burn. A total of 309 reference pixels were selected for the no burn class, 307 pixels were correctly classified as no burn, with two pixels misclassified as new burn. In the third class, old burn, there were 101 reference pixels chosen and 98 of them were correctly classified as old burn with one pixel misclassified as new burn and two pixels misclassified as no burn (Table 2). Burning tended to occur north of Lake Kyoga (Figure 4-7), but there were still burned areas throughout the entire image.

Out of all the 5 different scenes, 1995 had the largest area burned. The total area burned for 1995 was 2,341.5 km^2, with 711.0 km^2 new burn and 1,630.5 km^2 old burn (Figure. 8); the overall accuracy was 99.7% and a kappa coefficient of 0.995 (Table 3). The majority of the burned area occurred in the northeast quadrant of the scene and scattered burn scars towards the west central region (Figure 9-12).

2001 had the least amount of area burned compared to the other the 4 scenes. 2001 had 495.6 km^2 of total area burned, with 81.6 km^2 making up new burn, and 414.0 km^2

of old burn (Figure 13). The overall accuracy for 2001 was 99.0% with a kappa value of 0.983 (Table 4). Area burned tended to be in the west central area and in the upper northeast region (Figure 14-17).

The total area burned for 2003 was 748.2 km^2, with 150.3 km^2 of new burn and 597.9 km^2 of old burn (Figure 18). The overall accuracy for 2003 was 99.4% and a kappa coefficient of 0.976 (Table 5). 2003 had the second highest area burned of all five years, with the majority of the burned area located in the west central region of the northwest quadrant and some burning in the upper northeast (Figure 19-22). This year is the first year that the northwest quadrant had a larger total area burned than the northeast quadrant.

The last year, 2010, had a total of 634.9 km^2, with 142.9 km^2 of new burn and 492.0 km^2 of old burn (Figure 23). The overall accuracy for 2010 was 98.8% with a kappa coefficient of 0.934 (Table 6). 2010 was the second lowest burn year, after 2001. The majority of the burn is north of Lake Kyoga, with patches in the west central region, upper northeast, and the east central region (Figure 24-27).

The size of the each fire ranges from as small as 0.0018 km^2 up to 120.94 km^2 (Table 7-8.) A two pixel size fire was the threshold set to cancel out possible noise in the data, thus a fire smaller than 0.0018 km^2, two pixels, was not used to determine the averaged burn size of the new burn class and of the old burn class for each fire year. The year with the largest average burn size for both new burn and old burn classes was 1995. The largest single fire for both new burn and old burn classes was in 1995. The year with the smallest average burn size for the new burn and old burn classes was 2010.

Spatial trends in burned areas occur in the northern portion of the Landsat scene, and more specifically, in the northeast quadrant in all five scenes. The largest burn in 1995 is clustered in the northeast portion of the scene with some areas in the west central region. 2001 had the lowest area burned of all five scenes and had a similar geographical pattern of burned area as the rest of the images. The 2001 image is the first date that shows a more profound area burned in the central west region, and this area continues to show burning in 2003 and 2010. 2003 is the first year that the northwest quadrant had a larger total area burned than the northeast quadrant, but the northwest tends to contain the most total km^2 of area burned for all five years, with little to no burned area in the southern portion of the scenes (Table 9).

The frequency of fires can be seen in Figure 28. If no burning was classified in all five scenes a value of zero was given, if the pixel had only burned once during all five years it was given the value of 1. The most a single pixel and/or area can burn is five times, one per scene. Area burned and the frequency of the burn for each quadrant, northwest, northeast, southwest, and southeast, can been seen in Figures 29-32. Table 10-14 show the area burned for each frequency. The total of area burned that had only burned once for all five scenes was 3,533.7 km^2. The total area burned decreased by an order of magnitude for each number of times burned.

The March through February monthly z-score for precipitation rates from 1988 to 2010 showed expected variation, with wet years occurring during 1988-1989, 1994-1995, and 2009-2010, whereas 2000-2001 and 2002-2003 years were dry. The most negative z-score for precipitation rate occurred during the non-imaged period of 1993-1994 (Figure 33).

March through February's monthly z-score for soil moisture from 1988 to 2010 showed year to year variation. Wetter than average years occurred in 1988-1989, 1994-1995, and 2009-2010, whereas 2000-2001 and 2002-2003 years were drier than average years. Similar trends can be seen between soil moisture and precipitation rates, with negative values occurring during the same years for both climate variables; 1993-1994 had the most negative z-score value for both soil moisture and precipitation rate (Figure 34).

The monthly z-scores for surface temperature were compared in two different time periods, March through February and October through February. March through February, the Landsat scenes aligned with cooler temperatures occurring in 1988-1989 and 1994-1995, while 2000-2001 was the warmest year, and 2002-2003 and 2009-2010 were warmer than average, but not as hot as 2000-2001 (Figure 35). In October through February, 1988-1989, 1994-1995, 2000-2001, 2009-2010 were cool years, and 2002-2003 was a warmer than average year (Figure 36).

Climate variables z-scores, temperature, soil moisture, precipitation rate from October to February, one year average precipitation rate (March to February), two year average precipitation rate, were compared with one another and with the total area burned for the years 1989, 1995, 2001, 2003, and 2010 (Figure 37-41). The coolest and wettest years occurred during 1988-1989, but did not have the lowest area burned for all five years examined. 2000-2001 saw the least area burned and had cool temperatures, slightly positive October through February precipitation rate z-scores, and negative z-scores for one and two year precipitation rates. The year with the most total burn area was 1994-1995, yet was cool and wet.

The population within the study area from 1990 to 2010 has been increasing at an accelerating rate as seen in Table 15. Beginning in 1990 the total population for the study area was 209,507 people, and in 2010 the population had risen to 412,770, a rate of 50.76%. Population data were divided into four quadrants: northwest (NW), northeast (NE), southwest (SW), and southeast (SE). All of the quadrants increased in total population at an increasing rate over the twenty years of data (Table 16-19). Figures 42-46 show the spatial variation in population densities. The NE had the largest population increase; from 2005 to 2010 there was a 25% increase in the population and it ended with the second highest population of all quadrants. The SW had the lowest percent change in the study area during all time periods with a range from 10-14% change. The SE had the exact same percent change in population as the NW, but the SE has the largest total population out of the entire study region. The SE is more urbanized, and contains larger towns and/or cities.

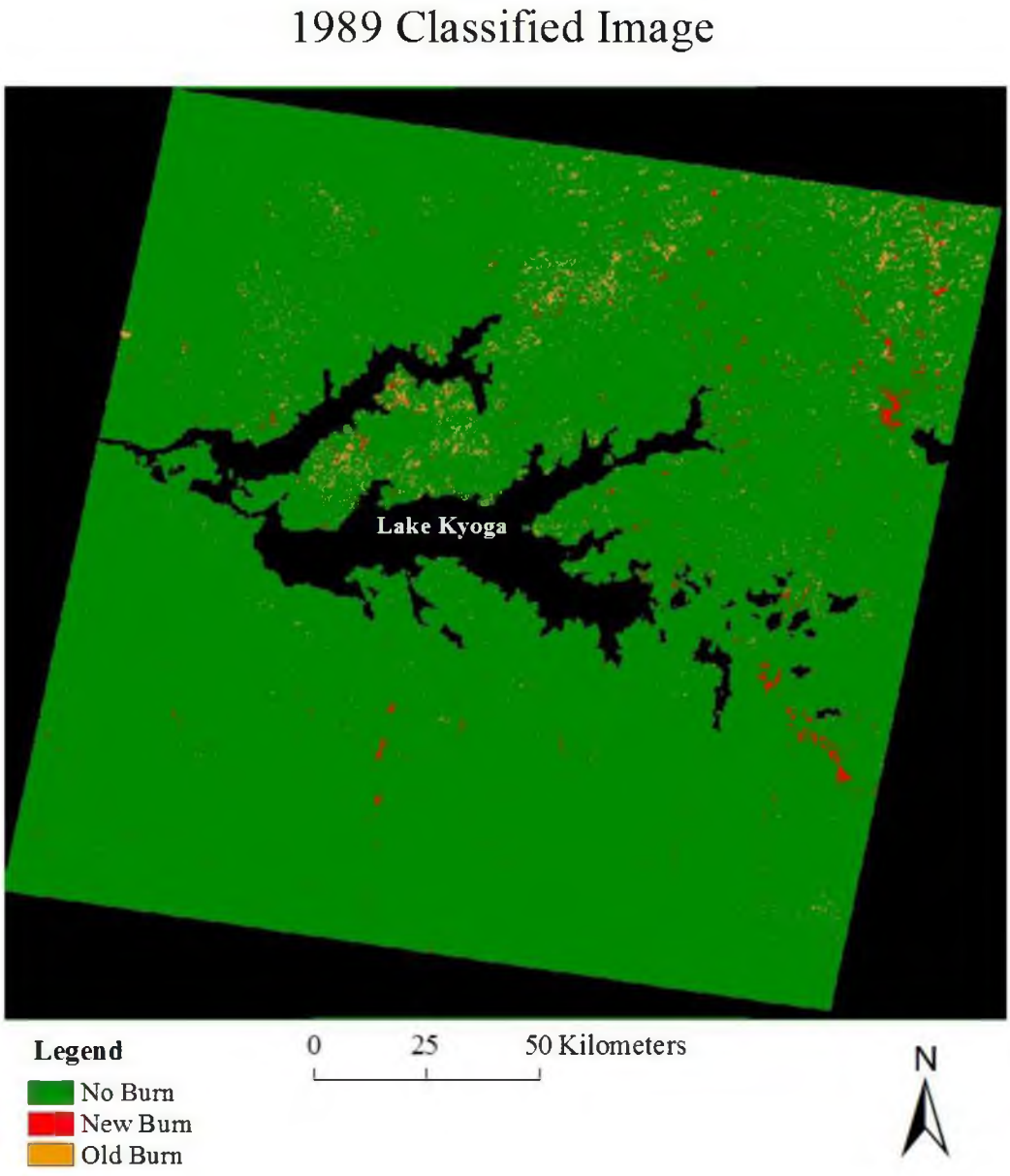

Figure 3. 1989 classified image of the study area within Uganda, containing the three decision tree classes: no burn, new burn, and old burn.

Table 2. Confusion Matrix for 1989 comparing the accuracy ROIs to the classified image ROIs.

Image Class 1989	New Burn ROI	No Burn ROI	Old Burn ROI	Total
New Burn	52	2	1	55
No Burn	8	307	2	317
Old Burn	0	0	98	98
Total	60	309	101	470

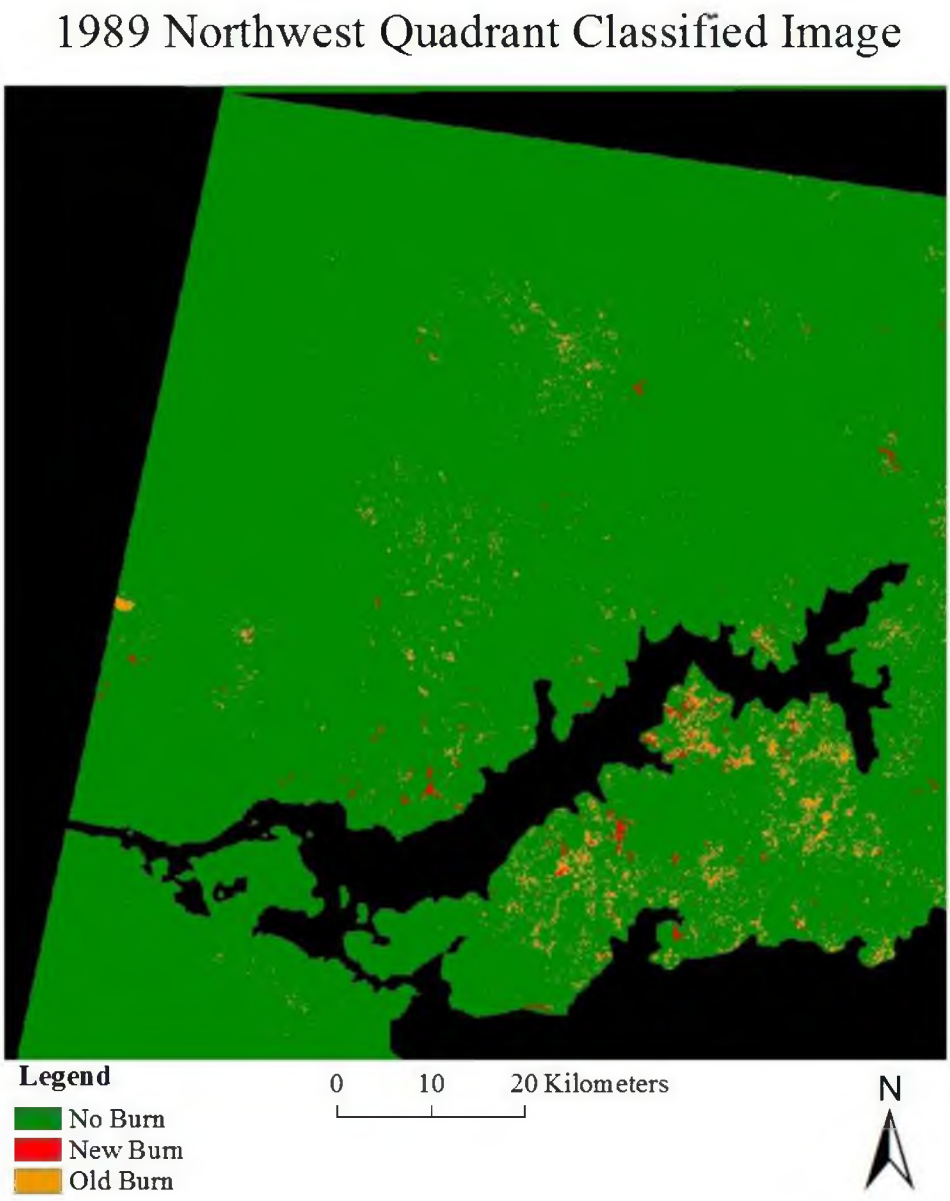

Figure 4. 1989 Northwest quadrant classified image within the study area of Uganda, containing the three decision tree classes: no burn, new burn, and old burn.

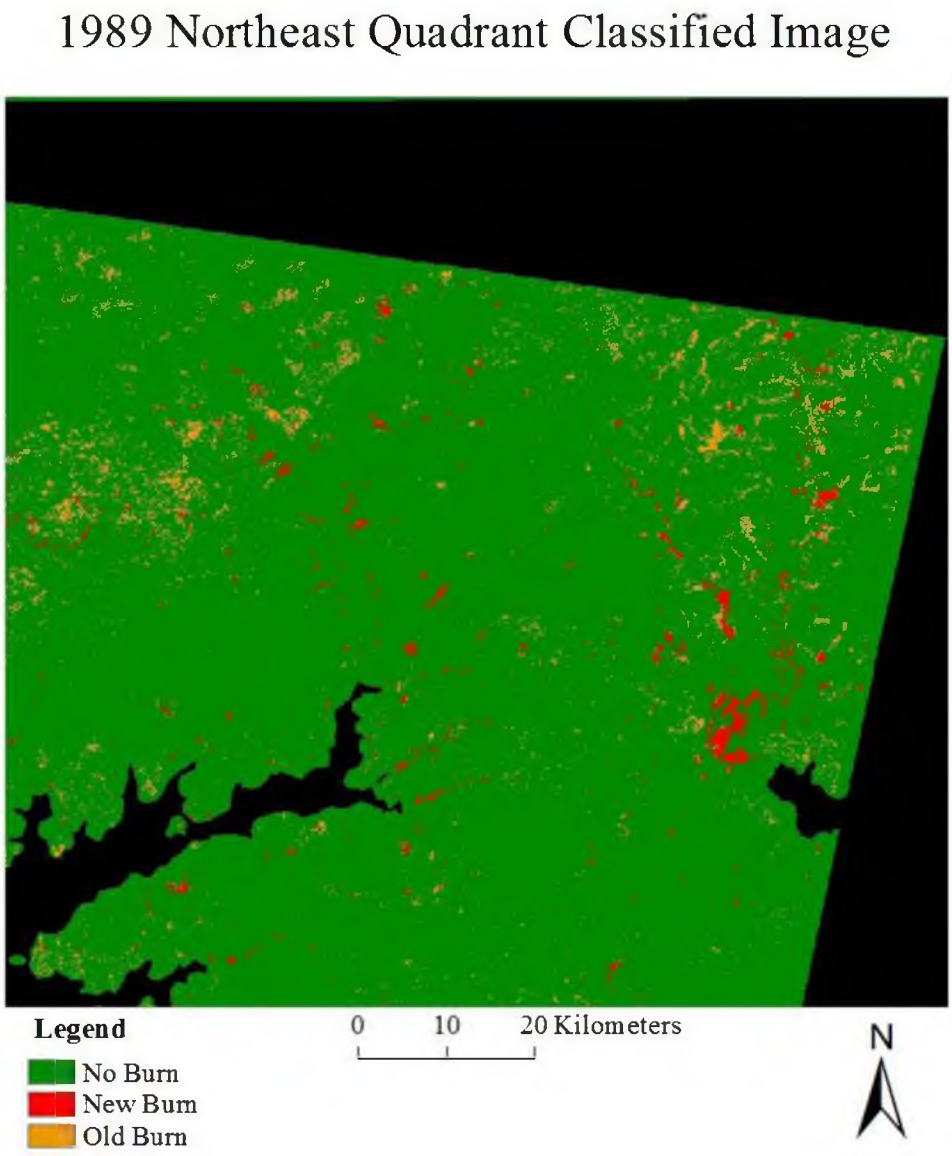

Figure 5. 1989 Northeast quadrant classified image within the study area of Uganda, containing the three decision tree classes: no burn, new burn, and old burn.

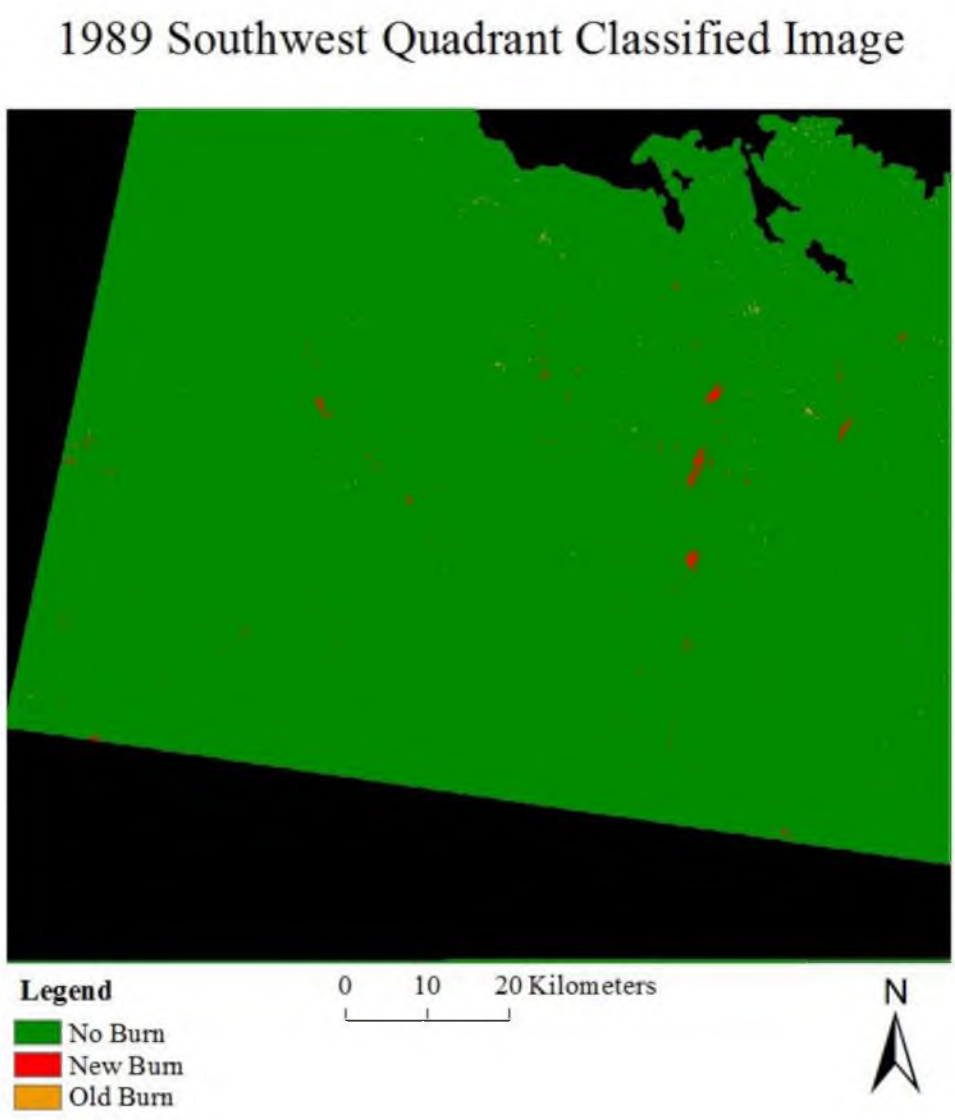

Figure 6. 1989 Southwest quadrant classified image within the study area of Uganda, containing the three decision tree classes: no burn, new burn, and old burn.

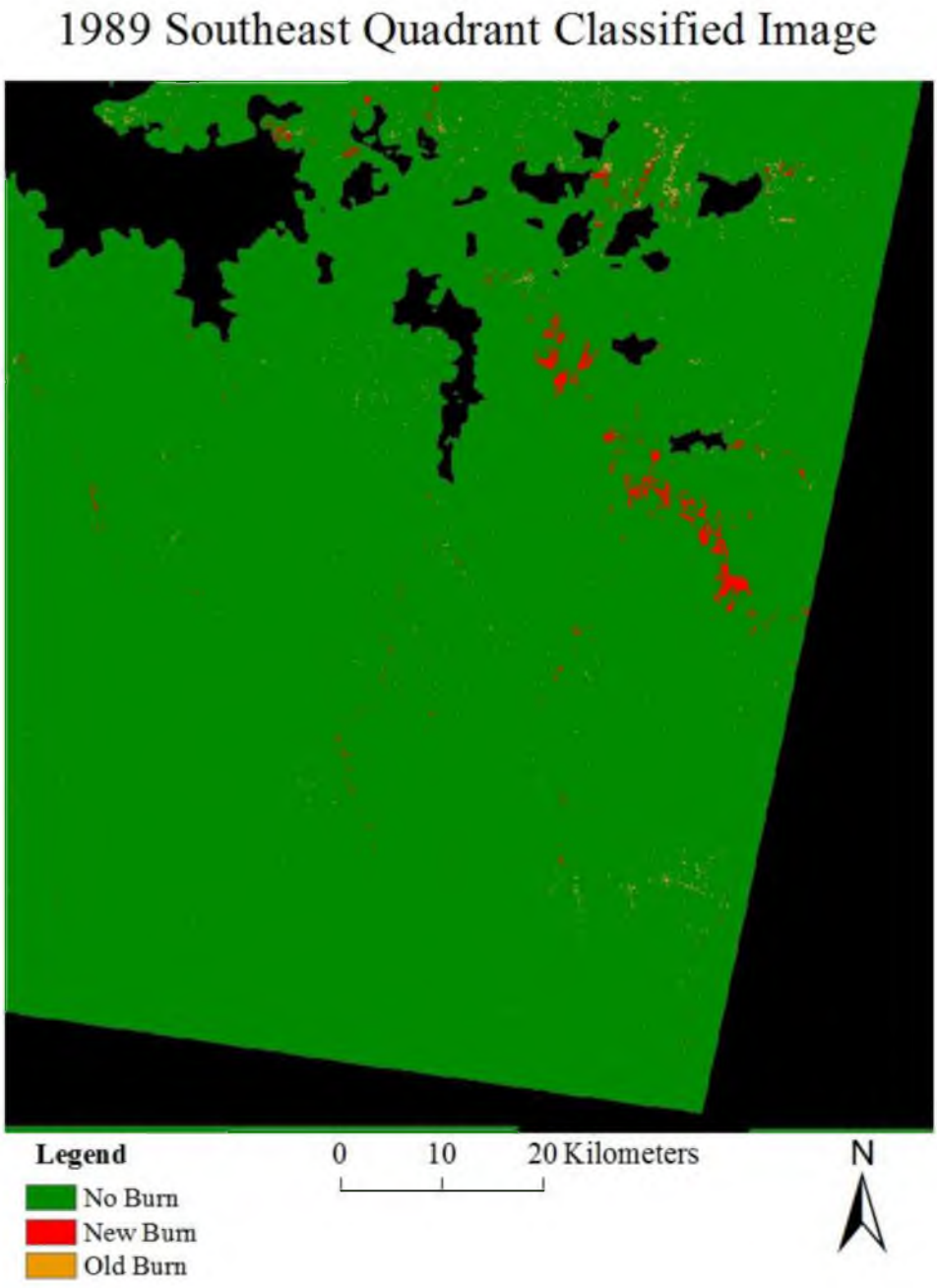

Figure 7. 1989 Southeast quadrant classified image within the study area of Uganda, containing the three decision tree classes: no burn, new burn, and old burn.

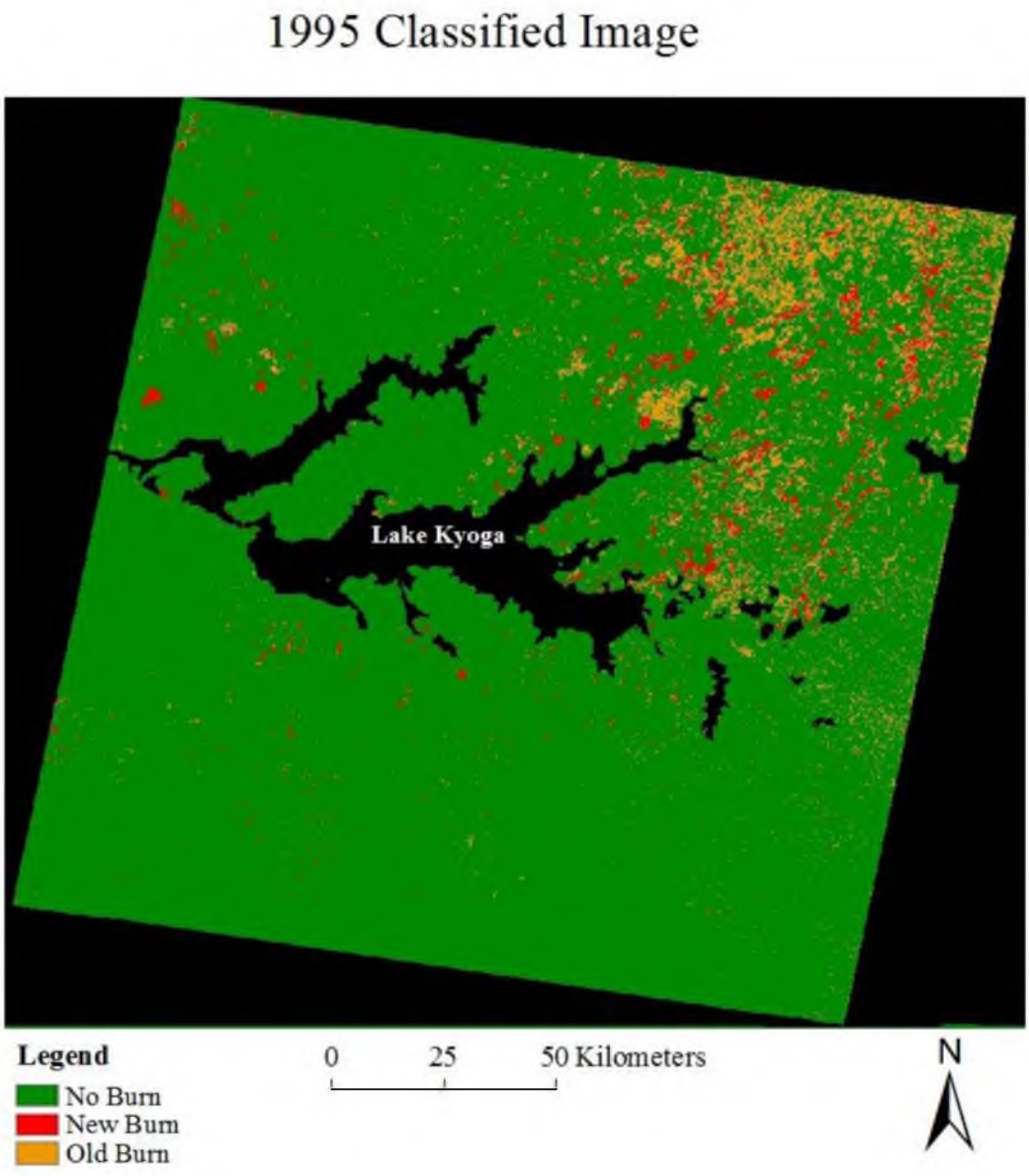

Figure 8. 1995 classified image of the study area within Uganda, containing the three decision tree classes: no burn, new burn, and old burn.

Table 3. Confusion Matrix for 1995 comparing the accuracy ROIs to the classified image ROIs.

Image Class 1995	New Burn ROI	No Burn ROI	Old Burn ROI	Total
New Burn	208	0	0	208
No Burn	0	330	2	332
Old Burn	0	0	109	109
Total	208	330	111	649

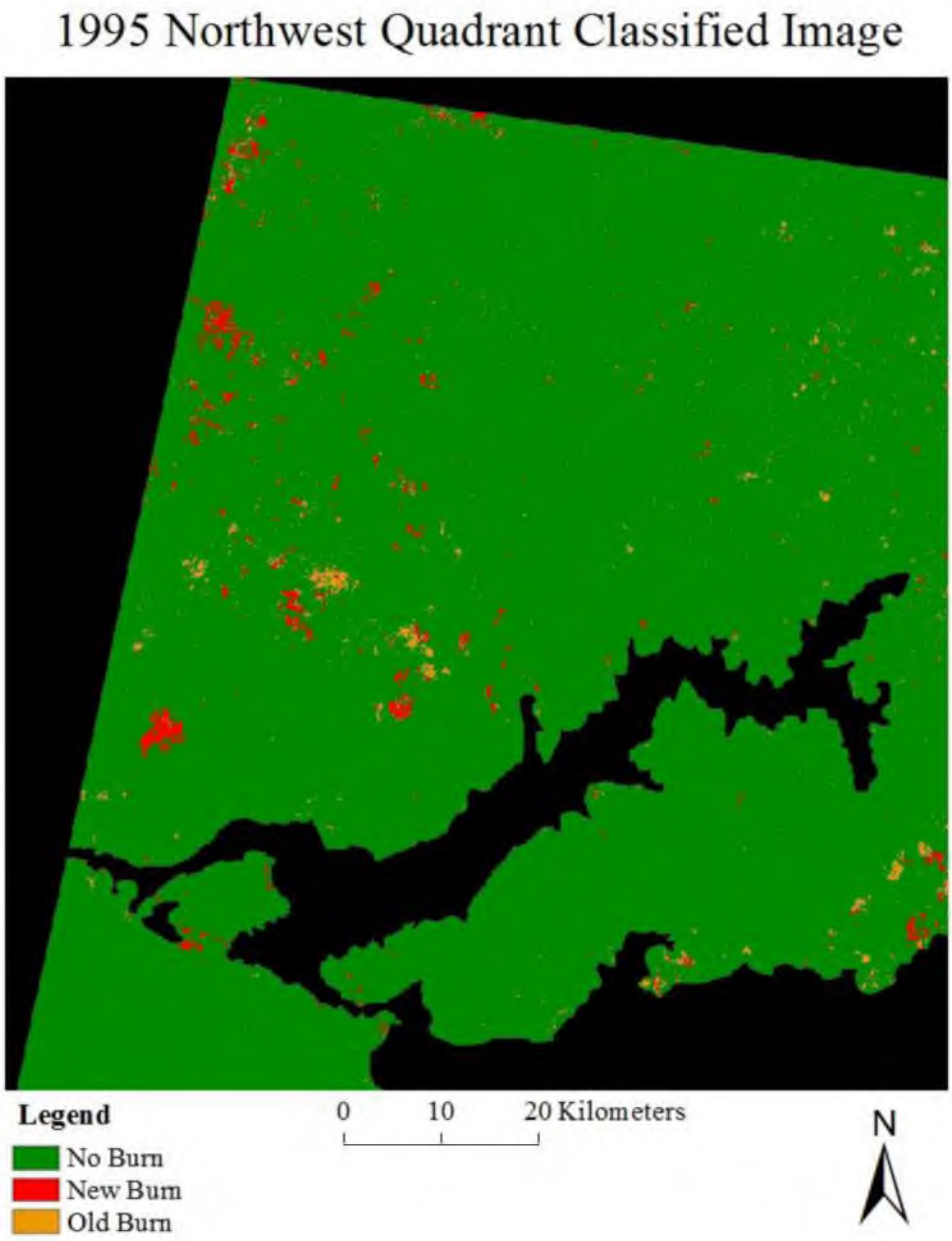

Figure 9. 1995 Northwest quadrant classified image within the study area of Uganda, containing the three decision tree classes: no burn, new burn, and old burn.

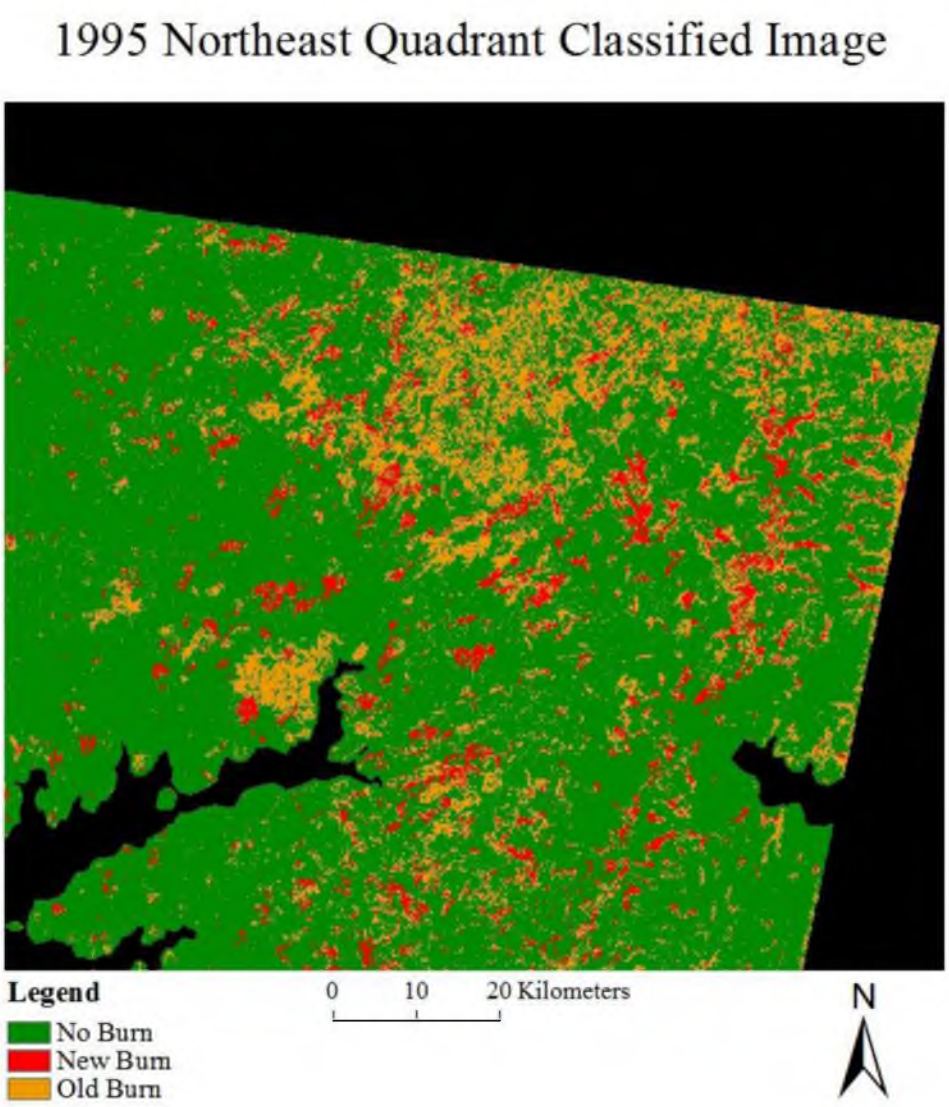

Figure 10. 1995 Northeast quadrant classified image within the study area of Uganda, containing the three decision tree classes: no burn, new burn, and old burn.

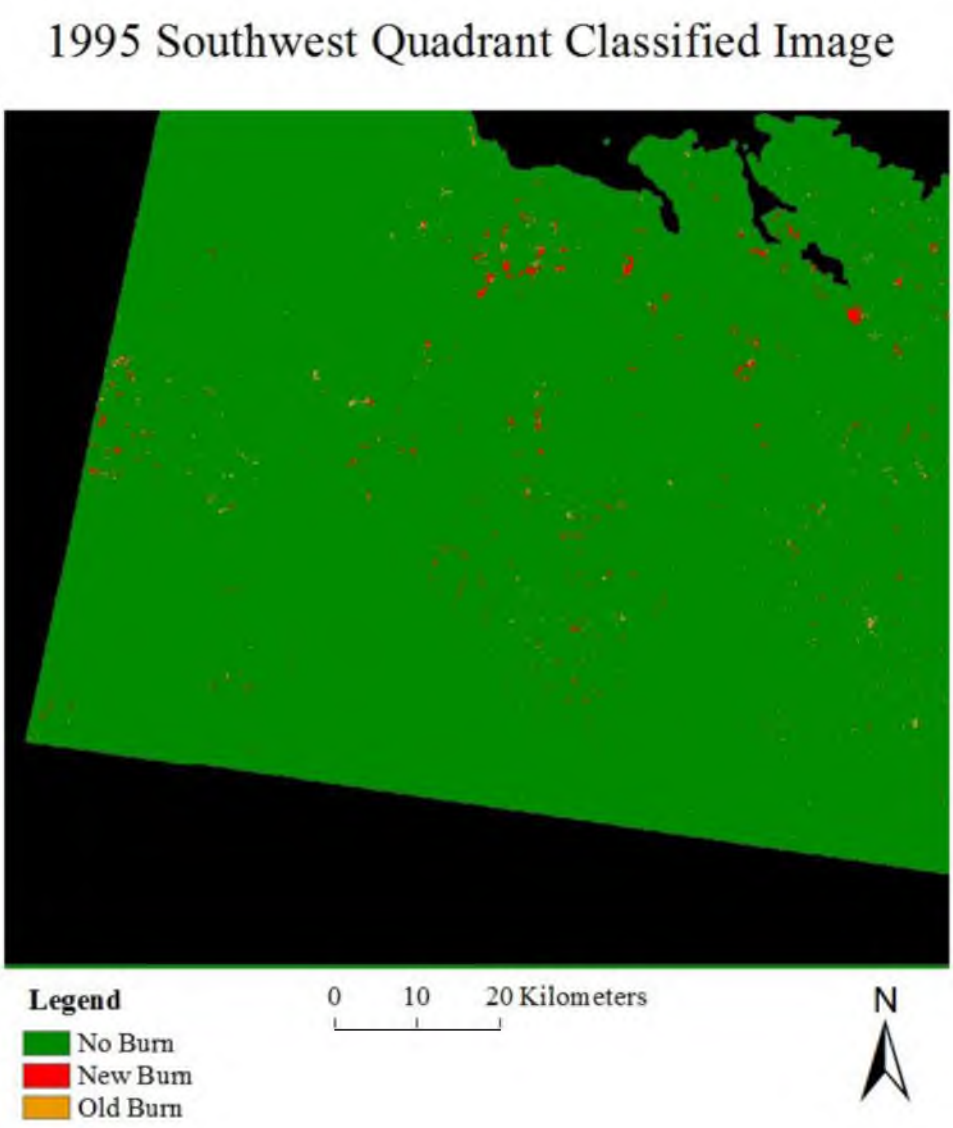

Figure 11. 1995 Southwest quadrant classified image within the study area of Uganda, containing the three decision tree classes: no burn, new burn, and old burn.

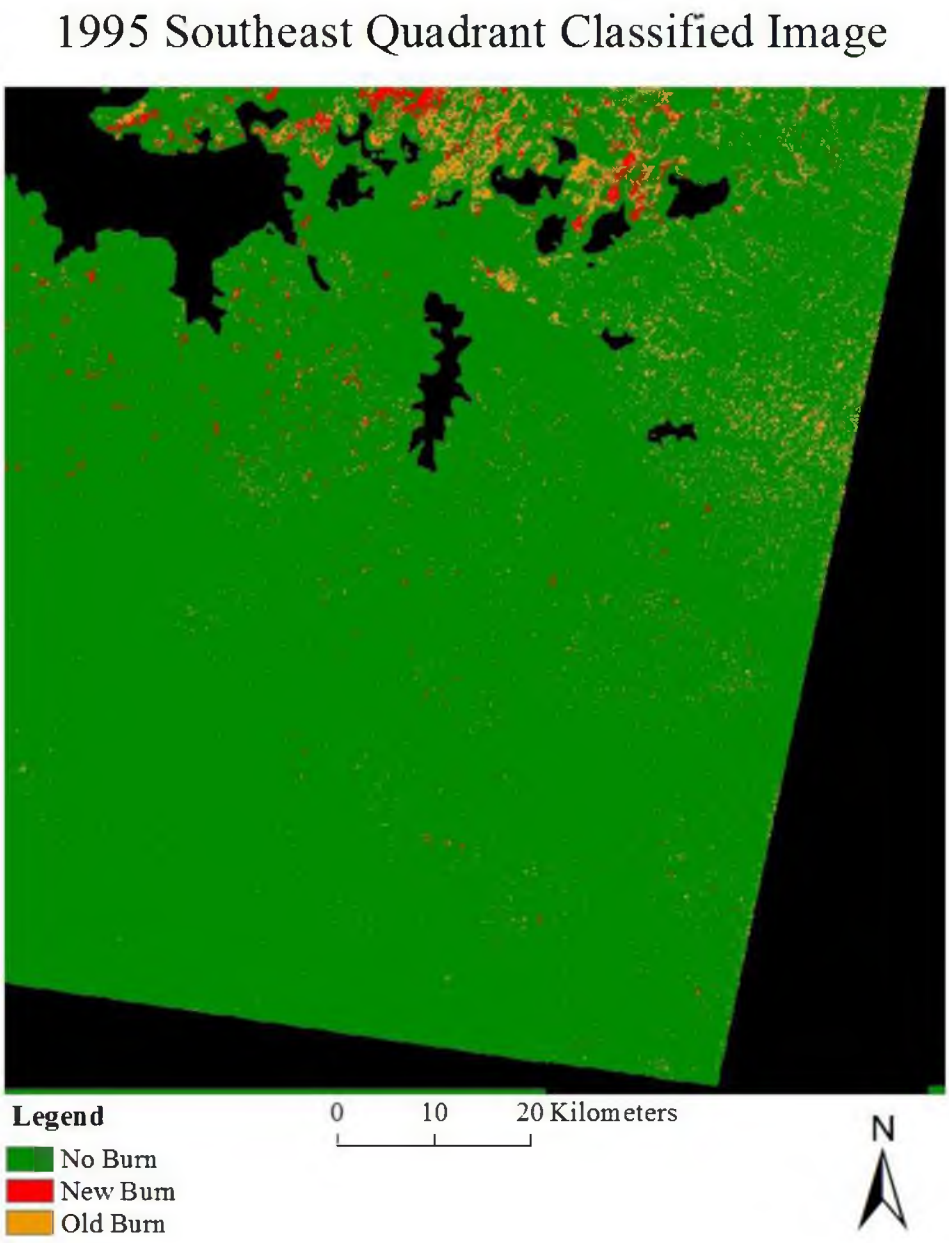

Figure 12. 1995 Southeast quadrant classified image within the study area of Uganda, containing the three decision tree classes: no burn, new burn, and old burn.

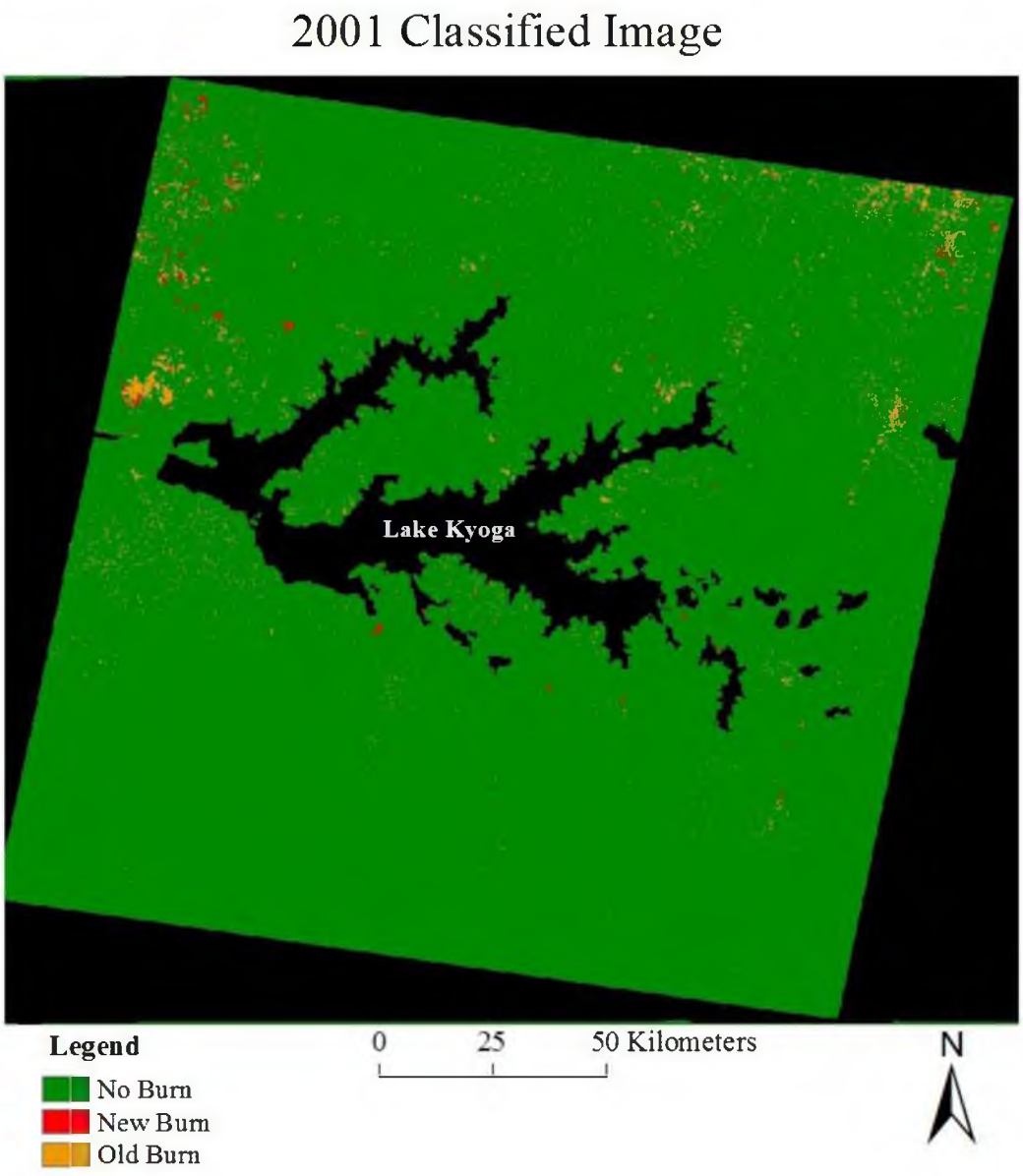

Figure 13. 2001 classified image of the study area within Uganda, containing the three decision tree classes: no burn, new burn, and old burn.

Table 4. Confusion Matrix for 2001 comparing the accuracy ROIs to the classified image ROIs.

Image Class 2001	New Burn ROI	No Burn ROI	Old Burn ROI	Total
New Burn	122	0	1	123
No Burn	1	269	3	273
Old Burn	0	0	92	92
Total	123	269	96	488

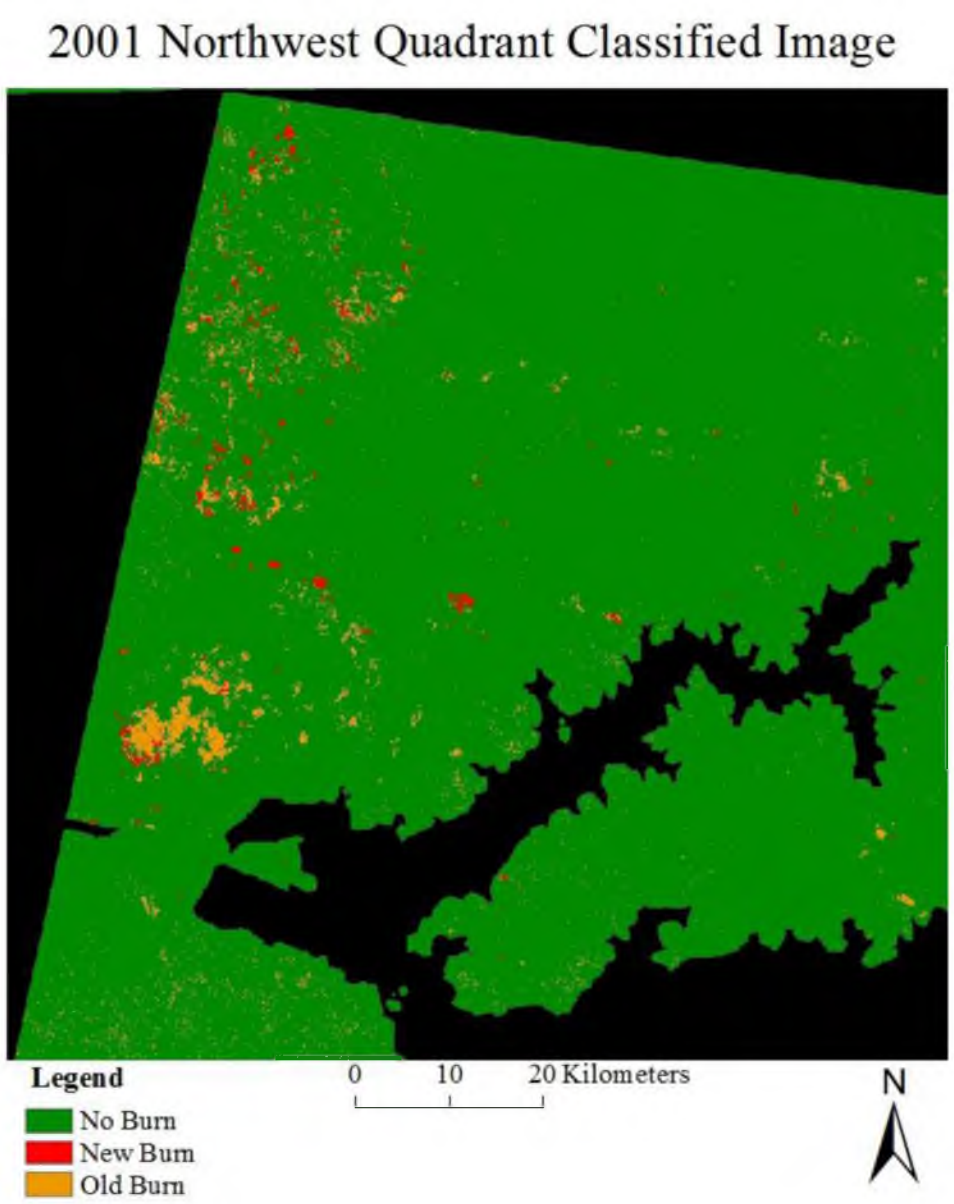

Figure 14. 2001 Northwest quadrant classified image within the study area of Uganda, containing the three decision tree classes: no burn, new burn, and old burn.

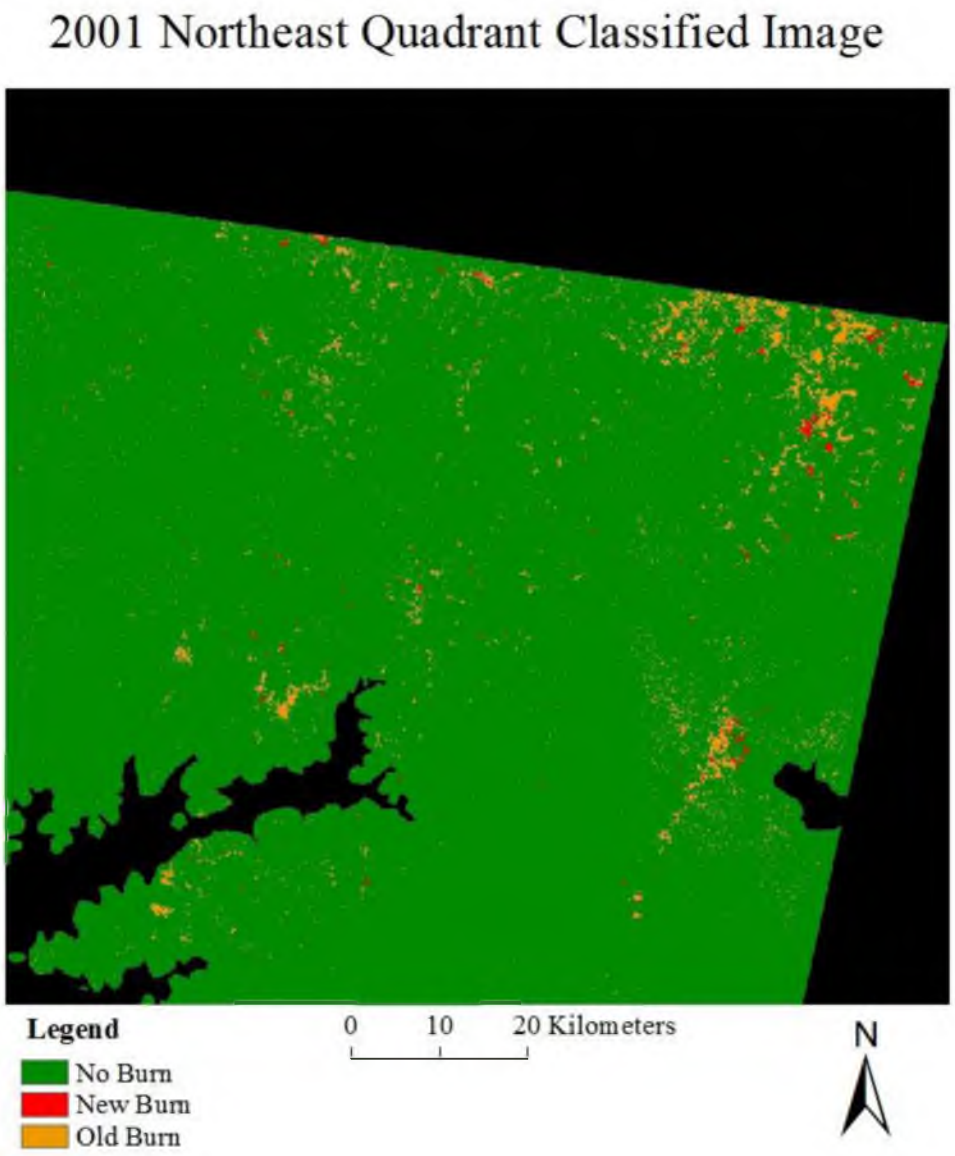

Figure 15. 2001 Northeast quadrant classified image within the study area of Uganda, containing the three decision tree classes: no burn, new burn, and old burn.

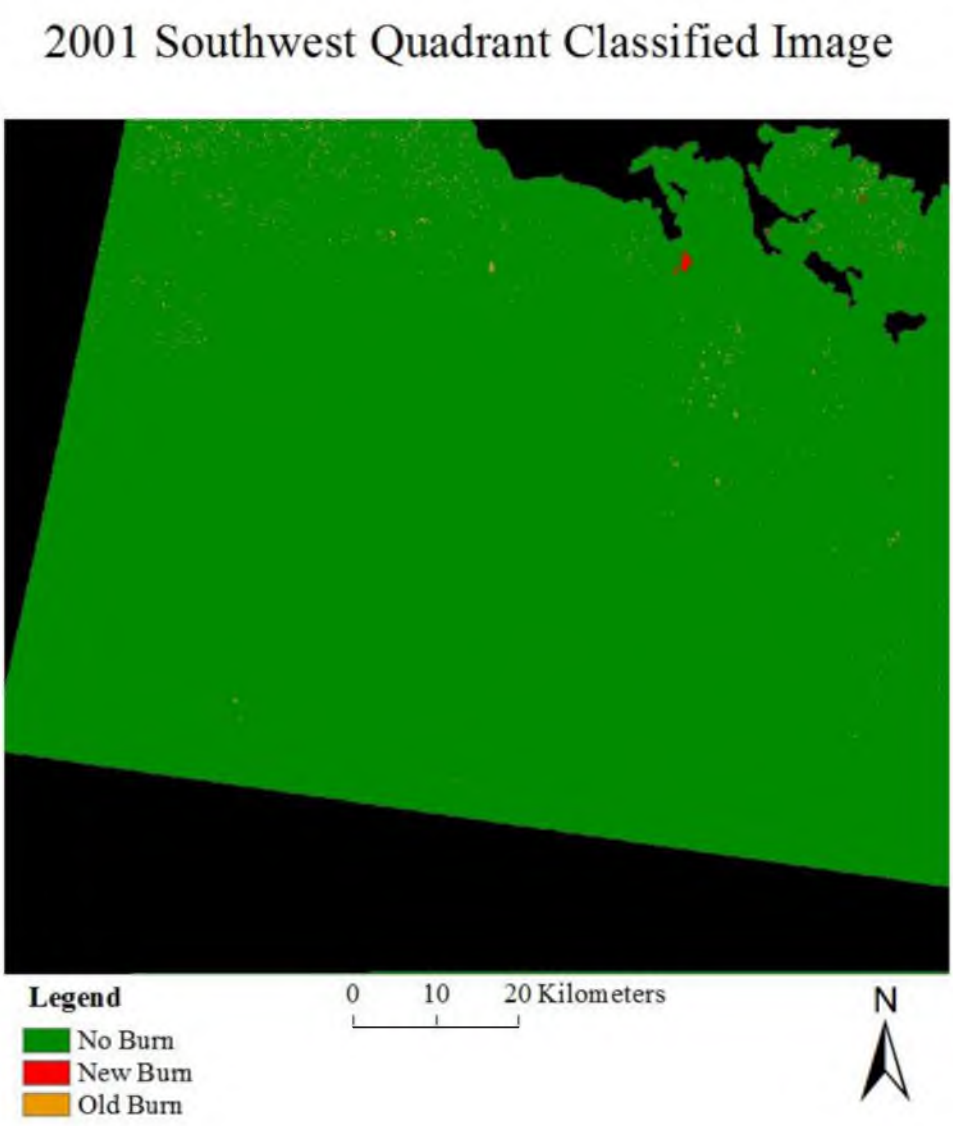

Figure 16. 2001 Southwest quadrant classified image within the study area of Uganda, containing the three decision tree classes: no burn, new burn, and old burn.

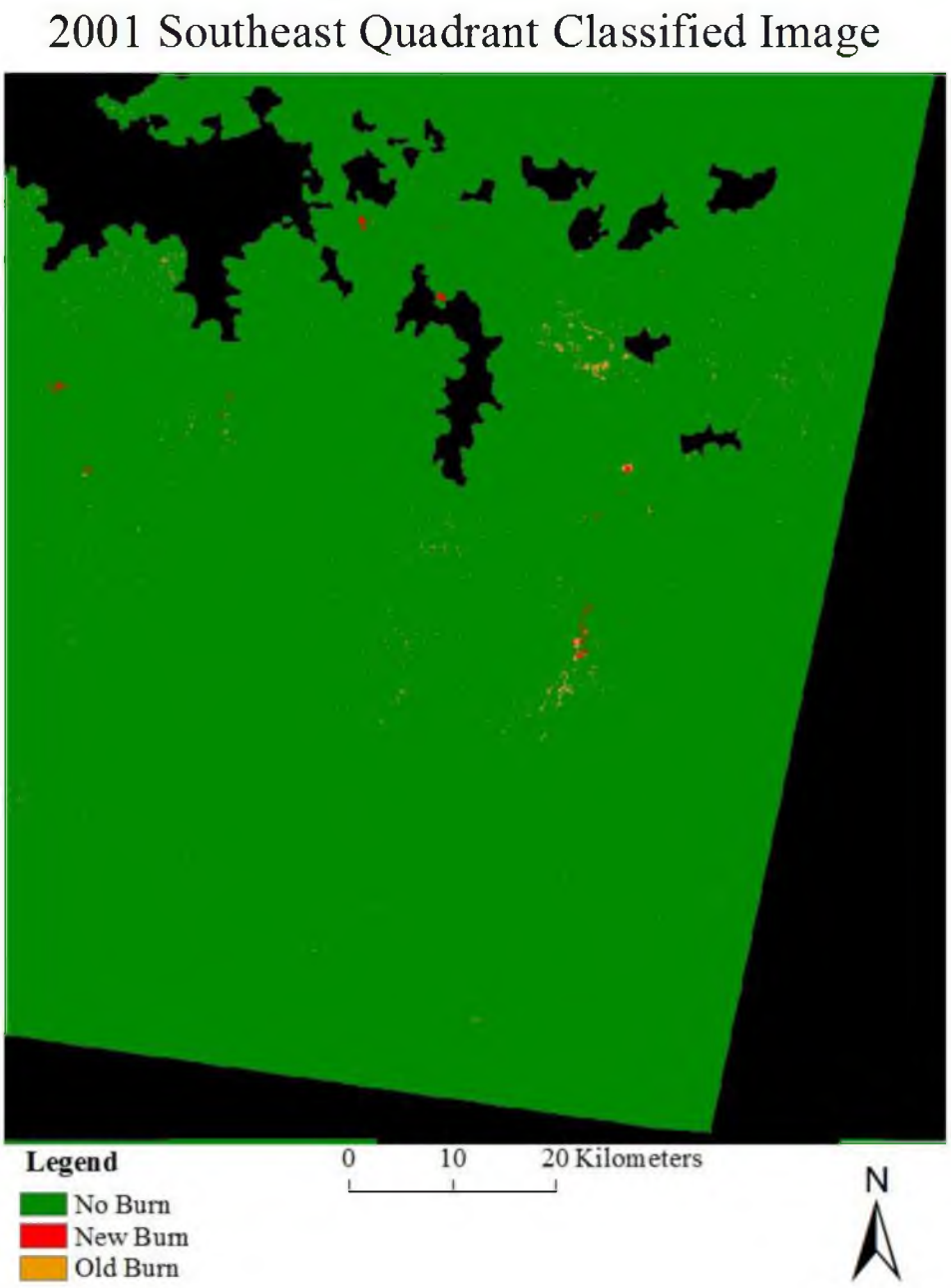

Figure 17. 2001 Southeast quadrant classified image within the study area of Uganda, containing the three decision tree classes: no burn, new burn, and old burn.

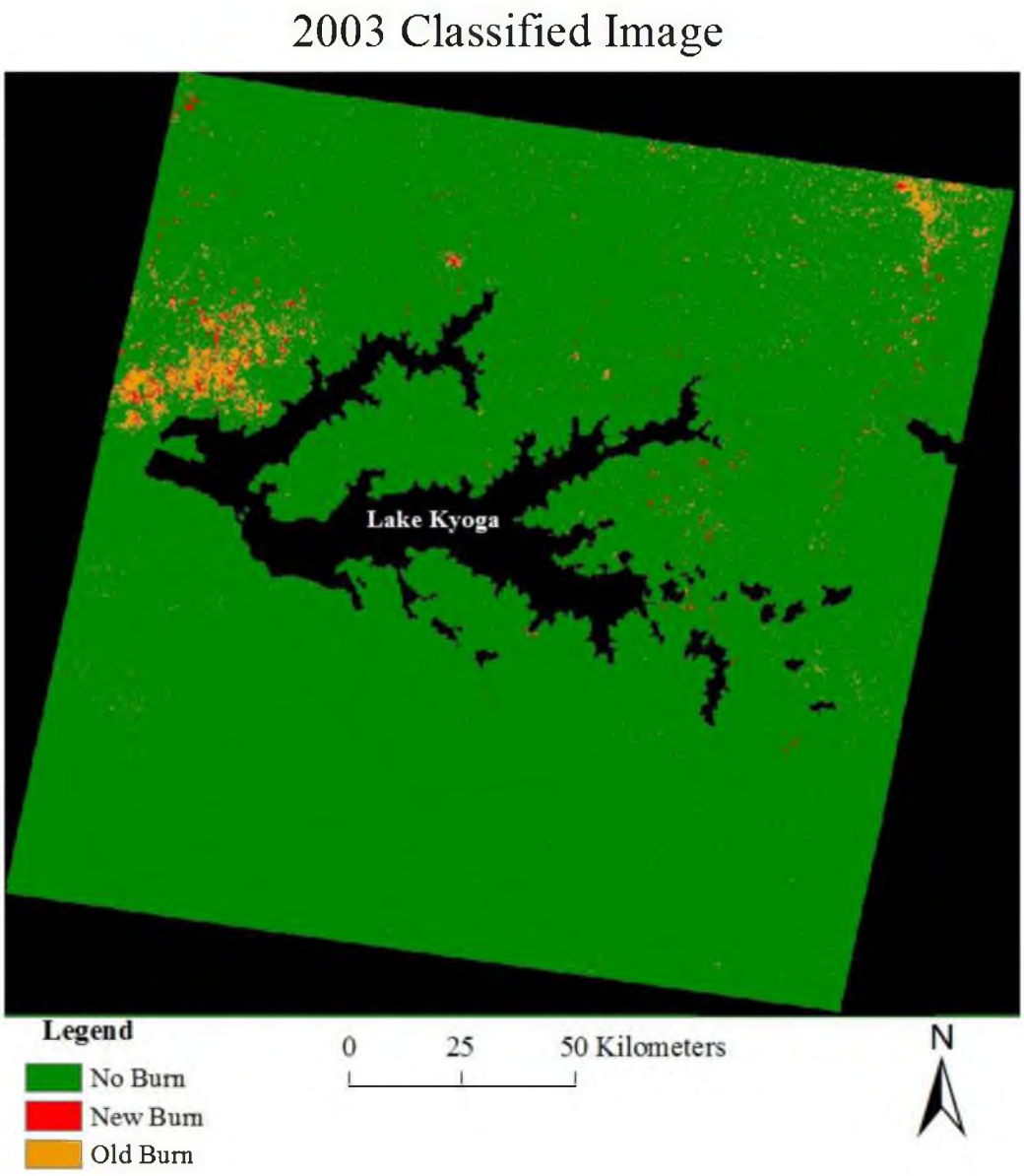

Figure 18. 2003 classified image of the study area within Uganda, containing the three decision tree classes: no burn, new burn, and old burn.

Table 5. Confusion Matrix for 2003 comparing the accuracy ROIs to the classified image ROIs.

Image Class 2003	New Burn ROI	No Burn ROI	Old Burn ROI	Total
New Burn	120	4	0	124
No Burn	0	1456	0	1456
Old Burn	0	6	112	118
Total	120	1466	112	1698

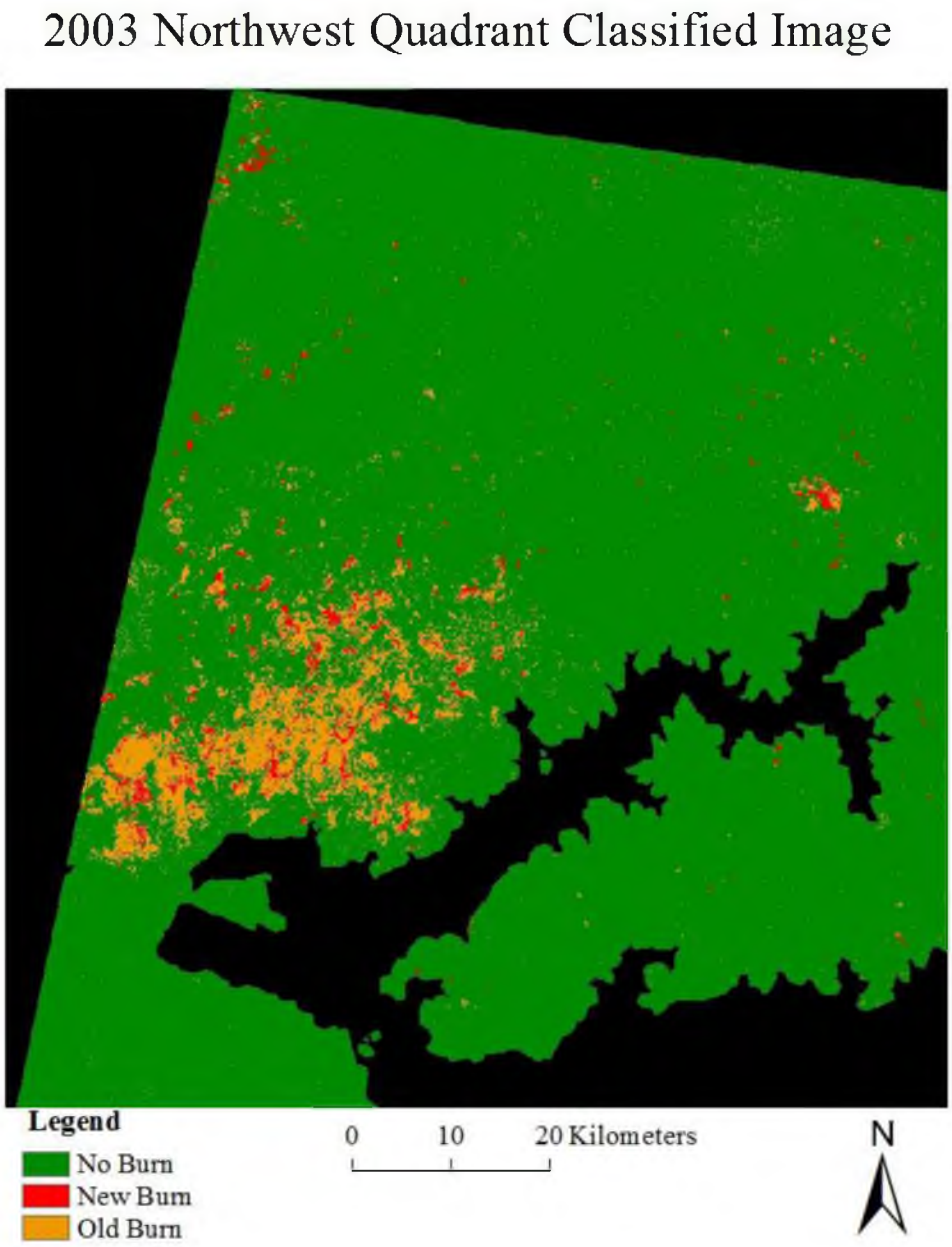

Figure 19. 2003 Northwest quadrant classified image within the study area of Uganda, containing the three decision tree classes: no burn, new burn, and old burn.

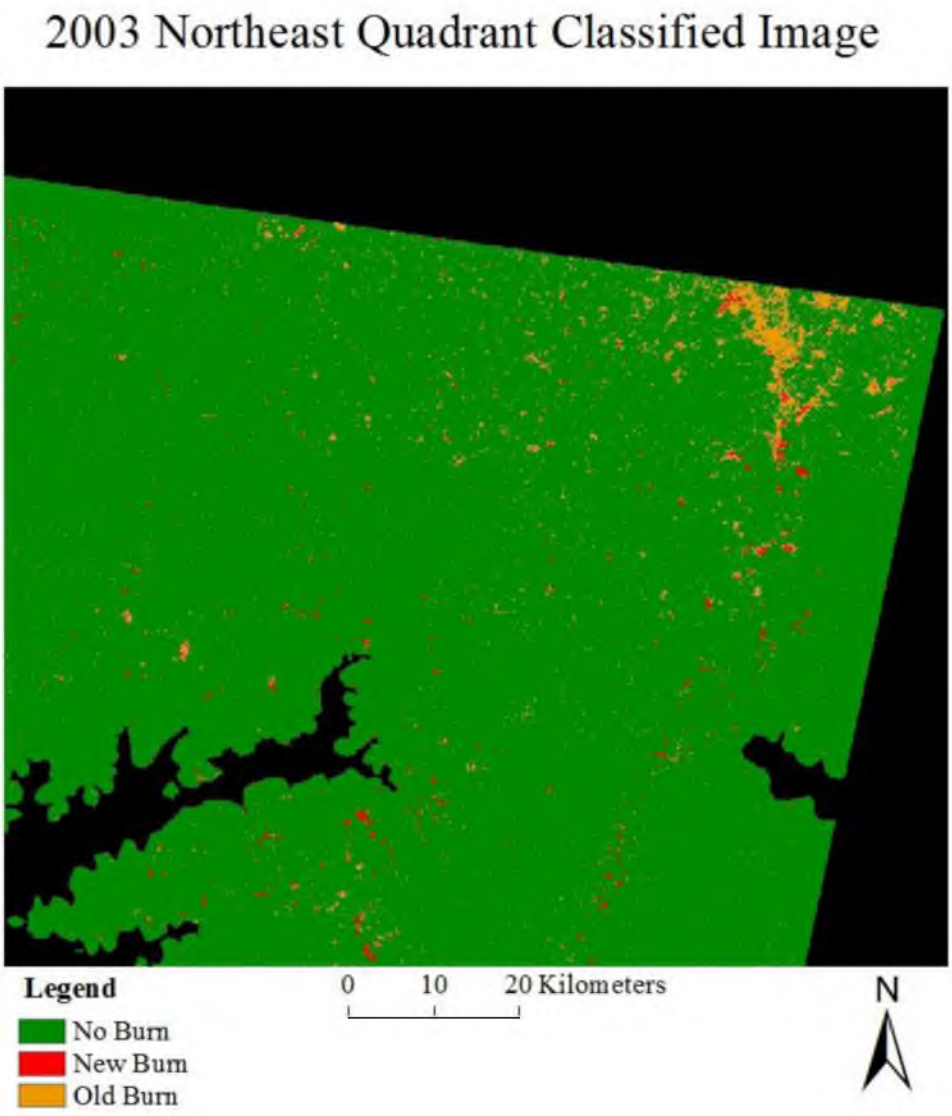

Figure 20. 2003 Northeast quadrant classified image within the study area of Uganda, containing the three decision tree classes: no burn, new burn, and old burn.

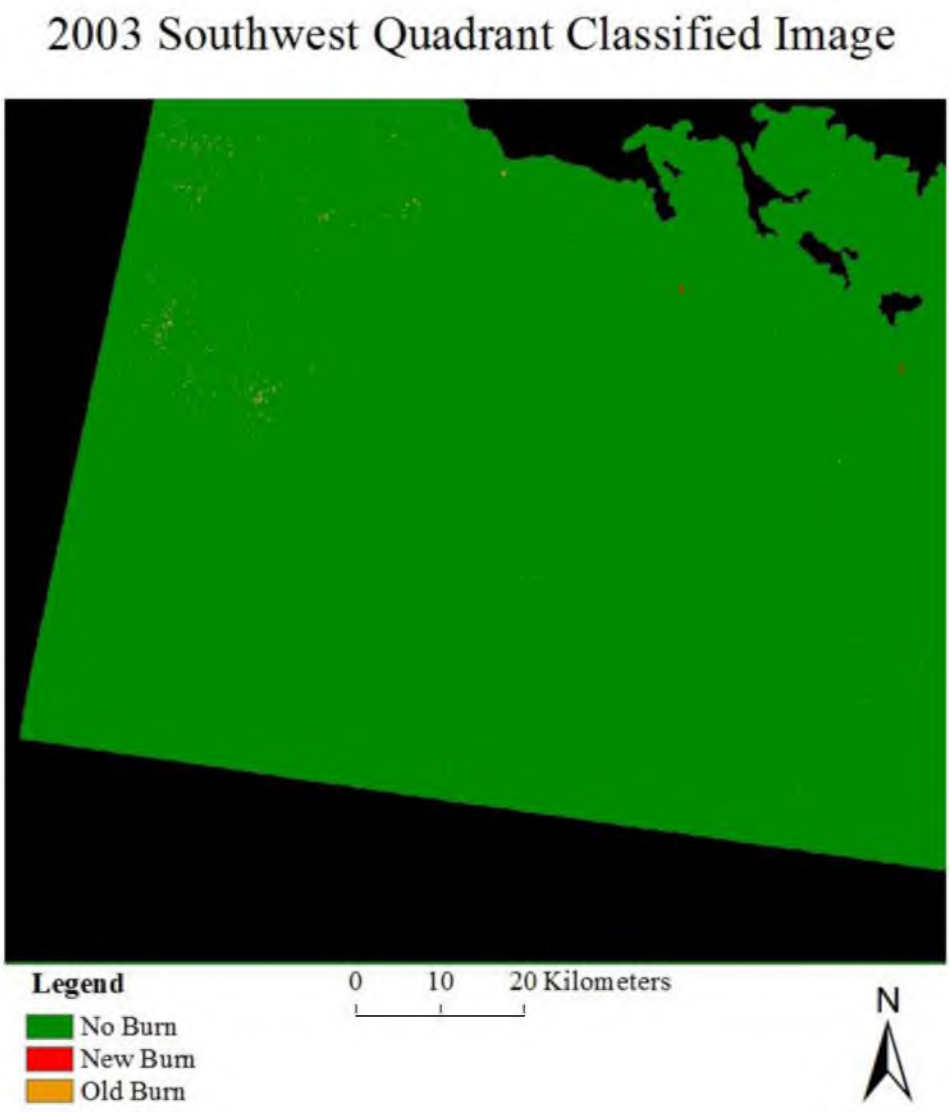

Figure 21. 2003 Southwest quadrant classified image within the study area of Uganda, containing the three decision tree classes: no burn, new burn, and old burn.

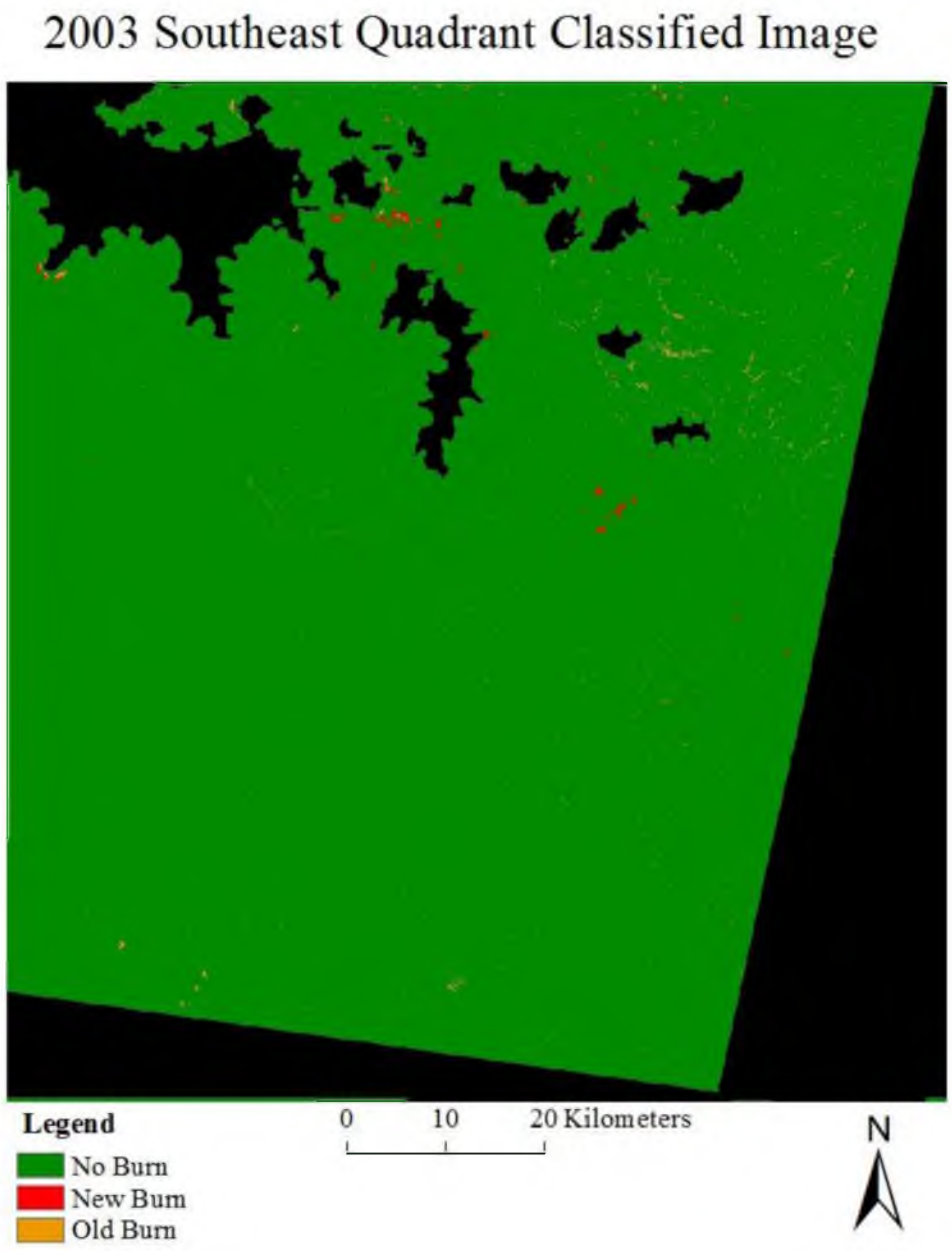

Figure 22. 2003 Southeast quadrant classified image within the study area of Uganda, containing the three decision tree classes: no burn, new burn, and old burn.

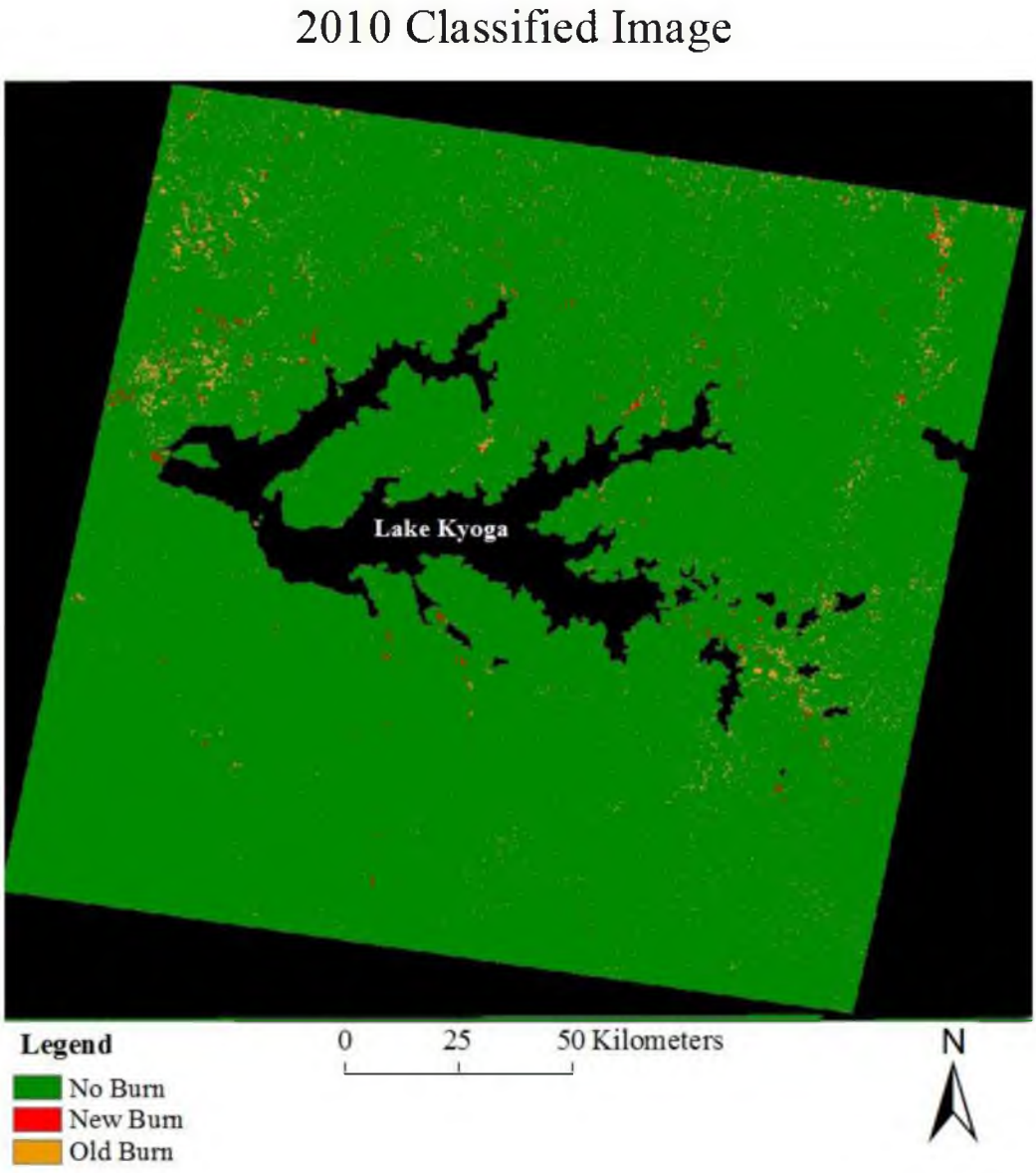

Figure 23. 2010 classified image of the study area within Uganda, containing the three decision tree classes: no burn, new burn, and old burn.

Table 6. Confusion Matrix for 2010 comparing the accuracy ROIs to the classified image ROIs.

Image Class 2010	New Burn ROI	No Burn ROI	Old Burn ROI	Total
New Burn	101	0	0	101
No Burn	0	225	0	225
Old Burn	2	4	120	126
Total	103	229	120	452

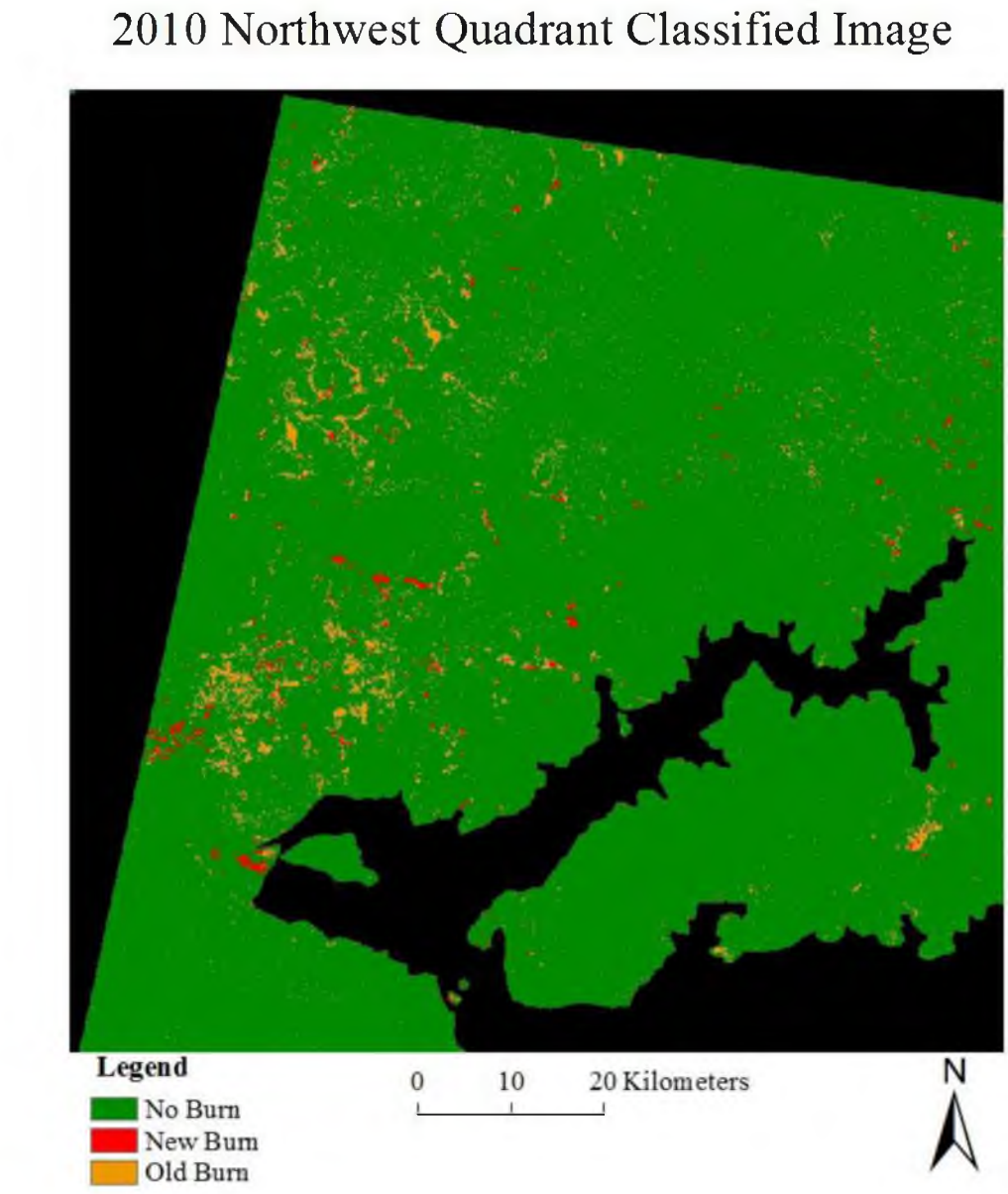

Figure 24. 2010 Northwest quadrant classified image within the study area of Uganda, containing the three decision tree classes: no burn, new burn, and old burn.

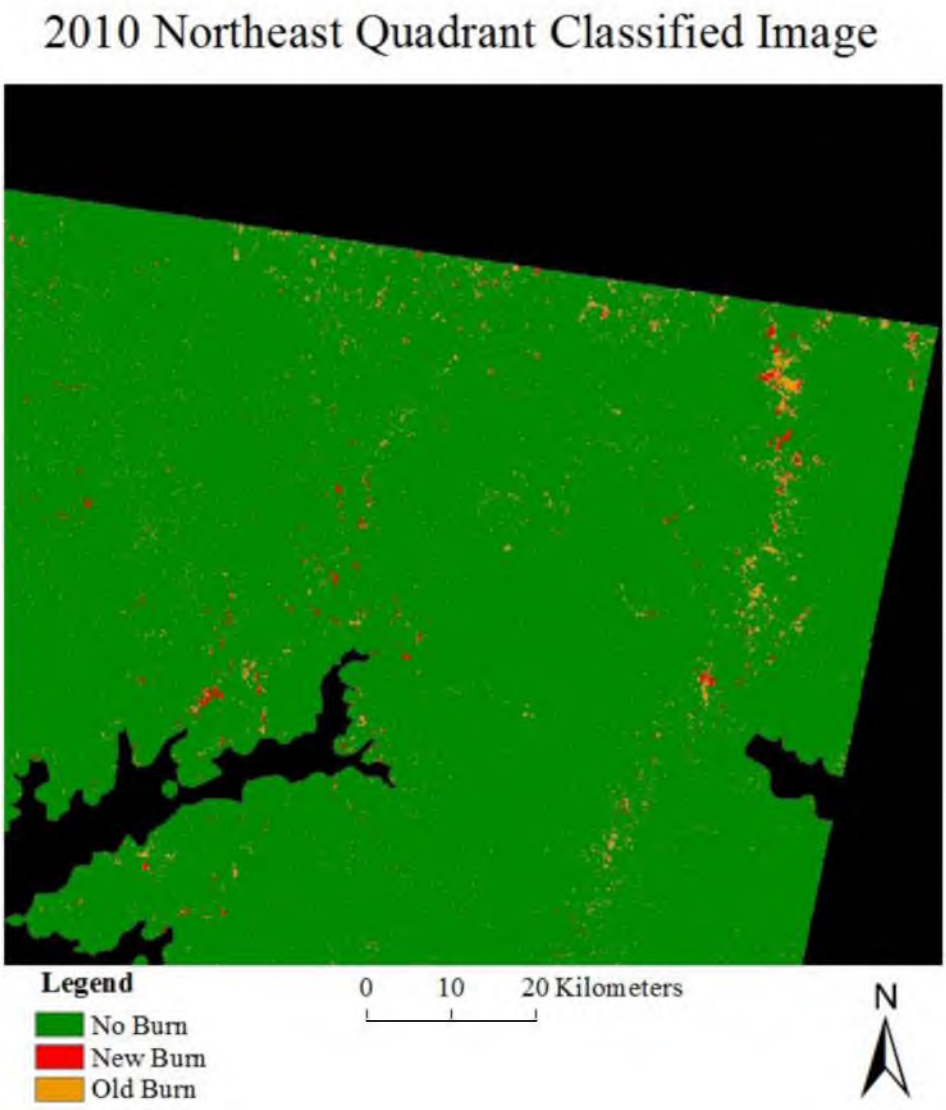

Figure 25. 2010 Northeast quadrant classified image within the study area of Uganda, containing the three decision tree classes: no burn, new burn, and old burn.

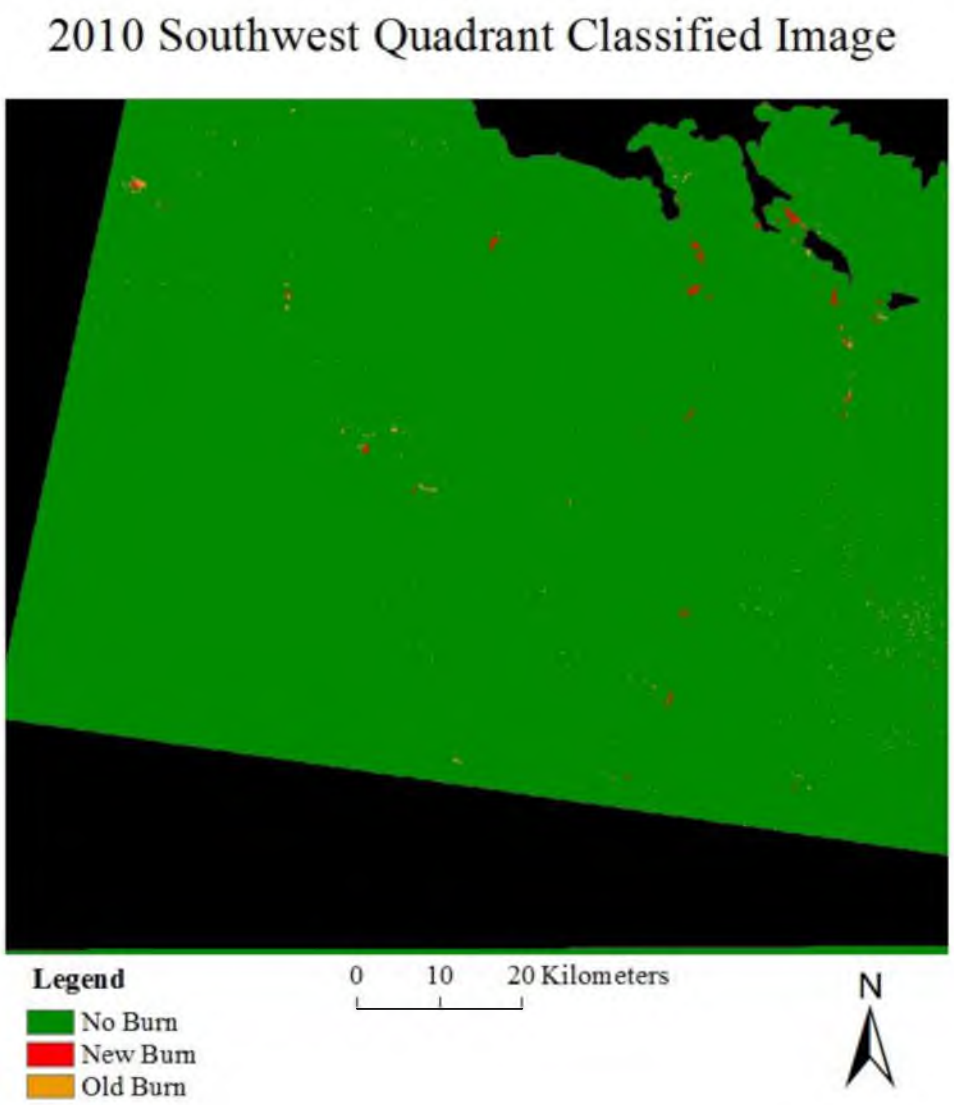

Figure 26. 2010 Southwest quadrant classified image within the study area of Uganda, containing the three decision tree classes: no burn, new burn, and old burn.

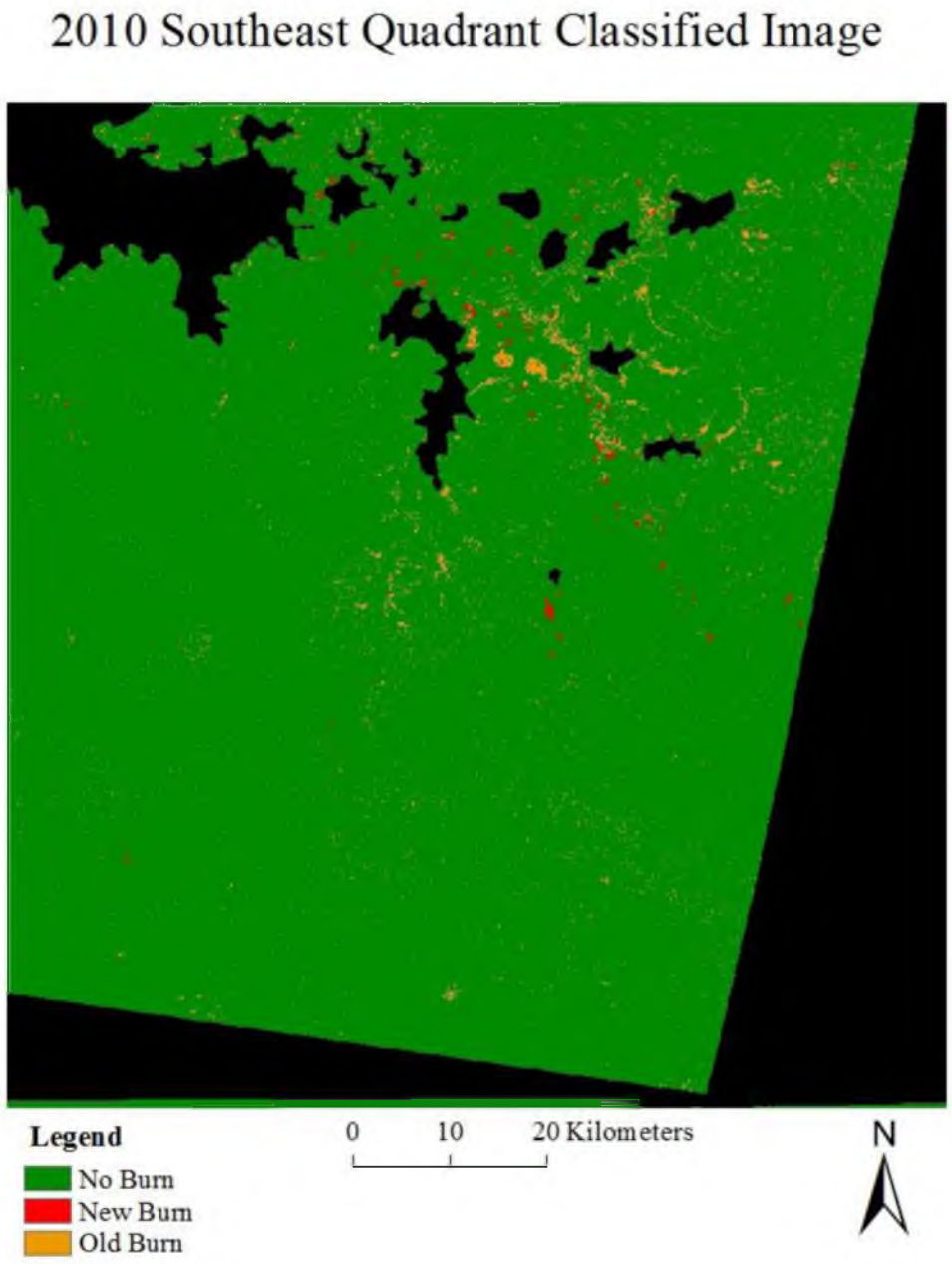

Figure 27. 2010 Southeast quadrant classified image within the study area of Uganda, containing the three decision tree classes: no burn, new burn, and old burn.

Table 7. Average burn size, smallest burn size and largest burn size for the new burn class for all fire years.

Year	Average Burn Size (km^2) New Burn	Smallest Burn Size (km^2) New Burn	Largest Burn Size (km^2) New Burn
1989	0.0230	0.0018	13.0869
1995	0.0307	0.0018	14.6331
2001	0.0205	0.0018	2.2707
2003	0.0214	0.0018	2.7171
2010	0.0167	0.0018	1.7226

Table 8. Average burn size, smallest burn size and largest burn size for the old burn class for all fire years.

Year	Average Burn Size (km^2) Old Burn	Smallest Burn Size (km^2) Old Burn	Largest Burn Size (km^2) Old Burn
1989	0.0143	0.0018	5.3730
1995	0.0316	0.0018	120.9366
2001	0.0122	0.0018	32.3964
2003	0.02188	0.0018	117.2439
2010	0.0115	0.0018	5.4036

Table 9. Summary of total area burned, new burn, and old burn in km^2 for the entire scenes and each quadrant: Northwest (NW), Northeast (NE), Southwest (SW), and Southeast (SE) for 1989, 1995, 2001, 2003, 2010.

Area Burned (km^2)	1989	1995	2001	2003	2010
Full: total	644.4	2341.5	495.6	748.2	634.9
Full: "new"	205.0	711.0	81.6	150.3	142.9
Full: "old"	439.4	1630.5	414.0	597.9	492.0
NW: total	180.0	149.9	213.9	447.2	264.8
NW: "new"	25.9	88.6	48.4	83.6	60.2
NW: "old"	154.1	61.3	165.5	363.6	204.6
NE: total	364.7	1794.3	227.9	256.4	184.3
NE: "new"	109.4	483.2	25.0	55.5	42.5
NE: "old"	255.3	1311.1	202.8	201.0	141.8
SW: total	26.3	78.6	20.0	11.2	34.3
SW: "new"	18.7	52.1	4.7	0.90	15.0
SW: "old"	7.6	26.5	15.4	10.3	19.3
SE: total	73.5	318.7	33.8	33.4	151.5
SE: "new"	51.0	87.0	3.6	10.4	25.2
SE: "old"	22.5	231.7	30.3	23.0	126.4

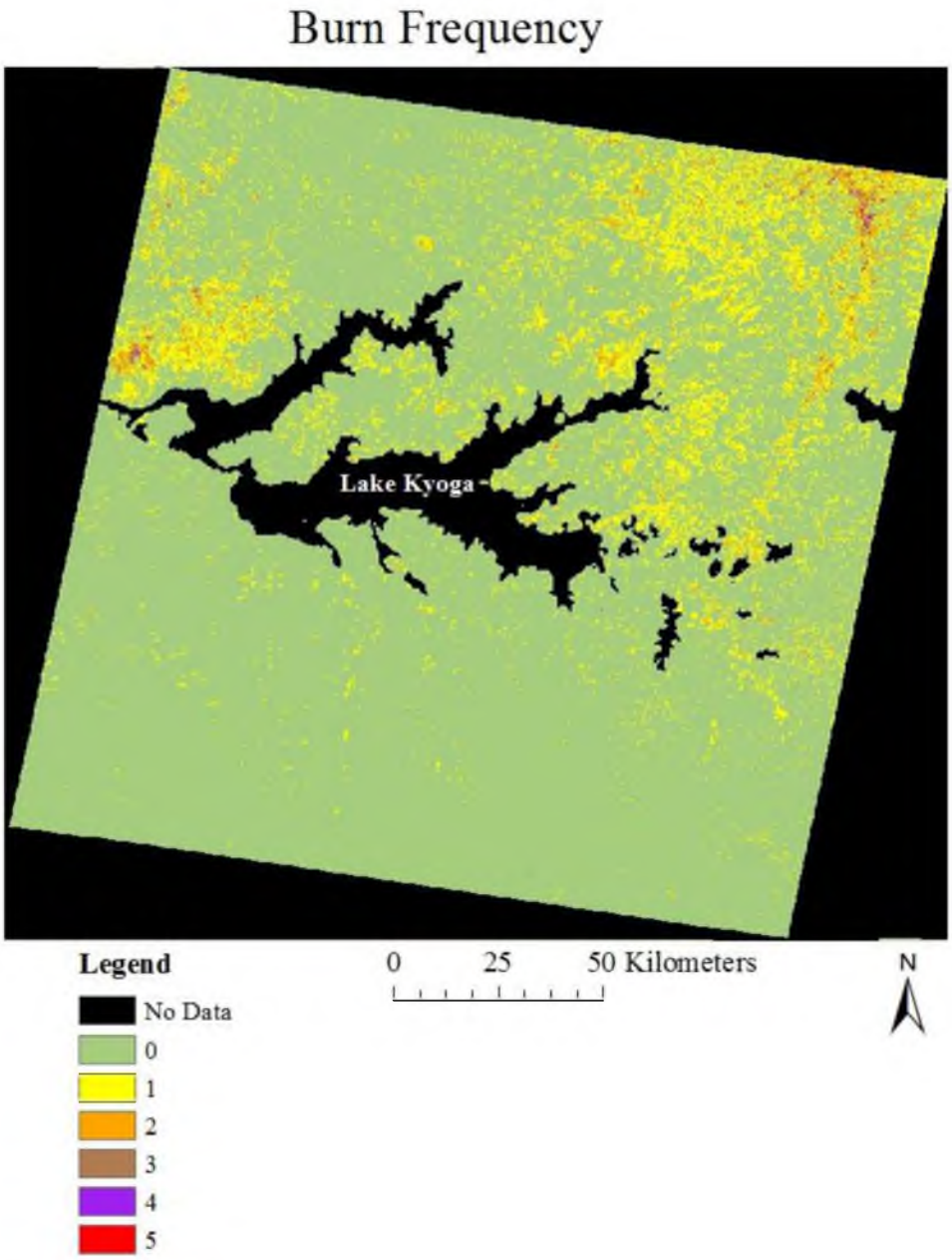

Figure 28. Burn frequencies for the entire scene.

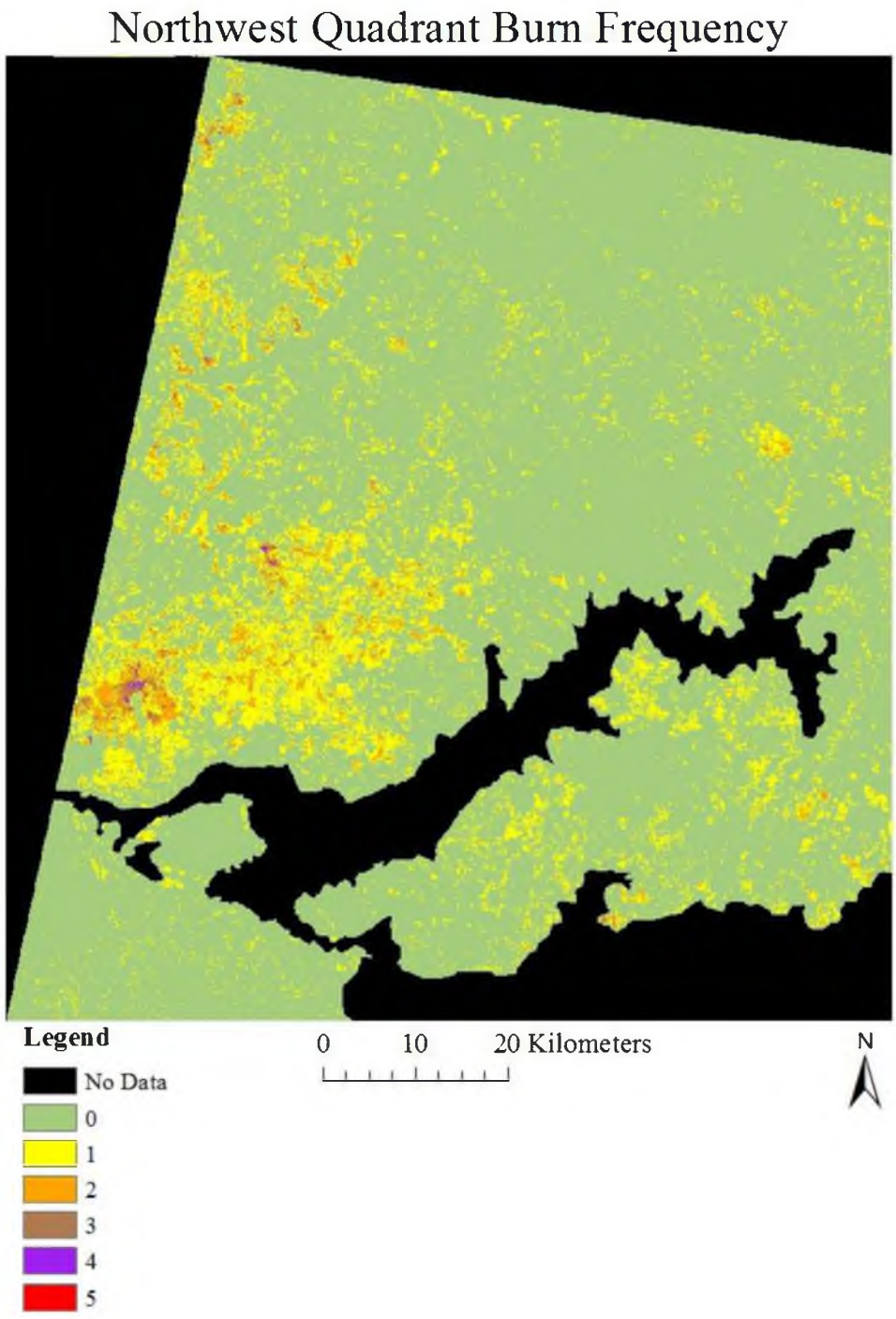

Figure 29. Northwest quadrant burn frequency.

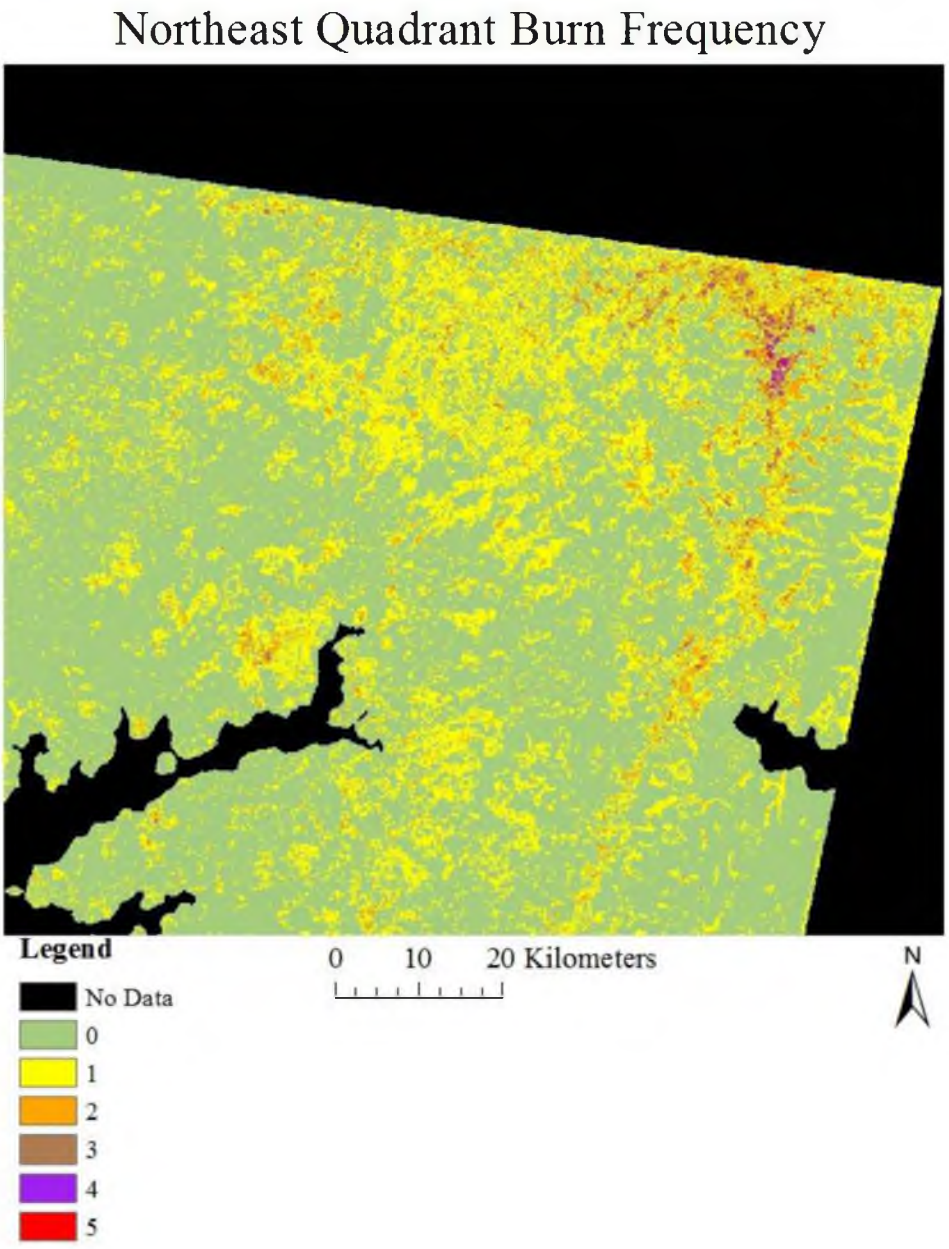

Figure 30. Northeast quadrant burn frequency.

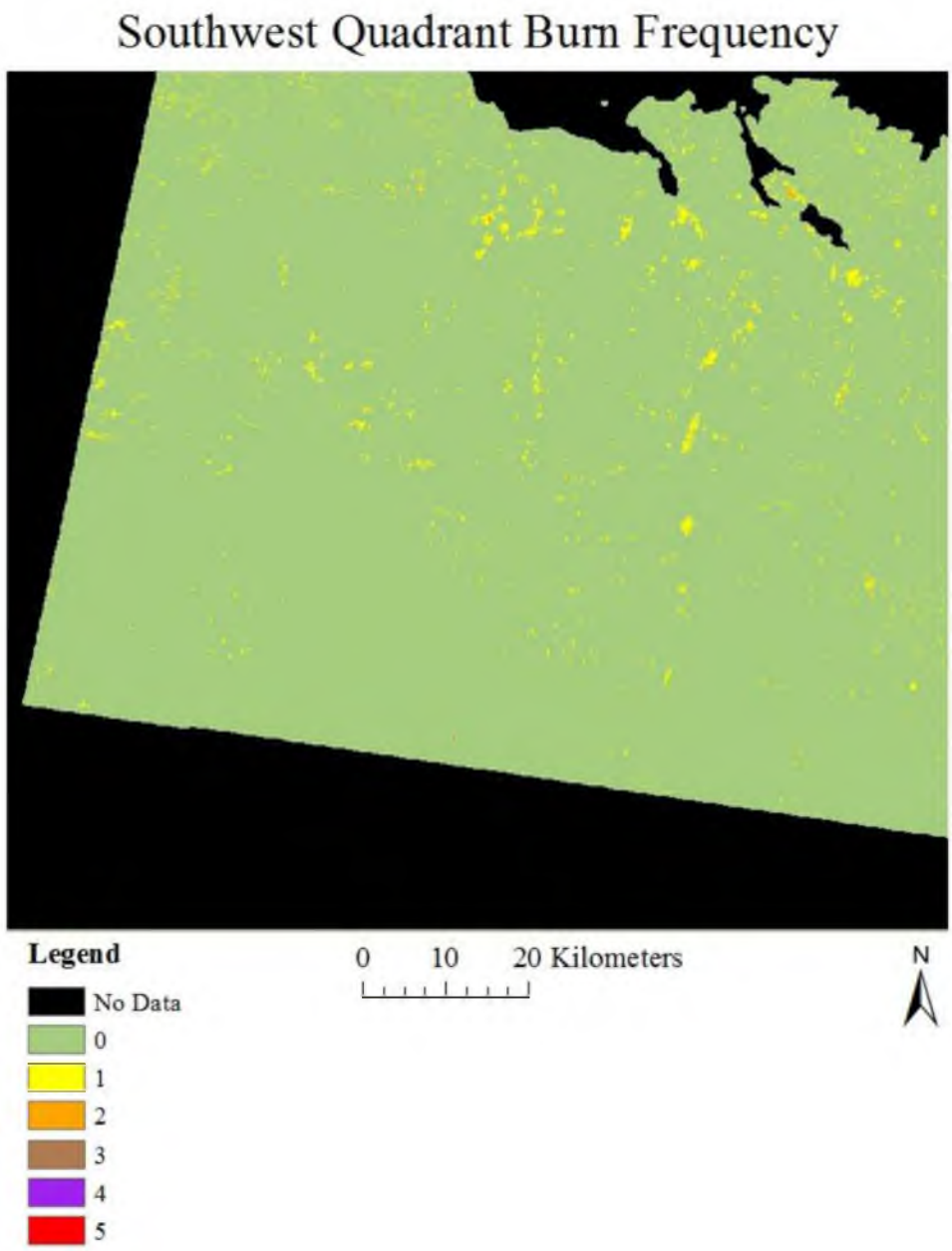

Figure 31. Southwest quadrant burn frequency.

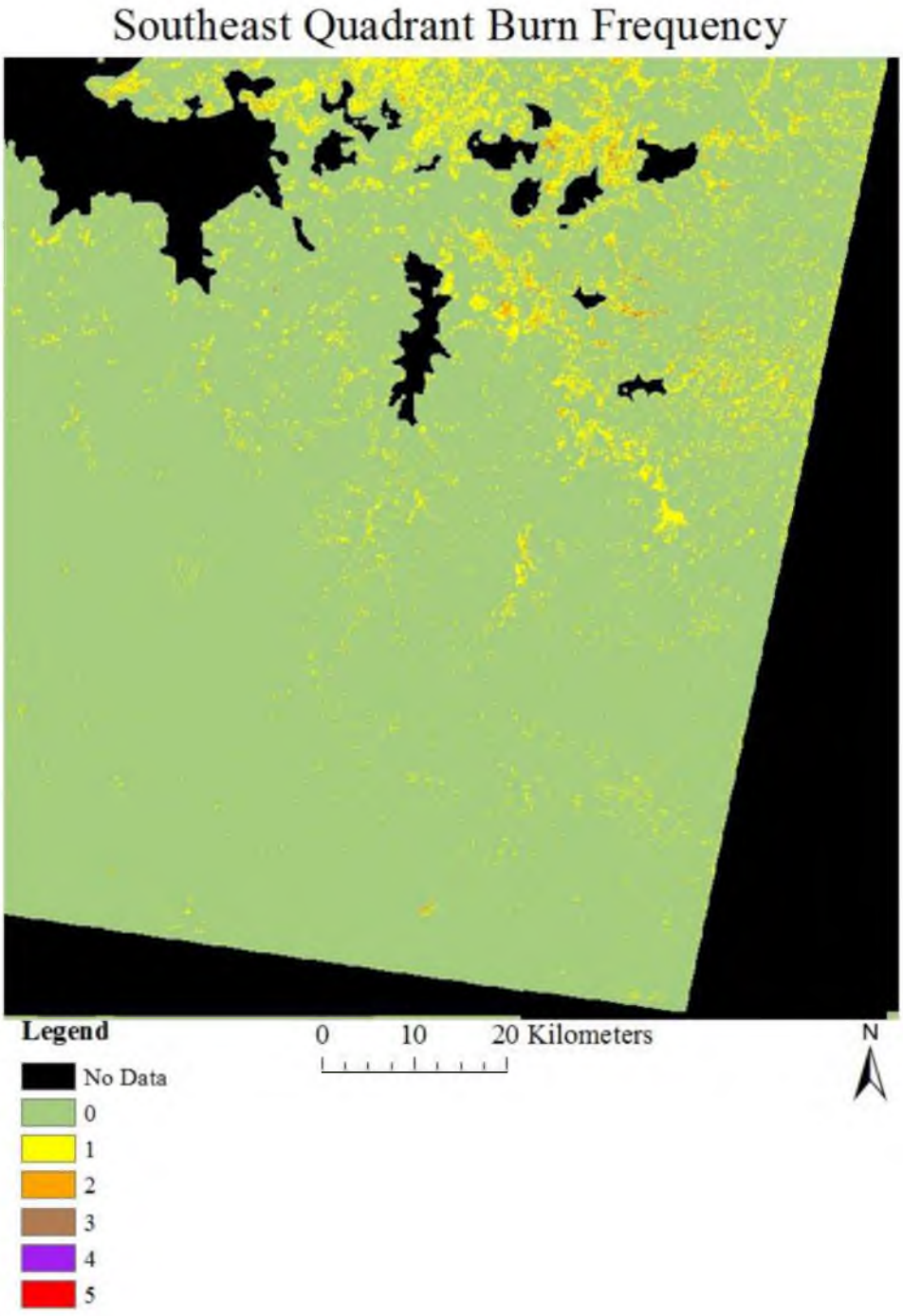

Figure 32. Southeast quadrant burn frequency.

Table 10. Burn frequency shows the area burned in km^2 that never burned, 0; burned once, 1; twice, 2, etc. The total times an area can burn is five times due to the number of scenes.

Burn Frequency Full Scene	Area Burned (km^2)
0	28,141.5
1	3,533.7
2	486.8
3	82.6
4	12.9
5	1.8

Table 11. Burn frequency for the northwest quadrant.

Burn Frequency Northwest Quadrant	Area Burned (km^2)
0	6,132.9
1	863.7
2	137.9
3	21.3
4	2.2
5	0.0

Table 12. Burn frequency for the northeast quadrant.

Burn Frequency Northeast Quadrant	Area Burned (km^2)
0	6,191.7
1	1,991.4
2	305.6
3	57.8
4	10.5
5	1.8

Table 13. Burn frequency for the southeast quadrant.

Burn Frequency Southeast Quadrant	Area Burned (km^2)
0	8,415.7
1	171.6
2	3.8
3	0.10
4	0.02
5	0.00

Table 14. Burn frequency for the southwest quadrant.

Burn Frequency Southwest Quadrant	Area Burned (km^2)
0	7,401.2
1	506.8
2	39.5
3	3.4
4	0.20
5	0.01

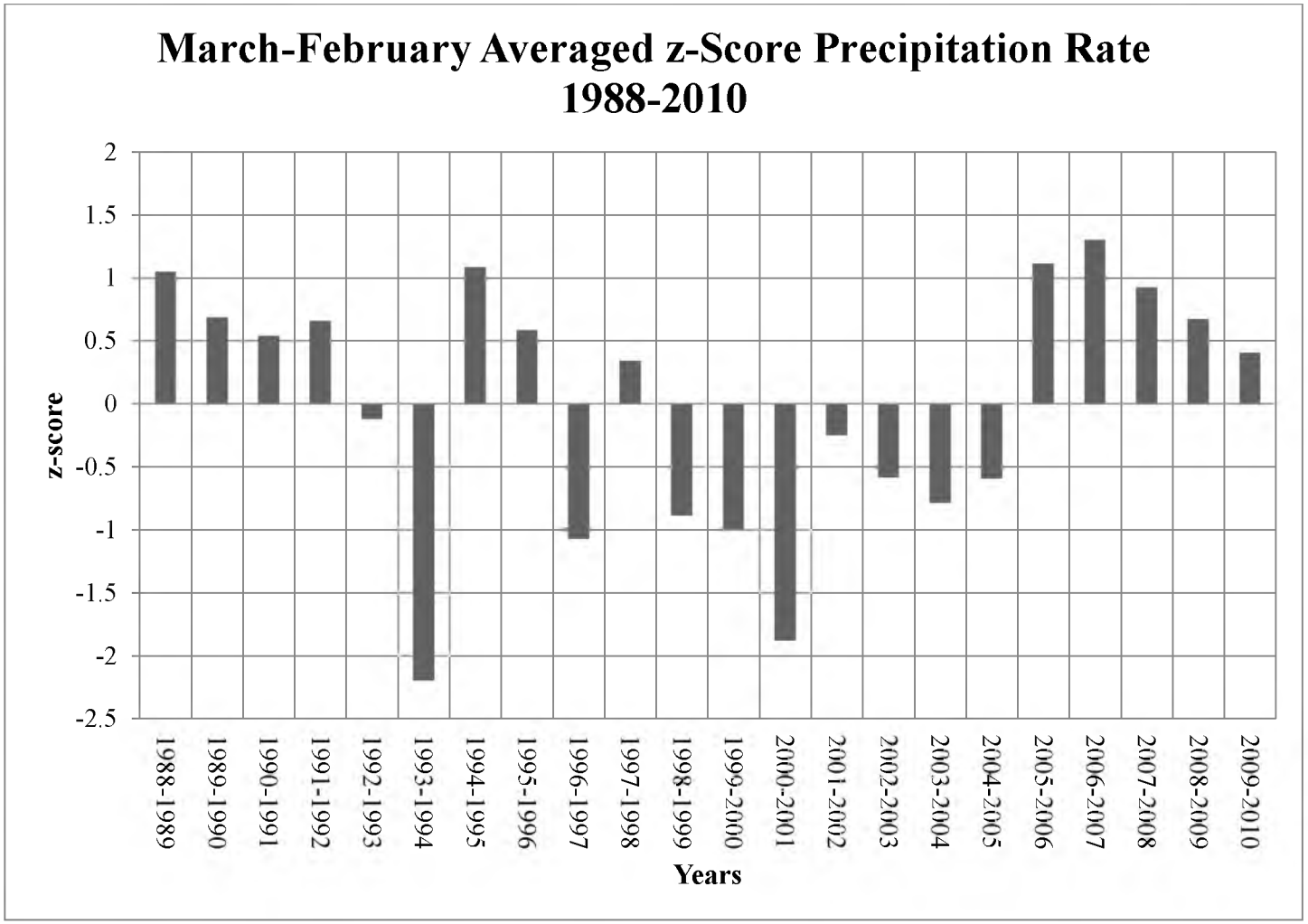

Figure 33. March through February monthly averaged z-score for precipitation rate from 1988 to 2010.

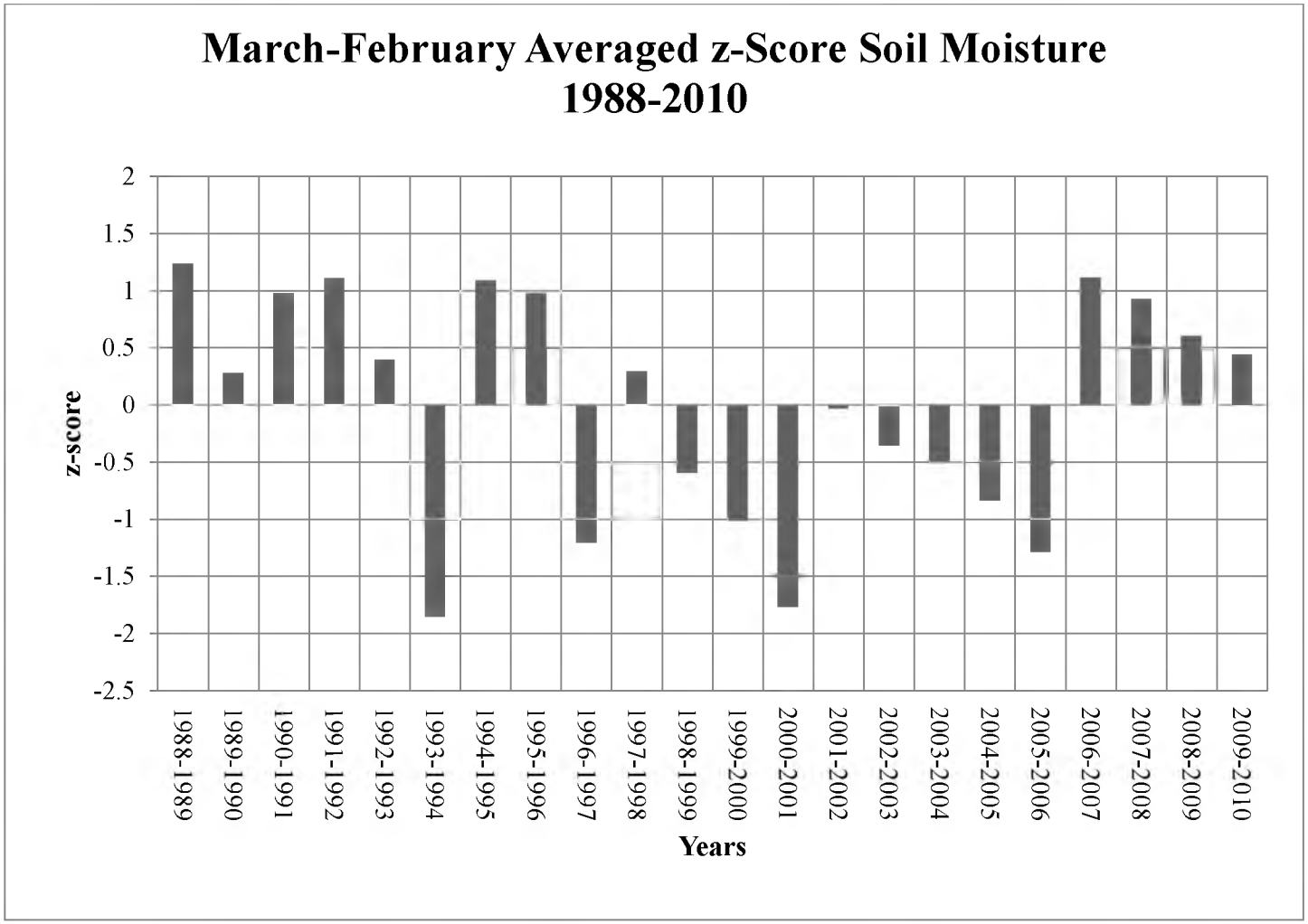

Figure 34. March through February monthly averaged z-scores for soil moisture from 1988 to 2010.

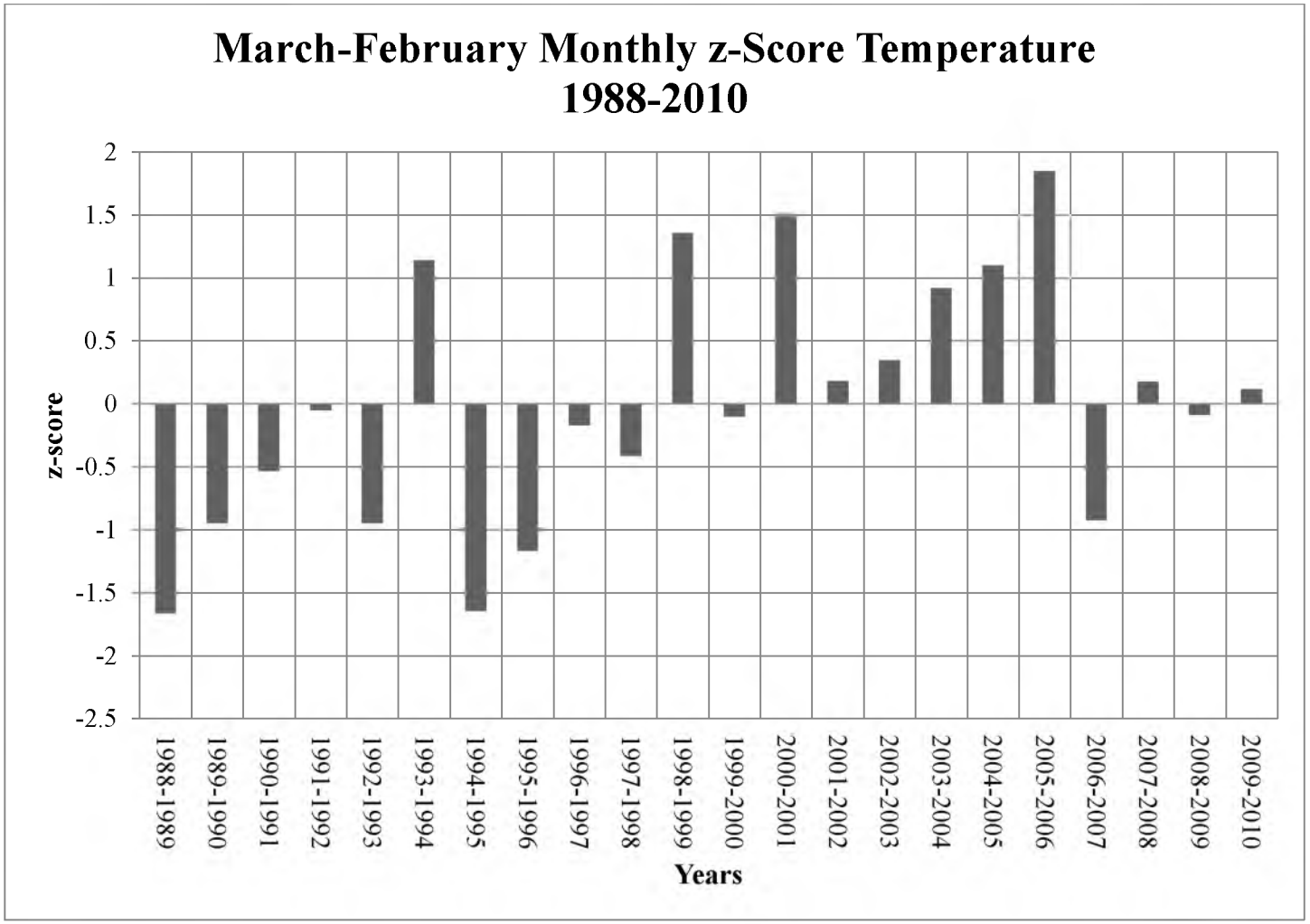

Figure 35. March through February monthly averaged z-score for temperature from 1988 to 2010.

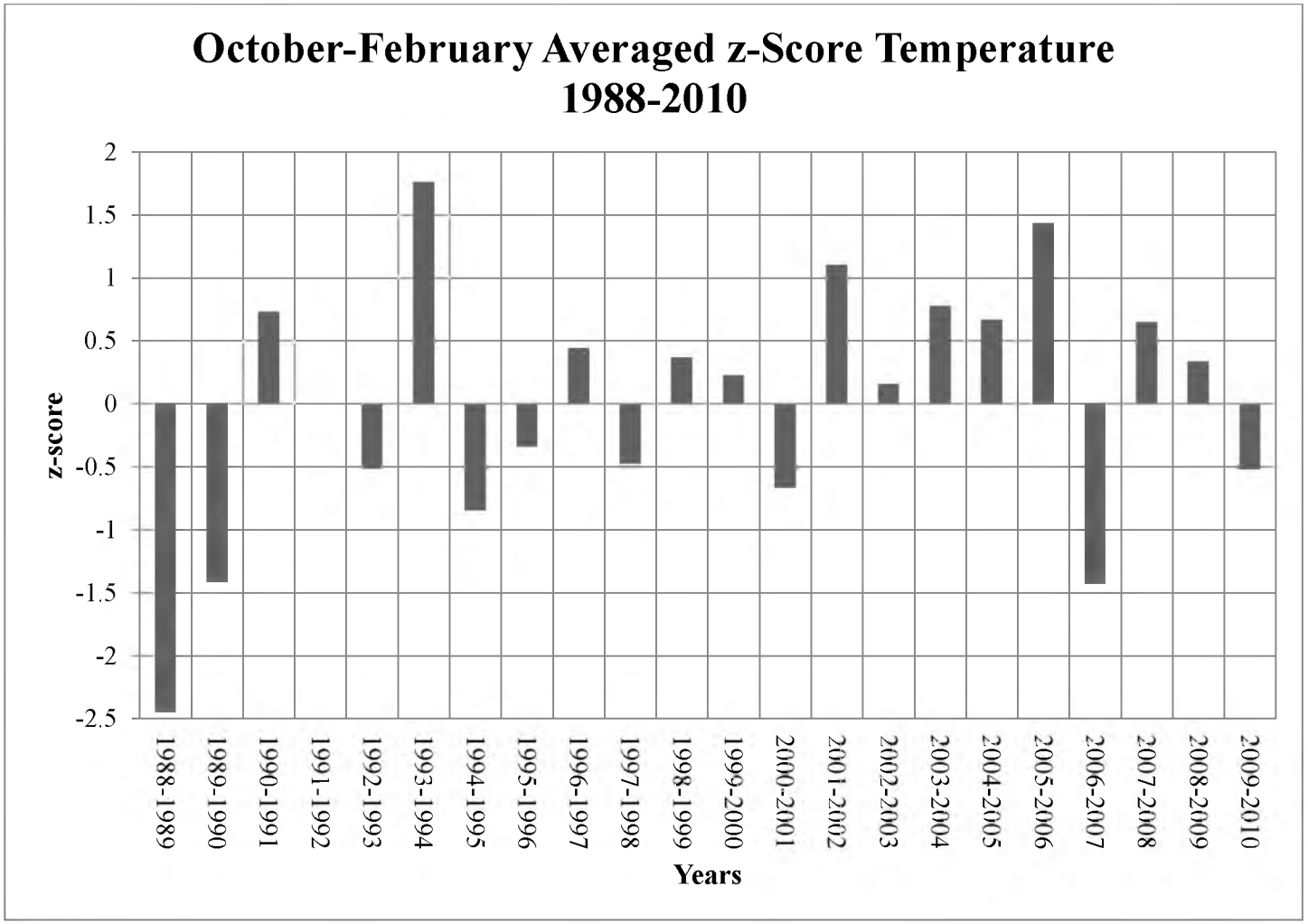

Figure 36. October through February monthly averaged z-score for temperature from 1988 to 2010.

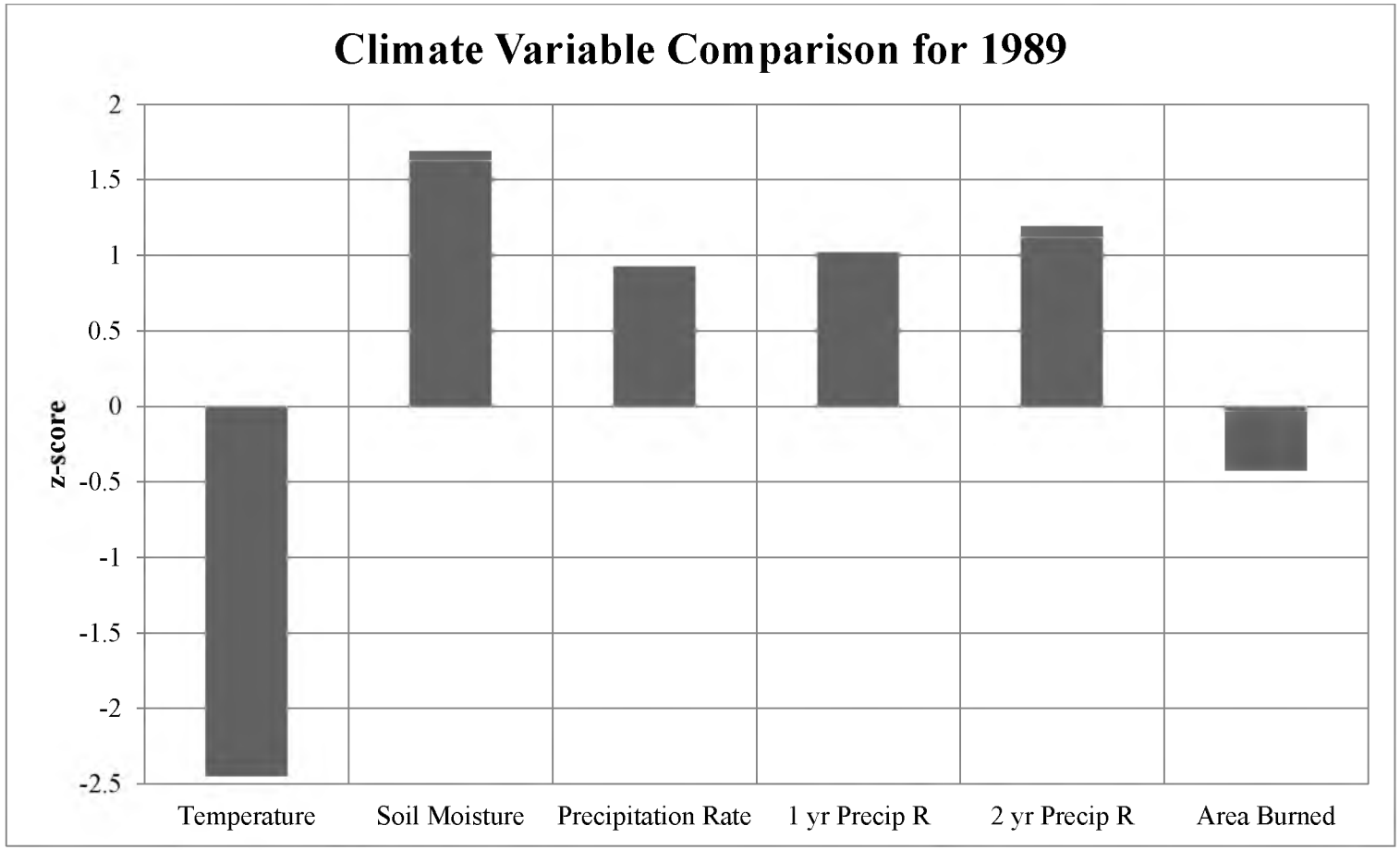

Figure 37. Comparing climate variable z-score values and the z-score value for the total area burned in km^2 for 1989. Climate variables: temperature, soil moisture, (March through February monthly averaged z score), precipitation rate (October through February monthly averaged z-score), 1 year precipitation (March through February monthly averaged z-score), 2 years precipitation rate (March, two years prior to the year the image was taken through February monthly averaged z-score). The total area burned for 1989 was 644.4 km^2.

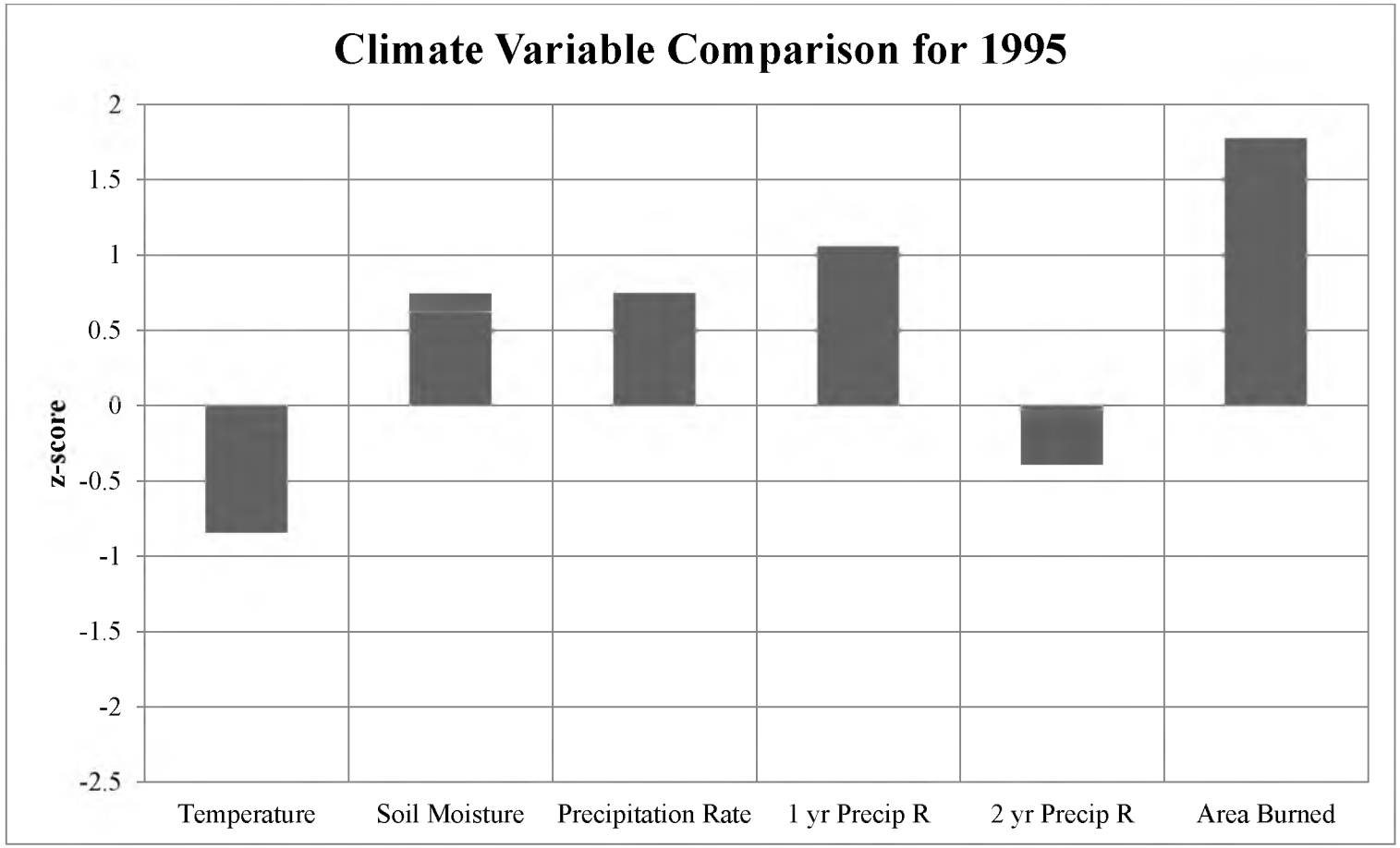

Figure 38. Comparing climate variable z-score values and the z-score value for the total area burned in km^2 for 1995. Climate variables: temperature, soil moisture, (March through February monthly averaged z-score), precipitation rate (October through February monthly averaged z-score), 1 year precipitation (March through February monthly averaged z-score), 2 years precipitation rate (March, two years prior to the year the image was taken through February monthly averaged z-score). The total area burned for 1995 was 2,341.5 km^2.

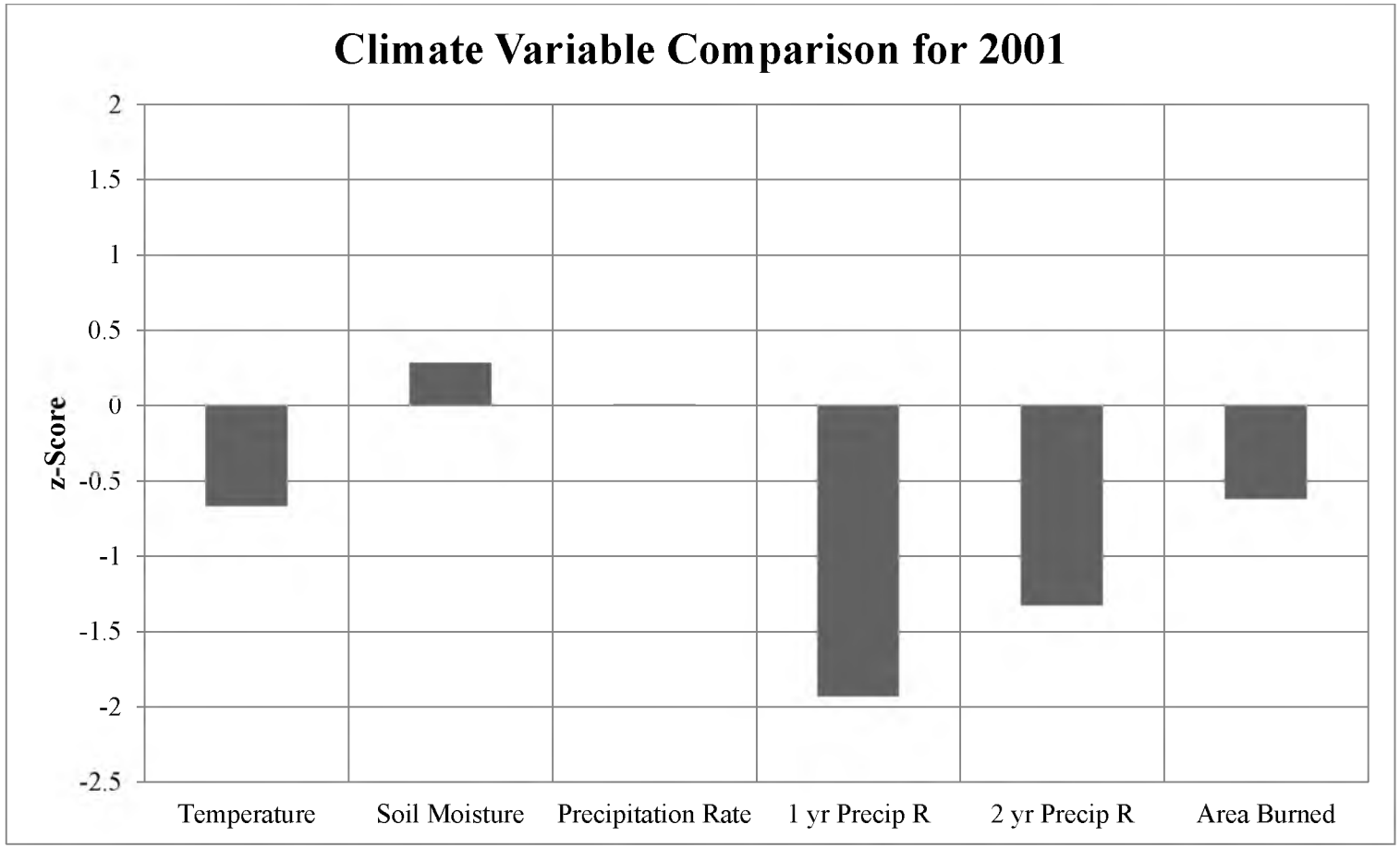

Figure 39. Comparing climate variable z-score values and the z-score value for the total area burned in km^2 for 2001. Climate variables: temperature, soil moisture, (March through February monthly averaged z-score), precipitation rate (October through February monthly averaged z-score), 1 year precipitation (March through February monthly averaged z-score), 2 years precipitation rate (March, two years prior to the year the image was taken through February monthly averaged z-score). The total area burned for 2001 was 495.6 km^2.

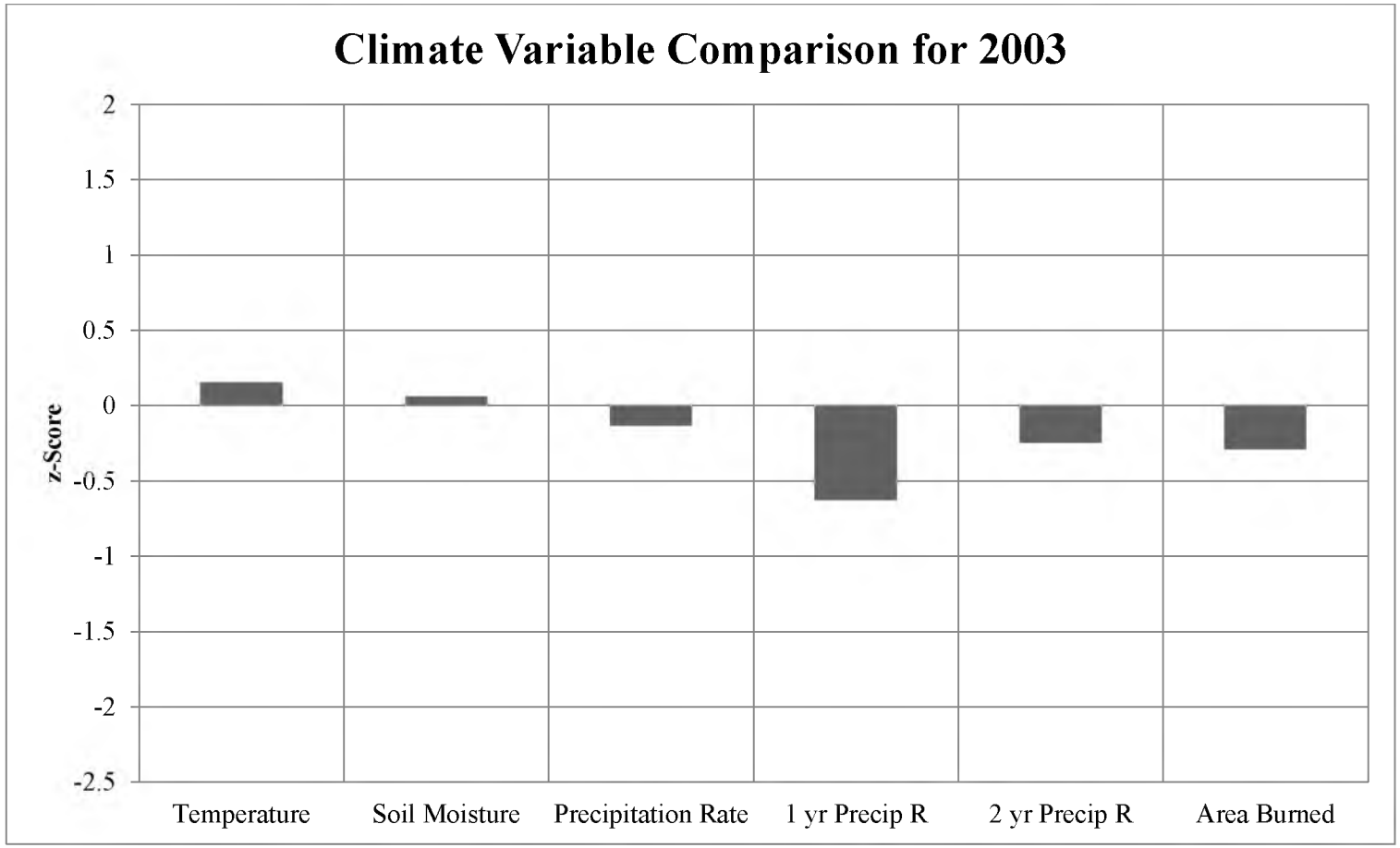

Figure 40. Comparing climate variable z-score values and the z-score value for the total area burned in km^2 for 2003. Climate variables: temperature, soil moisture, (March through February monthly averaged z-score), precipitation rate (October through February monthly averaged z-score), 1 year precipitation (March through February monthly averaged z-score), 2 years precipitation rate (March, two years prior to the year the image was taken through February monthly averaged z-score). The total area burned for 2003 was 748.2 km^2.

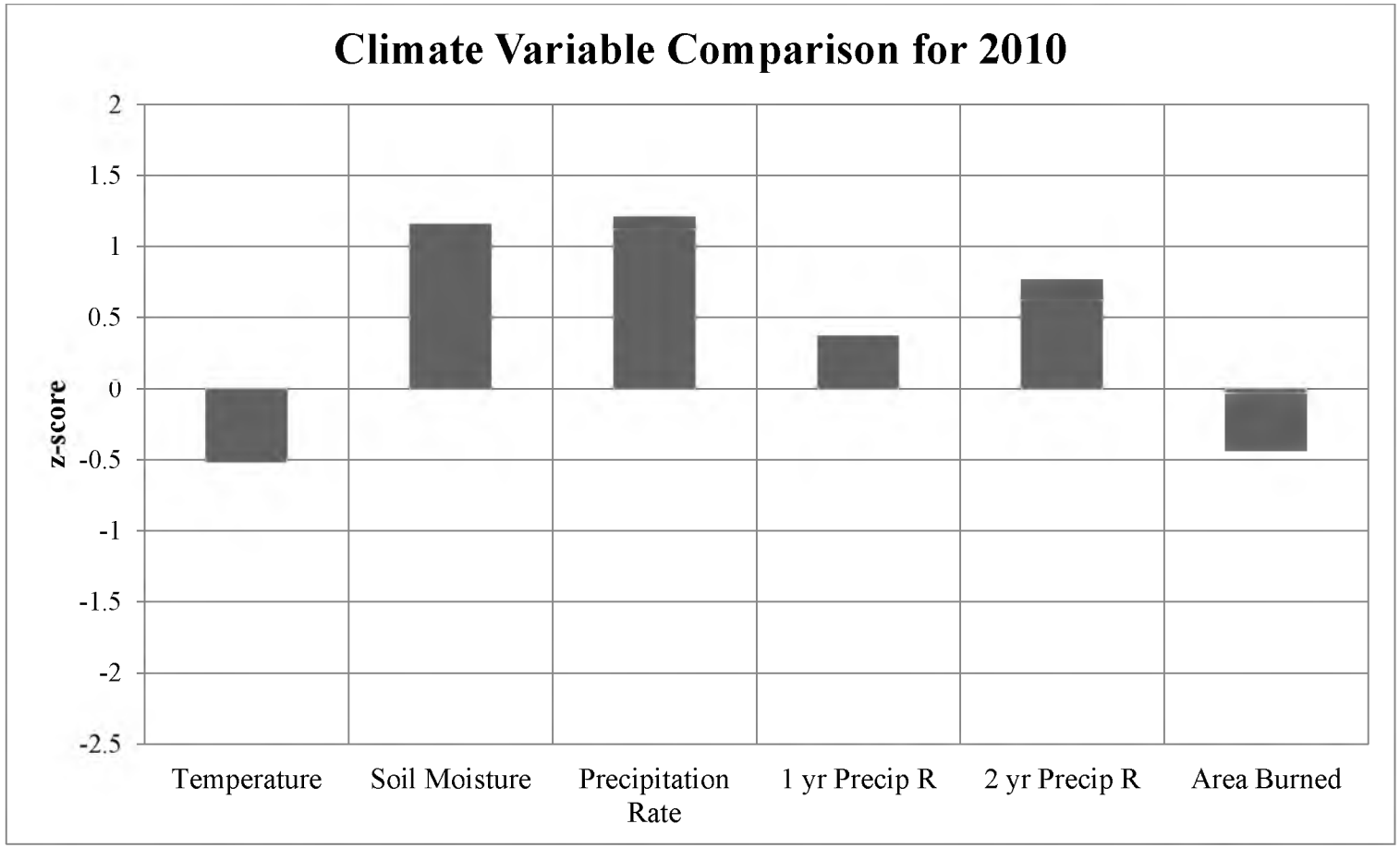

Figure 41. Comparing climate variable z-score values and the z-score value for the total area burned in km^2 for 2010. Climate variables: temperature, soil moisture, (March through February monthly averaged z-score), precipitation rate (October through February monthly averaged z-score), 1 year precipitation (March through February monthly averaged z-score), 2 years precipitation rate (March, two years prior to the year the image was taken through February monthly averaged z-score). The total area burned for 2010 was 634.9 km^2.

Table 15. Entire study area, gridded population densities.

Year	Average Population Density per 2.5'	Difference	% Change	Total Population	Difference
1990	93.8			209,507	
1995	110.8	17	18%	247,411	32,904
2000	129.8	19	17%	289,862	42,451
2005	153.7	24	18%	343,223	53,361
2010	184.9	31	20%	412,770	69,547

Table 16. Northwest (NW) quadrant of study area, gridded population densities.

Year	Average Population Density per 2.5'	Difference	% Change	Total Population	Difference
1990	64.6			36,475	
1995	77.2	13	20%	45,600	7,124
2000	91.4	14	18%	51,600	8,000
2005	109.0	18	19%	61,598	9,998
2010	131.9	23	21%	74,546	12,948

Table 17. Northeast (NE) quadrant of study area, gridded population densities.

Year	Average Population Density per 2.5'	Difference	% Change	Total Population	Difference
1990	59.3			33,913	
1995	73.4	14	24%	41,977	8,063
2000	89.8	16	22%	51,345	9,368
2005	110.6	21	23%	63.274	11,930
2010	138.1	27	25%	78,993	15,719

Table 18. Southwest (SW) quadrant of study area, gridded population densities.

Year	Average Population Density per 2.5'	Difference	% Change	Total Population	Difference
1990	84.4			49,889	
1995	93.1	9	10%	55,010	5,123
2000	102.4	9	10%	60,514	5,503
2005	114.5	12	12%	67,650	7,136
2010	130.7	16	14%	77,225	9,575

Table 19. Southeast (SE) quadrant of study area, gridded population densities.

Year	Average Population Density per 2.5'	Difference	% Change	Total Population	Difference
1990	166.1			98,328	
1995	195.6	32	20%	117,544	19,216
2000	234.7	36	18%	138,987	21,393
2005	279.6	45	19%	165,516	26,579
2010	337.5	58	21%	199,791	34,275

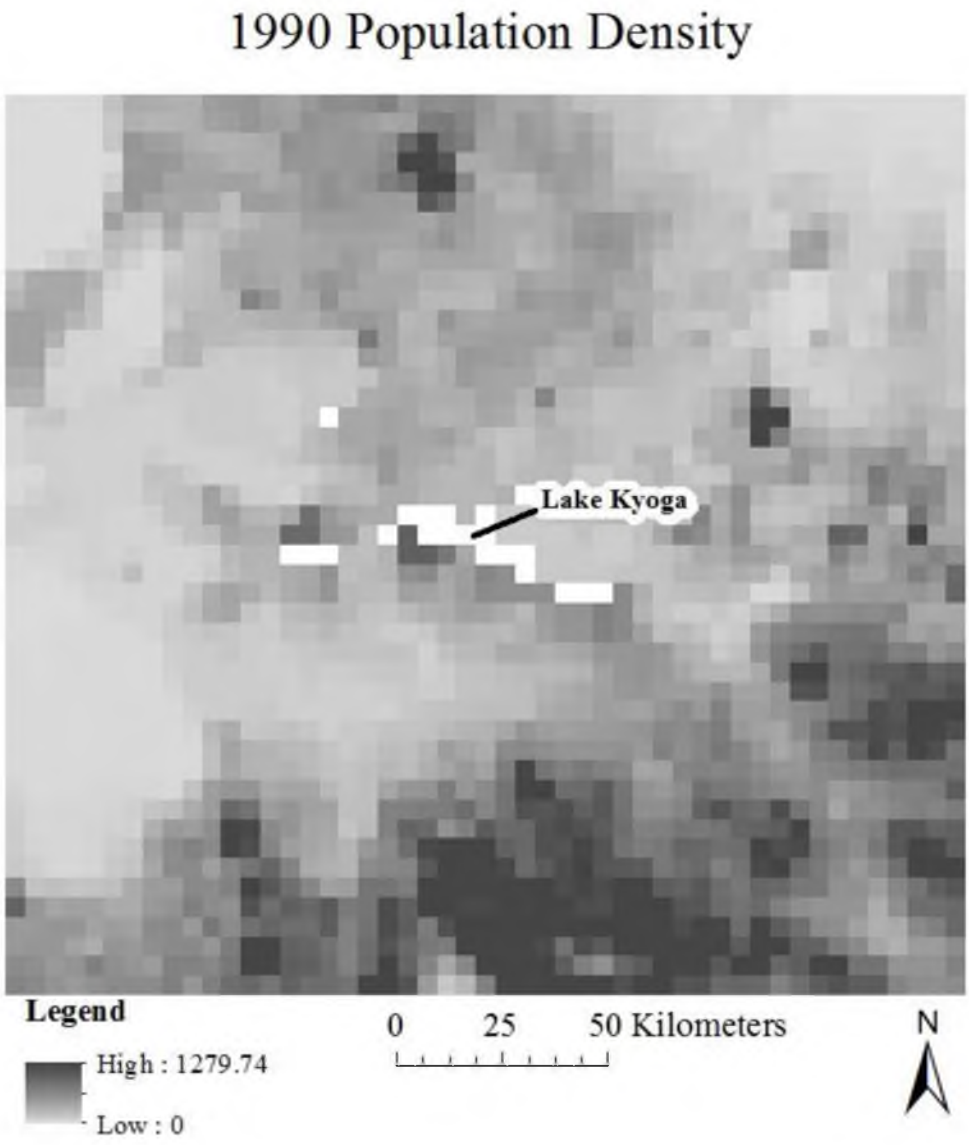

Figure 42. Gridded population density map with a spatial resolution of 2.5', for study area, 1990.

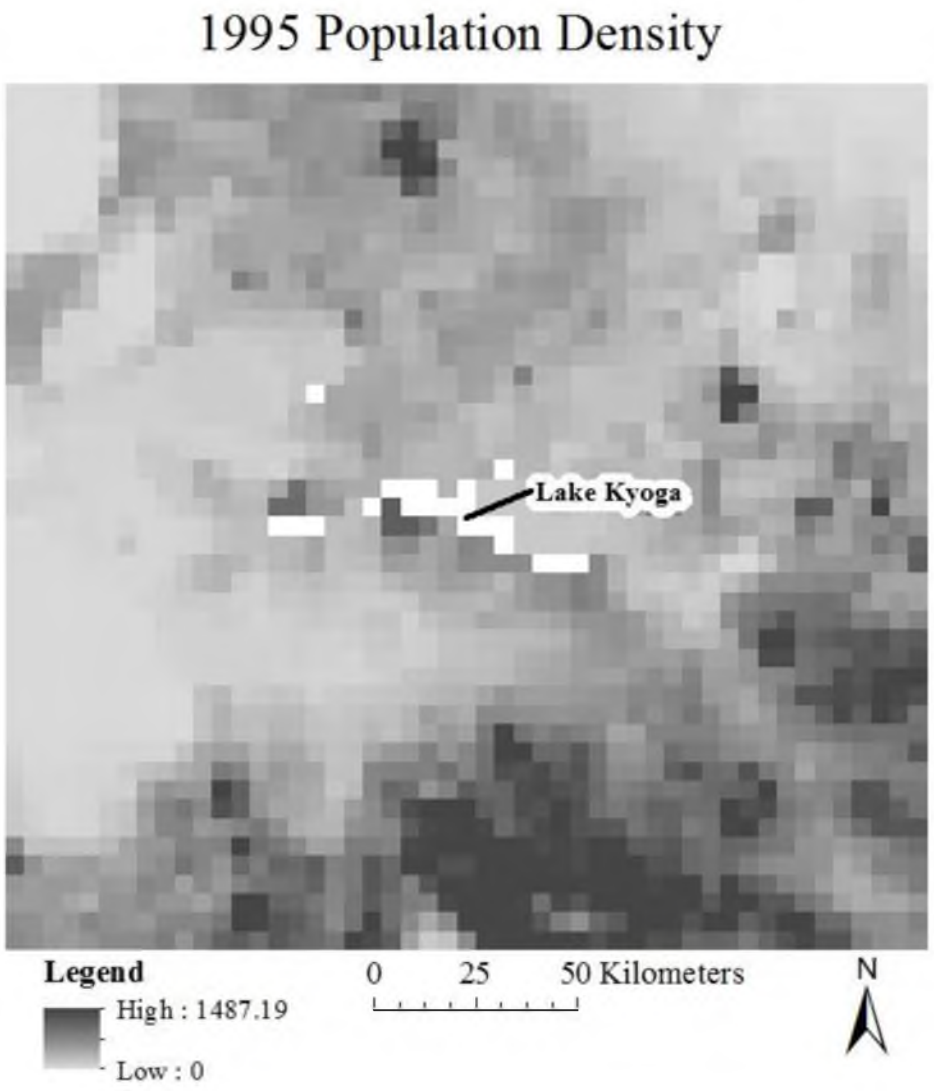

Figure 43. Gridded population density map with a spatial resolution of 2.5', for study area, 1995.

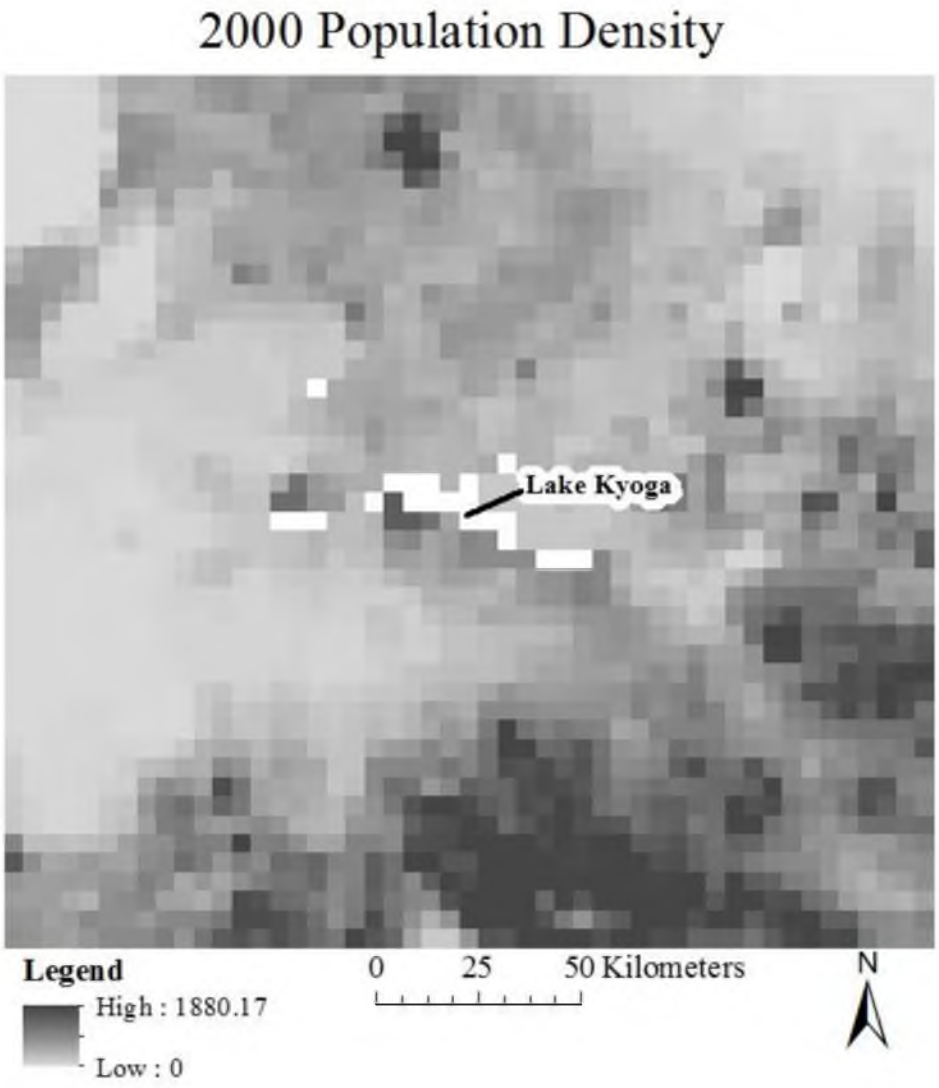

Figure 44. Gridded population density map with a spatial resolution of 2.5', for study area, 2000.

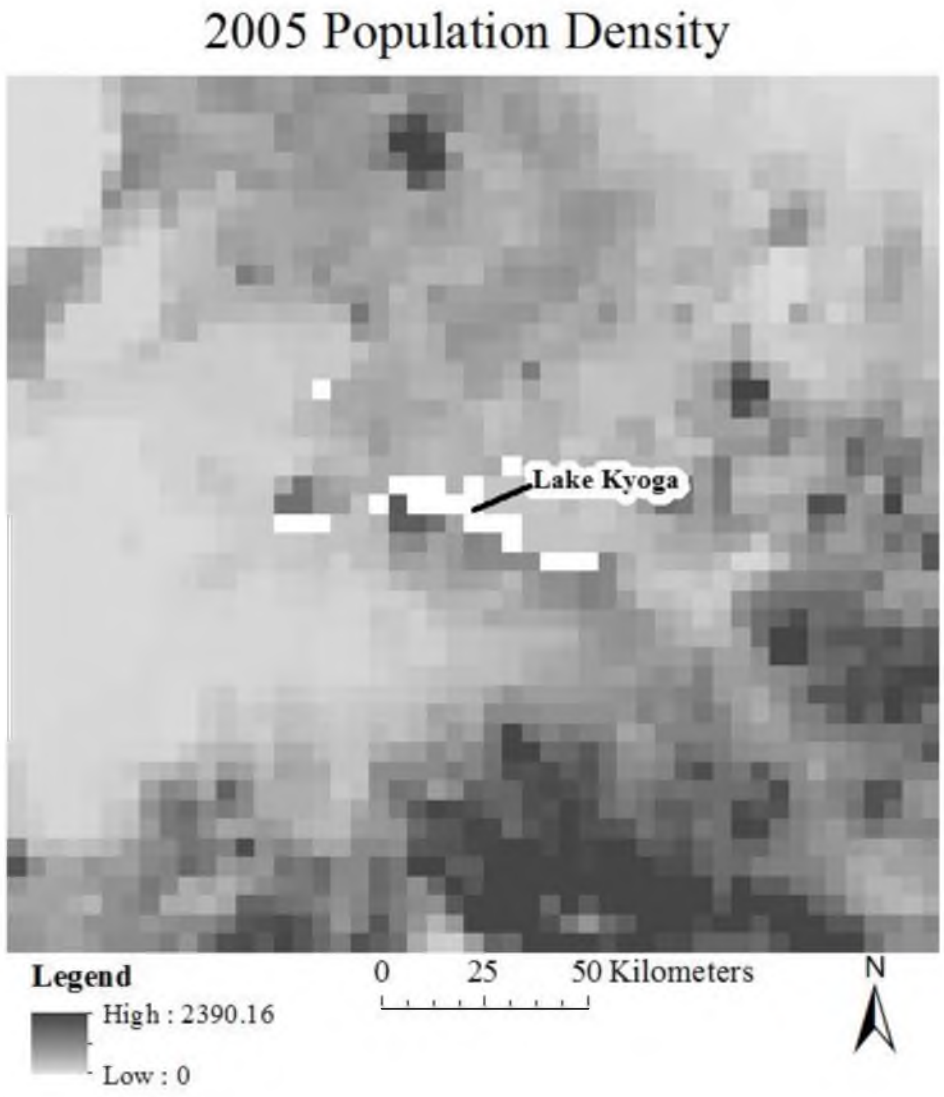

Figure 45. Gridded population density map with a spatial resolution of 2.5', for study area, 2005.

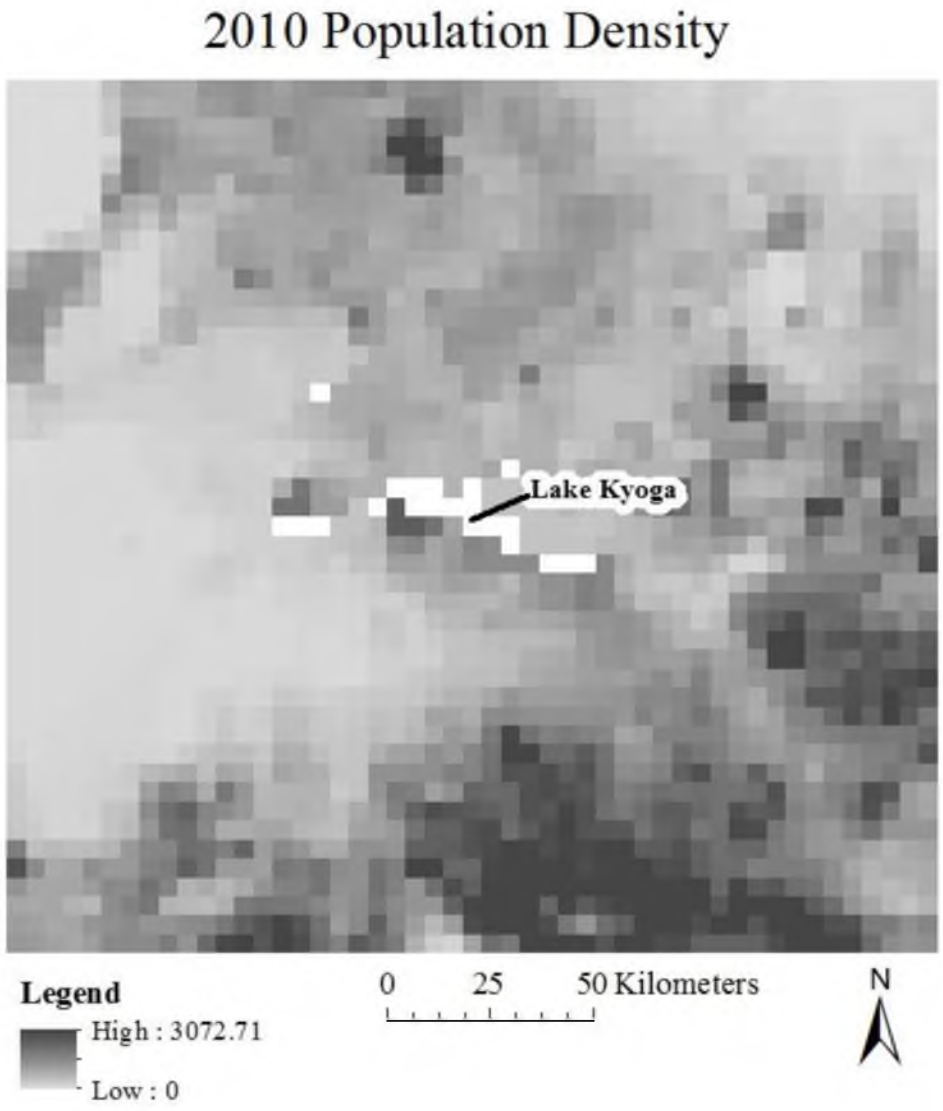

Figure 46. Gridded population density map with a spatial resolution of 2.5', for study area, 2010.

5 DISCUSSION

The northern portion of the Landsat scene burned more area more frequently compared to the southern half of the scene. On average, the north is drier than the south, receiving less annual precipitation which would likely lead to occurrence of more fire. A direct link between the precipitation rate, soil moisture, and temperature to the amount of area burned was not established with the available datasets. The climate data has a coarse resolution; one cell encompasses the entire study area, thus not capturing the known precipitation and temperature gradient of drier and hotter conditions in the north and wetter and cooler conditions in the south.

The 1995 image taken had the largest area of new burn, old burn, and total area burned. The z-score values for precipitation rate and soil moisture for 1995 are positive values prior to the 1995 image date, signifying wetter than normal conditions. Low z-scores indicate less than average precipitation rate and soil moisture, which could lead to senesced vegetation that is likely to ignite. However, the actual values for precipitation rate and soil moisture are higher than average, greater than 1, opposite of what would be expected with the large amount of area burned. Temperatures during the preceding months were cooler than average, with a z-score value of -0.95. With cooler temperatures, more available water, and a large area burned, the climatic mechanisms contributing to increased area burned are likely complex. The climate data are unable to confirm that climate is driving the variation in burned area.

The scene taken in 2003 had the second highest area burn, 748.2 km^2, and had negative z-score values of -0.59 for precipitation rate and -0.36 for soil moisture while temperature was slightly positive with a value of 0.35. The values of the z-scores seem reasonable and would indicate that climatic conditions were conducive to increased burning.

The image from 1989 had 644.4 km^2 burned with positive z-score values for precipitation rate of 1.1 and 1.2 for soil moisture. Z-score values were negative for a temperature of -1.7 for the same time period. The scene with the least area burned of 495.6 km^2 was in 2001. The image from 2001 had high z-score values for temperature, 1.5, indicating warmer than average temperatures. Precipitation rate values were -1.8 and soil moisture was -1.7, but 2001 had the least amount of area burned out of all 5 images. The 2001 preceding months were drier and hotter but less fire was burned that year. High temperatures, and lower than normal precipitation rates and soil moisture, conditions would be conducive to increased burning, but that is not the case for this year. The years with the most burn or least burn do not line up with the climate variables that would indicate that climate is driving the total area burned. The relationship between the climate variables, precipitation rate, soil moisture, and temperature and the amount of area burned was not as expected as fire occurred during wet and cool years, such as during 1995. Burning land during wet and cool conditions prevents fire from burning out of control; it is more difficult for a fire to ignite naturally under cool and wet conditions. More area burned aligns with wet and cool weather conditions indicating that humans may be driving total area burned.

The size of each fire was determined and averaged for each fire year. The 1995 fire year had the largest burn size and the largest average burn size for both new burn and old burn classes compared to the other four years. The average burn size for each year has less than a tenth of a km^2. Small burn patches are characteristic of humans burning the landscape in a non-contiguous manner. Smaller fires area easier for people to contain, whereas climate driven fires tend to be contiguous and larger in size, and harder to contain or to extinguish.

The population within the study region is known for using fire as a means to clear the landscape of grasses and shrubs for various reasons such as re-mineralizing the soils to produce a more nutritious diet for grazing animals and the removal of biomass for energy production. An increase in the total population was more than 50% from 1990 to 2010 within the study area. The majority of the population resides in the southeast region, with a little more than two times as many people than the other quadrants. The total area burned from all five Landsat images for the southeast quadrant was $608km^2$, the second lowest. The southwest quadrant had the least total area burned, $169km^2$, and had the second highest total population for all years data are available, 1990, 1995, 2000, 2005, and 2010. The northeast quadrant had the most total area burned for all five years, 2,825 km^2 and had the lowest total population until 2005. In 2005 and 2010 the northeast had the second lowest total population, ahead of the northwest.

The northeast had the most area burned and had the fewest number of people in 1990, 1995, 2000 and the second lowest total population in 2005 and 2010. Pastoralist and agriculturalist lifestyles, which use fire as a tool to manage crops and control pests, are more common in the north versus the south, and the southern region is more

urbanized. A relationship between total area burned and fewer people exist in the northeast quadrant. An inverted U-shaped relationship exists between fires frequency and land use intensity, where fires are predominately ignited by humans (Lavorel et al., 2007).

The inverted U-shaped relationship is the combination of benefits of fires controlling pests and managing crops and the risks of fire endangering human life, property, and infrastructure. Ecosystems dominated by pastoralist and agriculturalist are inclined to burn more frequently because fire is used as a land management tool. As the population increases, land use intensifies and fire is replaced with machinery and labor. Agriculture intensification changes the role of fire from clear cutting of forests to burning smaller plots of land for farming. The population data support the claim that the variation in burned area is related to the population density and/or population change, but more data are be needed to confirm this hypothesis.

Areas of high-fire frequencies occurred in the northern portion on the region. In the uppermost section of the northeast quadrant, there are areas that were burned in all 5 scenes (Figure 30). There are five villages that are within 20 kilometers in this area: Kapelenbyong, Achumet, Achwa, Usuku, and Adachal. The specific pixels that burned in all five scenes tend to be in low-lying areas; about 30 meters lower than surrounding areas. These specific areas of high-burn frequency have a small waterway going through it and appears to contain thicker vegetation. Burning in this area may be related to agricultural or transportation uses along this waterway.

Another area that has multiyear burns is in the lower-left region of the northeast quadrant (Figure 29). In this area pixels burned up to four times over the time series.

This area is within 15 kilometers of four villages: Teboke, Awila, Akokoro, and Itwara. There does not appear to be water bodies or rivers within this area with little topographic variation. Imagery available on Google Earth in July 2012 shows what appears to be agriculture occurring in grid like formations in and around the multiyear burn sites, which indicates humans are likely burning this area intentionally.

The accuracy assessment was a way to examine how well the decision tree was able to accurately produce a classified image. The high overall accuracies and kappa coefficients were high due to the agreement between the classified image ROIs and the accuracy assessment ROIs. Ground-truth data would provide information as to what the exact spectral response would be for each class, rather than an educated guess, and would provide an improved assessment of classification accuracy. It is not clear how old the old burn class is; a better temporal resolution and/or ground-truth data would provide the necessary information to more accurately divide up the burn classes. Ground-truth data could have also provided the type of vegetation and fuel loading found throughout the study region. If the vegetation has not burned for a few years, the biomass can accumulate resulting in increased fuel loading. Different types of vegetation and the amount of biomass available can change how severe the fire will burn and change how a land surface will look spectrally.

The image taken in 1995 had by far the most area burned, but it is difficult to say if this is an anomaly given the coarse temporal resolution. There were 5 good images, within 20 years, available from the Landsat suite of sensors starting from when the first Landsat TM sensor was launched until the end of 2010. The 5 images that were available were close to the same day year after year. Four out of the 5 scenes were within 10 days

of each other and were all in the month of January, whereas the image from 1989 was taken in mid February. The end of February is the end of the dry season and when vegetation is at its driest. If scenes could have been acquired later in the season it is possible that the total area burned could have been greater. The timing of when scenes are taken is just as important as the temporal resolution.

Additional remote sensing datasets such as those from the Moderate Resolution Imaging Spectroradiometer (MODIS) could fill in the gaps. MODIS has a lower spatial resolution than Landsat, thus, additional cross calibrations would be needed and it is possible that decision trees as a means to create a classified image would not be the appropriate method to determine burned areas.

The climate data are spatially coarse and do not account for the spatial variation in burned area that occurs within the study region. Access to high spatial resolution climate data could provide a better understanding of how climate interacts with not only the landscape but the population. Additional drought data would be helpful for determining the timing, geography, and the intensity of dry periods. Drought data were available for Uganda, but also had a low spatial resolution and did not seem to be helpful in determining why and where fires had burned.

An alternative method to mapping the total area burned for each scene would be to map the active fires. Again, more remote sensing data would be helpful in understanding the year to year variations. Another limitation in the study was the lack of prior research that has been done in Uganda on this topic. Little to no modern information was available as to why, where and how fires are burning.

6 CONCLUSION

This study aimed to map and determine the total area burned, explain temporal trends in the remote sensing data, and obtain a better understanding of the relationships between fire, climate, and population in Central Uganda from 1989 to 2010. Climate variables (precipitation rate, soil moisture, and temperature) were used to gain a better understanding of the interaction between fire and climate. The years with the most fire unexpectedly aligned with wetter and cooler weather conditions, which indicate climate is likely not driving fire in Uganda.

Fire is a tool that the rural and urban population in Uganda use for an energy source, and agriculturalist and pastoralists use fire to regenerate soils and clear land. Regions of the study area with less population saw more area burned, while areas with higher population densities saw less area burned. The northeast region had the lowest population density and had the most area burned for 1989, 1995, and 2001.

Fire has been used throughout human existence in Africa. While fire is also a natural disturbance that can impact the landscape in a positive and negative way, it is a challenging disturbance to understand. How and why fire burns is not well understood in Africa and particularly in Uganda. Due to the size of the rural population in Uganda and how they use fire for their livelihood, human activity is likely a more important contributor to area burned than climate. There is a need for more research on fires in Uganda to better comprehend how climate may be affecting fire.

LITERATURE CITED

Apuuli, B., Wright, J., Elias, C., & Burton, J. (2000). Reconciling national and global priorities in adaptation to climate change: with an illustration from Uganda. *Environmental Monitoring and Assessment 61*, 145-159.

Asner, G.P., Elmore, A.J., Olander, L.P., Martin, R.E., & Harris, A.T. (2004). Grazing systems, ecosystem responses, and global change. *Annual Review of Environment and Resources 29*, 261–299.

Buechner, H. K., & Dawkins, H. (1961). Vegetation change induced by elephants and fire in Murchison Falls National Park, Uganda. *Ecology Society of America 42*(4), 752-766.

Chander, G., Markham, B. L., & Helder, D. L. (2009). Summary of current radiometric calibration coefficients for Landsat MSS, TM, ETM+ and EO-1 ALI sensors. *Remote Sensing of Environment 113,* 893-903.

Christopherson, R. W. (2000). Geosystems (4th ed.). Upper Saddle River, NJ: Prentice Hall.

Cooke, W. F., Grégoire, J. M., & Koffi, B. (1996). Seasonality of vegetation fires in Africa from remote sensing data and application to a global chemistry model. *Journal of Geophysical Research 101*, 21,051-21,065.

Copeland, J. H., Pielke, R. A., & Kittel, T. G. F. (1996). Potential climate impacts of vegetation change: A regional modeling study. *Journal of Geophysical Research*, 101(D3), 7409-7418.

Coppin, P., Jonckheere, I., Nackaerts, K., & Muy, B. (2004). Digital change detection methods in ecosystem monitoring: A review. *International Journal of Remote Sensing 25*(9), 1565-1596.

Ericksen, S., O'Brien, K., & Rosentrater, L. (2008). Climate change in eastern and southern Africa: Impacts, vulnerability and adaptation. *Global Environmental Change and Human Security Report 2.* Oslo: University of Oslo.

Funk, C., Husak, G., Michaelsen, J., Love, T., & Pedreros , D. (2007). Third generation rainfall climatologies: Satellite rainfall and topography provide a basis for smart interpolation. Crop and Rangeland Monitoring Workshop, Nairobi (Kenya), March 2007.

Healey, S. P., Warren. B. C., Zhiqiang, Y., & Krankina, O. N. (2005). Comparison of Tasseled Cap-based Landsat data structures for use in forest disturbance detection. *Remote Sensing of Environment 97*, 301-310.

Huang, C., Goward, S. N., Masek, J. G., Thomas, N., Zhu, Z., & Vogelmann, J. E. (2010). An automated approach for reconstructing recent forest disturbance history using dense Landsat time series stacks. *Remote Sensing of Environment*, 114, 183-198.

Jensen, J. R. (2005). Introductory digital image processing: A remote sensing perspective (3rd ed.). Upper Saddle River, NJ: Prentice Hall.

Kokaly, R. F., Rockwell, B. W., Haire, S. L., & King, T. V.V. (2007). Characterization of post-fire surface covers, soils, and burn severity at the Cerro Grande Fire, New Mexico, using hyperspectral and multispectral remote sensing. *Remote Sensing of Environment 106*, 305 – 325.

Lavorel, S., Flannigan, M. D., Lambin, E. F., & Scholes, M. C. (2007). Vulnerability of land systems to fire: Interactions among humans, climate, the atmosphere, and ecosystems. *Mitigating and Adaptation Strategies for Global Change 82*, 33-53.

MacDonald, G. (2003). Biogeography: Introduction to space, time and life. New York, NY: John Wiley and Sons.

McSweeney, C., New, M., Lizcano, G., & Lu, X. (2010). UNDP climate change country profiles: Improving the accessibility of observed and projected climate information for studies of climate change in developing countries. *Bulletin of the American Meteorological Society,* 157–166.

Miller, J. D., & Thode, A. E. (2007). Quantifying burn severity in a heterogeneous landscape with a relative version of the delta Noramlized Burn Ratio (dNBR). *Remote Sensing of Environment 109,* 66-80.

Mills, A.J., & Fey, M.V. (2004). Frequent fires intensify soil crusting: Physicochemical feedback in the pedoderm of long-term burn experiments in South Africa. *Geoderma, 121*, 45–64.

Milne, A. K. (1988). Change direction analysis using Landsat imagery: A review of methodology. Proceedings of the IGARSS'88 Symposium Edinburgh, Scotland, ESA SP-284 (Noordwijk, Netherlands: ESA), pp. 541-544.

Mugisha, S. (2002). Patterns and root causes of land cover/use change in Uganda: An account of the past 100 years. The Land Use Change, Impacts and Dynamics (LUCID) Project. Working paper number 14. Nairobi, Kenya.

Mutai, C. C., & Ward, N, W. (2000). East African rainfall and the tropical circulations/convection on intraseasonal to interannual timescales. *American Meterological Society 13*, 3915-3939.

Nakakaawa, C. A., Vedeld, P. O., & Aune, J. B. (2011). Spatial and temporal land use carbon stock changes in Uganda: Implications for a future REDD strategy. *Mitigation and Adaptation Strategies for Global Change 16*, 25-62.

Namaalwa, J., Hofstad, O., & Sankhayan, P. L. (2009). Achieving sustainable charcoal supply from woodlands to urban consumers in Kampala, Uganda. *International Forestry Review 11*(1), 64-78.

Nicholson, S.N., (2001). Climate and environmental change in Africa during the last two centuries. *Climate Research 14*, 123-144.

Ogallo, L. J. (1989). The spatial and temporal patterns of the East African seasonal rainfall derived from principal component analysis. *International Journal of Climatology 9*, 145-167.

Ogallo, L.J. (1988). Relationships between seasonal rainfall in East Africa and the Southern Oscillation. *International Journal of Climatology 8*, 31-43.

Osbahr, H., Dorward, P., Sterns, R., & Cooper, S. (2011). Supporting agricultural innovation in Uganda to respond to climate risk: Linking climate change and variability with farmer perceptions. *Experimental Agriculture 47*(2), 293-316.

Otukei, J. R., & Blaschke, T. (2010). Land cover change assessment using decision trees, support vector machines and maximum likelihood classification algorithms. *International Journal of Applied Earth Observation and Geoinformation 12S*, S27-S31.

Pettorelli, N., Olav Vik, J., Mysterud, A., Gillard, J. M., Tucker, C. J., & Stenseth, N. C. (2005). Using the satellite-derived NDVI to assess ecological responses to environmental change. *Trends in Ecologoy and Evolution 20*(9), 503-510.

Phillips, J., & McIntyre, B. (2000). ENSO and interannual rainfall variability in Uganda: Implications for agricultural management. *International Journal of Climatology 20*, 171–182.

Pyne, S.J., Andrews, P.L., & Laven, R.D. (1996). Introduction to wildland fires. New York, NY: John Wiley & Sons, Inc.

Reich, P. B., Peterson, D. A., Wrage K., & Wedin, D. (2001). Fire and vegetation effects on productivity and nitrogen cycling across a forest–grassland continuum. *Ecology 82,* 1703–1719.

Sala, O. E., Chapin, Stuart III., Armesto, J. J., Berlow, E., Bloomfield, J., Dirzo, R., Huber-Sanwald, E., Huenneke, L. F., Jackson, R. B., Kinzig, A., Leemans, R., Lodge, D. M., Mooney, H. A., Oesterheld, M., Poff, N. L., Sykes, M. T., Walker, B. H., Walker, M., & Wall, D. H. (2000). Global biodiversity scenarios for the year 2100. *Science 287,* 1770–1774.

Van de Vijver, C. A. D. M., Poot, P., & Prins, H. H. T. (1999). Cause of increased nutrient concentrations in post-fire regrowth in an East African savanna. *Plants and Soils 214*, 173-185.

Vitousek, P. M. (1994). Beyond global warming: Ecology and global change. *Ecology 75*(7), 1861-1876.